INVESTIGATION OF NATURAL AND ANTHROPOMORPHIC SOURCES OF ATMOSPHERIC INFRASOUND

By

ARNESHA THREATT

Bachelor of Science in Mechanical Engineering

Oklahoma State University

Stillwater, Oklahoma

2014

Submitted to the Faculty of the
Graduate College of the
Oklahoma State University
in partial fulfillment of
the requirements for
the Degree of
MASTER OF SCIENCE
December, 2016

INVESTIGATION OF NATURAL AND ANTHROPOMORPHIC SOURCES OF ATMOSPHERIC INFRASOUND

Thesis Approved:

Dr. Brian Elbing

Adviser

Dr. Richard Gaeta

Committee Member

Dr. James Manimala

Committee Member

ACKNOWLEDGEMENTS

Special thanks to John Gage, Dr. Joe Conner, Collin Boettcher for their help in the installation of the roof deployment on the roof of the Fab Lab. Special thanks to Greg Vinyard for his help installing the roof system and help in the choice for the location of the second and third microphone deployments. Special thanks to Shannon Maher for her help in the design and building of platform system for deployment. Thanks to Yasaman Farasani for her help in the roof deployment and her endless support during my work on this project. Thanks to Shahrouz Mohagheghian for his and his team's work in improving the oscillating propane torch. Special Thanks to Dr. Brian Elbing for all of the guidance and wisdom he has shared with me throughout my tenure in his lab group.

Thanks to:
Jalen Golphin
Alexis Vance
Real KC
Jacob Niles
Chris Petrin

Name: ARNESHA THREATT

Date of Degree: DECEMBER 2016

Title of Study: INVESTIGATION OF NATURAL AND ANTHROPOMORPHIC SOURCES OF ATMOSPHERIC INFRASOUND

Major Field: MECHANICAL ENGINEERING

Abstract: Numerous geophysical and anthropogenic events emit infrasonic frequencies (<20 Hz), including volcanoes, hurricanes, earthquakes and tornadoes. These sounds, which cannot be heard by the human ear, can be detected from large distances (in excess of 100 miles) due to low frequency acoustic signals having a very low decay rate in the atmosphere. Data collected from researchers in the past suggest that infrasound could be used for long-range, passive monitoring and detection of these events. Currently there is an effort to establish an infrasonic monitoring station at Oklahoma State University (OSU) to determine the relationship between infrasonic signals produced during severe storms (as well as other events) and the flow-field that produced them. The current thesis reports on the deployment of the first infrasonic microphone on the roof of the OSU Fabrication Laboratory, which includes laboratory testing to compare the performance of available microphones and assess the windscreen performance. The microphone was able to record a variety of events including severe storms, fireworks, and earthquakes. Spectra from a sampling of these events are provided in the thesis as well as background atmospheric infrasound from a “typical day” (i.e. behavior on days without these events). In addition, preliminary work for the deployment of 2 additional microphones is discussed, including their utilization for acoustic localization.

Table of Contents

List of Tables

List of Figures

CHAPTER I

1. INTRODUCTION

1.1 Motivation

Tornadoes cause 60 to 65 fatalities and roughly 1,500 injuries per year. These numbers are due in part to the inaccuracy of tornado warnings and relatively short lead times. As shown in Figure 1 (Wurman et al., 2012), since about 2002 improvements in tornado detection, warning lead times and false alarms have plateaued due to limitations of existing technology and understanding of tornado dynamics. Consequently, there is a need for a new approach to tornado detection that could reduce the number of false alarms and possibly improve lead times.

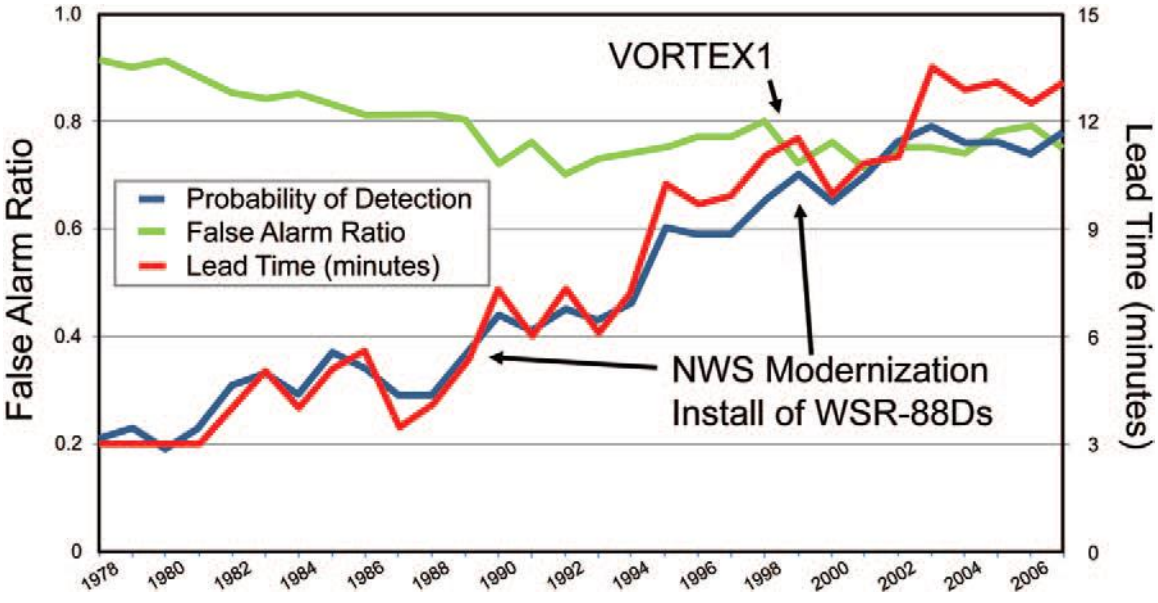

Figure 1: Graph showing improvements in tornado detection, lead times, and false alarms from 1978-2006 (Wurman et al., 2012).

Numerous natural and anthropomorphic occurrences emit infrasound. These occurrences include nuclear explosions, volcanos, earthquakes, and tornadoes (Bedard, 1998). Infrasound attenuates over very large distances due to an "acoustic ceiling" in the atmosphere (Bedard & Georges, 2000) and weak atmospheric absorption at low frequencies (Cook, 1962), meaning infrasonic sound signals can be detected from extremely far distances. These infrasonic signals carry information about source that produced it, which suggests it could possibly be used for early and more accurate detection of tornadoes, which is one of the primary motivations of this project.

This project is a small part of the overall NSF funded Collaboration Leading Operational UAS Development for Meteorology and Atmospheric Physics (CLOUD-MAP) project. This projects primary objective is to create and demonstrate unmanned aircraft systems (UAS) capabilities needed to support UAS operating in extreme conditions, such as a tornado producing storm system. The data collected will give

insight into the developing atmospheric boundary layer, which plays a significant role in severe storm systems and is currently poorly understood due to limited spatial and temporal resolution available from current instrumentation (e.g. radar, balloons, and towers). The UASs will gather information that will give more insight into the physics governing the formation and life of tornadoes. The aim of the infrasonic effort of CLOUD-MAP is to correlate the information from the UAS (as well as other available sources) with the data recorded from infrasonic microphones. In addition, the technical challenges associated with integrating an infrasonic microphone on a UAV will be examined. This thesis focused on establishing a trusted ground-based infrasonic array as well as recording the infrasonic signatures of various sources including severe storms, earthquakes, and fireworks.

1.2 Literature Review

1.2.1 Infrasonic Sources

An infrasonic sound source is necessary to confirm the capabilities of an infrasonic system. Since most infrasonic systems are used for field testing, the infrasonic source also must be portable. This significantly complicates things because most simple infrasonic generators have to be very large (e.g. lower the frequency range the larger a speaker). A review of the literature shows that an ideal compact infrasonic source remains elusive, but several alternative options that successfully created infrasound sources were found including explosives (Golden et al., 2008; Waxler et al., 2015), subwoofers (Shams et al., 2005; Ahuja et al., 1993), spherical Helmholtz resonator

(Bedard & Georges, 2000), pulsed gas combustion torches (Smith & Gabrielson, 2015; Elbing & Gaeta, 2016; Threatt & Elbing 2015, 2016), and rotary subwoofers (Park et al., 2009; Park & Robertson, 2009). The most novel (and least historically utilized) of these approaches are the pulsed gas combustion torch and the rotary subwoofer. The pulsed torch is discussed in more detail subsequently, so a review of the rotary subwoofer is provided here. Note that there are also high-end options such as the Mobile Acoustic Source (MOAS), commonly referred to as the "mother of all speakers", which can generate a high intensity low frequency sound source. However, the current work focuses on relatively low cost options.

According to Park et al. (2009), the rotary subwoofer or as it is often referred the Thigpen rotary woofer (TRW), is essentially a baffled fan with blades that have dynamically controlled pitch. A schematic and picture of the TRW is provided in in Figure 2. The hub of the fan is rotated at a constant frequency, while the fan blades pitch is modulated by a control signal based on the input signal. The motion results in pulses of air at high amplitudes.

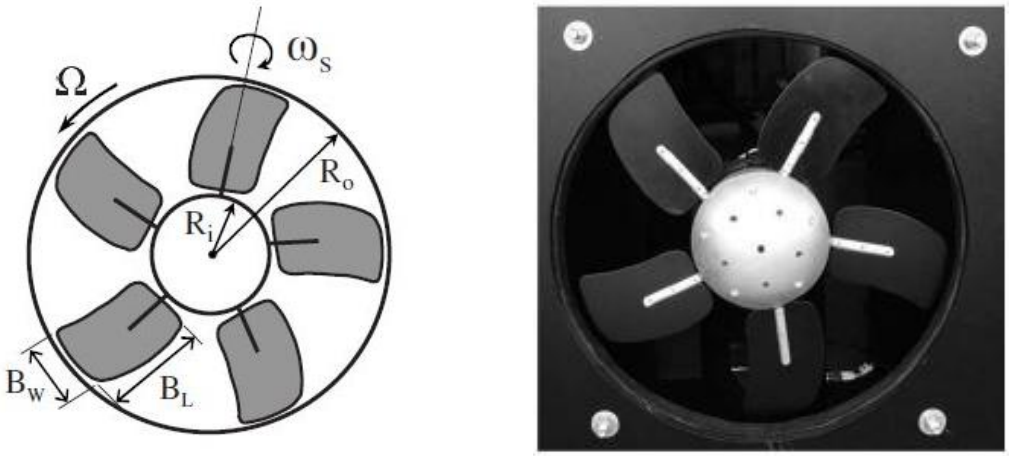

Figure 2: A (left) schematic and (right) image of the TRW from the work of Park et al. (2009). In the schematic R_i is the hub of radius, Ω is fixed rate of rotation of the hub, B_L and B_w are the

blade lengths and widths, respectively, and ω_s is the frequency of the pitch used to modulate the signal.

The TRW was made portable via its installation into the back of a U-Haul moving van. This installation involved bolting the fan housing to boards of wood clamped to the sides of the U-Haul (Figure 3, from Park & Robertson, 2009). A portable generator provided power to the TRW and the resulting signals were recorded with infrasonic microphones (Model 2.2A, Chaparral Physics) placed closer than 4.9 km (Park & Robertson, 2009). Favorable results were produced during this outdoor testing. A sample of the data is reproduced from Park & Robertson (2009) in Figure 4. They demonstrate that frequencies as low as 5 Hz can be produced by the TWR, while the MOAS mentioned earlier in this section can only reach frequencies as low as 10 Hz. Due to the time and effort it would take to build a TWR, it was not utilized in the current work. However it may be beneficial to perform experiments with the TWR in the future.

Figure 3: (left) Picture from Park & Robertson (2009) of the TRW mounted on the side of a moving truck to make it portable. (right) Same picture zoomed in on the TRW.

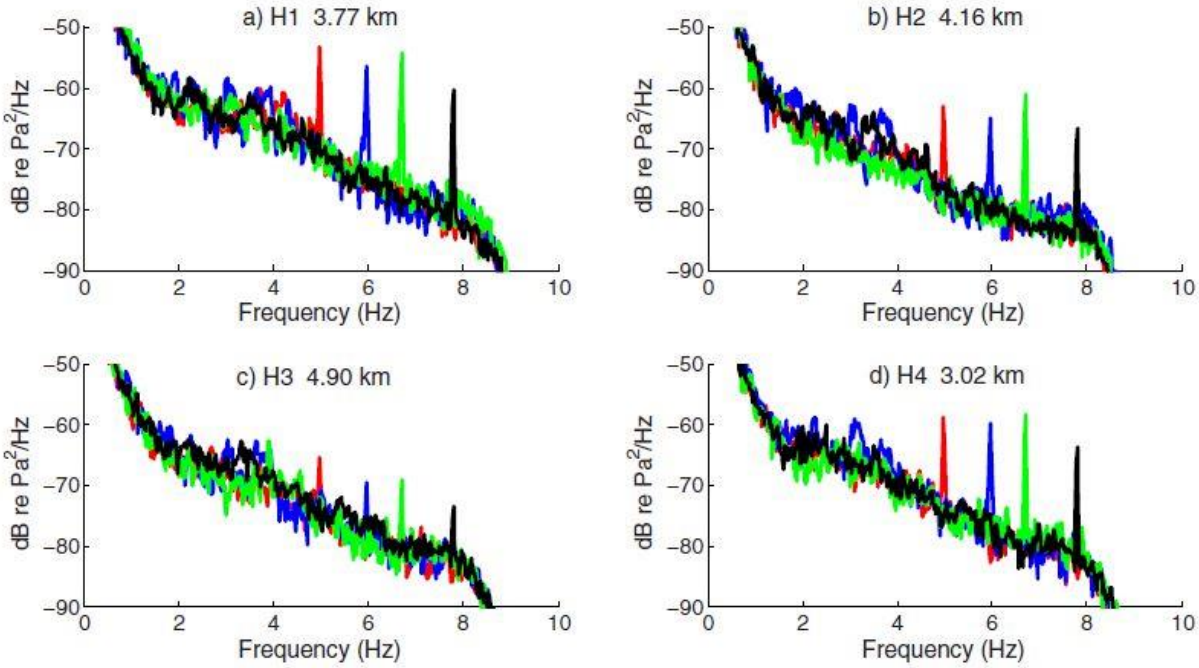

Figure 4: Results reproduced from Park & Robertson (2009). Power spectral density from the outdoor testing with TRW using sources at 5, 6, 7, and 8 Hz. The distance between the TRW source and the microphone varied from (a) 3.77 km, (b) 4.16 km, (c) 4.90 km, and (d) 3.02 km.

1.2.2 Infrasonic Measurements

Numerous papers have been written about the potential use of infrasound (Bedard, 1998; Bedard & Georges, 2000; Waxler & Gilbert, 2006; Farges & Blanc, 2010; Shams et al., 2013; Lorenz & Christie, 2015), including several focused on tornado detection and/or monitoring (Abdullah, 1966; Arnold et al., 1976; Bedard, 2005; Schecter et al., 2008; Ash et al., 2011; Frazier et al., 2014; Dean et al., 2015). Many of the papers on tornadic infrasound reference Abdullah (1966), which proposed that a radial mode of oscillation within a tornado could generate sounds in the infrasonic range. Other seminal infrasound work has been led by Alfred J. Bedard from NOAAs Earth System Research

Laboratory and more recently Roger Waxler's group at the University of Mississippi in the Department of Physics and Astronomy. Below key results from both groups are reviewed, though it should be stressed that this review is not exhaustive.

Bedard & Georges (2000) provides an excellent introduction to atmospheric infrasound in general with an overview of the history of infrasonic research, measuring and generating infrasound, potential applications and future infrasound research, and a brief synopsis of a couple research areas including severe storms. Here Bedard & Georges (2000) mention that infrasound radiating from the strongest thunderstorms can be measured from more than a thousand kilometers away. It is also noted that these infrasonic sounds seem to particularly come from storms that spawns tornadoes. This paper also suggests a connection between infrasonic frequency and funnel diameter.

Bedard's pioneering work is due in large part the establishing of the InfrasSonics Network (ISNet) in 2003. It consists of three separate infrasonic arrays located in Pueblo, CO; Boulder, CO; and Goodland, KS. Background information and the initial results from the ISNet are published in Bedard et al. (2004a, 2004b). The creation of ISNet was inspired by observations presented in Bedard (2005) and NOAA (2002). An example of data acquired in NOAA (2002) is provided in Figure 5. Here measurements of the infrasound in the atmosphere on a calm day and on a day with tornadoes are shown. The "path" of sound travel (or relative bearing angle) with and without tornadoes was determined by correlating data acquired from multiple infrasonic sensors. As can be seen the correlation on a calm day and the day with tornadoes is very different. On the day with tornadoes, the dominating sound appears to be following the path of a storm that is producing tornadoes (bearing angle of tornadoes shown with red dots). It is of note that

the correlation graph shows the path of the storm one hour before a tornado actually occurs.

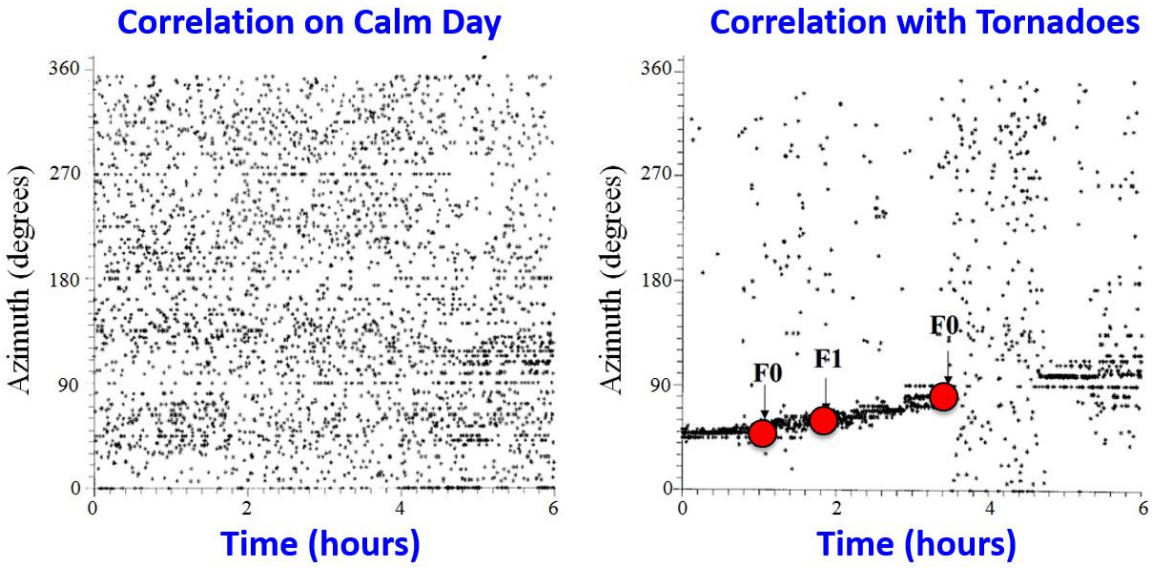

Figure 5: Data from NOAA (2002) showing the bearing (azimuth) angle of the peak correlation of infrasound on (left) a calm day and (right) a day with tornadoes. The red circles represent the bearing angle location of three tornadoes.

Bedard (2005) had suggested that the data recorded from tornadic thunderstorms have signals in the 0.5-10 Hz band, with maximum correlation between the 4-element array in the 0.5-2.5 Hz band. However, there is evidence suggesting that these frequency bands depend highly on the instrumentation used and the size of the array. Waxler's group (Frazier et al., 2014; Talmadge & Waxler, 2016) provide infrasonic data measured from several tornadoes near Stillwater, OK in 2011. Two arrays with digital NCPA sensors measuring at a sample rate of 1,000 samples per second recorded during the tornado outbreak. These arrays were roughly 700 to 1,200 meters away from the path of the tornadoes. Data from these tornadoes are shown in with the signals being generally

broadband peaking around 50 Hz. However, it should be noted that this group had expected the tornadoes to be further away, and consequently their configuration was not ideal for how close the tornadoes were to the array.

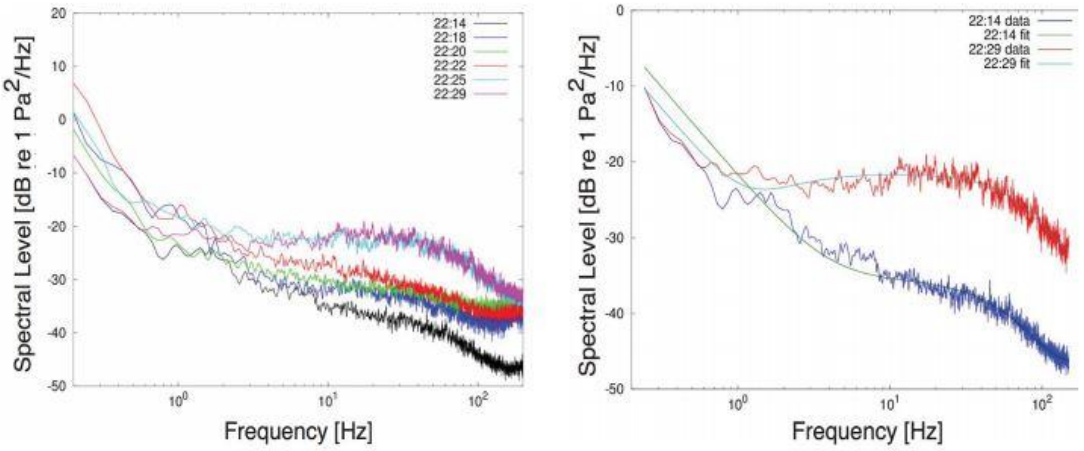

Figure 6: Figures reproduced from Talmadge & Waxler (2016) showing (left) spectra as tornadoes approach array and (right) best fit lines with spectra using model given in Equation (1).

Frazier et al. (2014) examined potential mechanisms for the "shoulder" seen in the spectra shown in Figure 6. It was concluded that the mostly likely source for the sound generated was the tornado vortex, which was replicated using a modified model for sound radiation from aeroacoustic jet turbulence (Powel, 1959). The modified model is provided in Equation (1), which states that the power spectrum $S(\omega,r)$ at a given frequency ω and distance r from the source is determined from the sum of three terms. The first term is associated with turbulent pressure fluctuations and based on traditional Kolmogorov scaling of the inertial-subrange turbulence should be proportional to $\omega^{-7/3}$ (e.g., Shields, 2005). The second term is the jet turbulence model, which represents the audible sound generated by the tornado as measured by a distant sensor. This term has

several free parameters to "fit" the data including A_s that sets the overall noise level, ω_n that sets the peak frequency, ζ sets the width of the peak, and g_a accounts for effects of attenuation and the propagation losses within the atmosphere (Bass et al. 1995). The third term A_n is simply the noise floor for the given arrangement. While there are several other publications reporting infrasonic data from tornadoes (e.g. Noble & Tenney, 2004; Dean et al., 2015), this review illustrates the need for an increase in the quantity and quality of available infrasonic data from severe storms.

$$S(\omega,r) = A_f \omega^{-7/3} + \frac{A_s \omega_n^2 \omega^2}{\omega^4 + 4\zeta^2 \omega_n^2 \omega^2 + \omega_n^4} g_a(\omega,r) + A_n \quad (1)$$

CHAPTER II

2. EXPERIMENTAL METHODS

2.1 Infrasonic Measurements

2.1.1 Microphones

The first infrasonic microphones purchased were low cost microphones (Infra20, Infiltec) shown in Figure 7, which the company advertises itself as "The Inexpensive Infrasound Monitor Project." This microphone is a simple device consisting of a basic circuit with a microcontroller and a couple of filters connected to a pressure transducer. The microphone is powered by a laptop/computer via the USB connection and records to that same computer. Figure 7 also shows the circuit along with a picture of the aluminum housing containing the entirety of the microphone.

The acoustic inlet for the microphone is attached to a clear plastic hose, which can be seen in Figure 7. This hose makes it easier to take measurements from specific locations and also helps reduce noise by attaching a windscreen to the port. It records in a frequency range of 0.05 to 20 Hz. This microphone records directly to a program normally used to monitor seismic activity (Amaseis, IRIS) and has a fixed sample rate of 50 samples per second. The sensitivity of this microphone was not provided by the

manufacturer but was deduced by microphone comparison experiments. The sensitivity of this microphone and the experiments used to find it will be discussed subsequently.

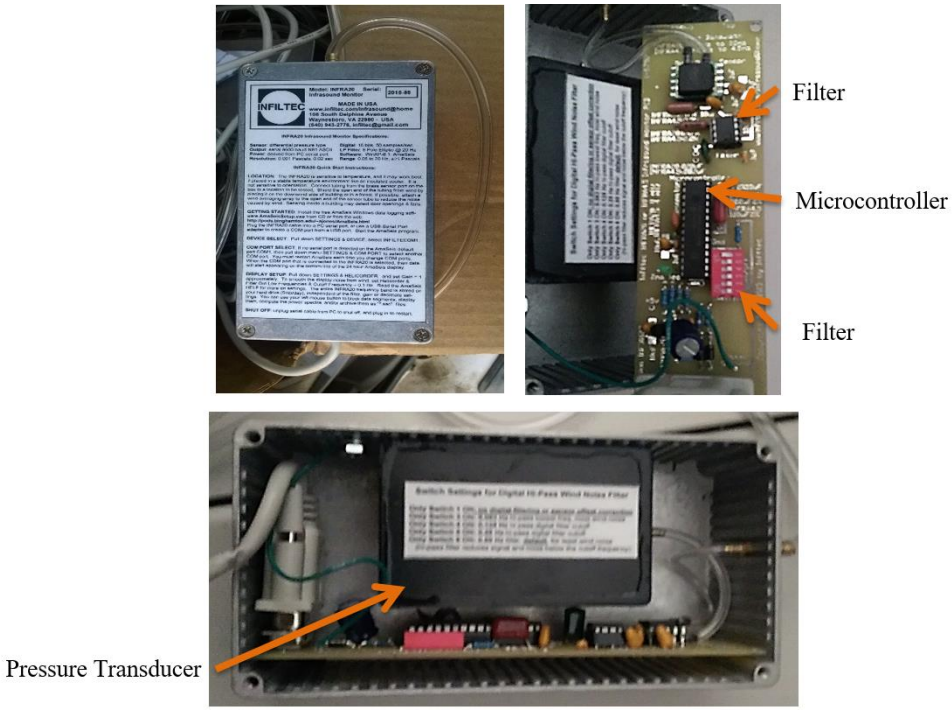

Figure 7: Pictured are the components of low-cost infrasonic microphone (Infra20, Infiltec) including (top left) the aluminum housing, (top right) circuit board with filters and controllers, and (bottom) the pressure transducer with the clear plastic hose attached.

With funding support from CLOUD-MAP, the microphones could be upgraded to state-of-the-art infrasonic microphones (Model 24, Chaparral Physics). These microphones are differential, low-air pressure sensors, and is considered by the manufacturer to be an ultra-low frequency microphone or microbarometer. These sensors have 4 inlet ports, which can be connected to soaker hoses to act as windscreens. They are specifically designed to be used in rugged environments, which is ideal for its

eventual uses in this project measuring during severe storms. An image of one of the purchased Chaparral Physics microphones is shown in Figure 8.

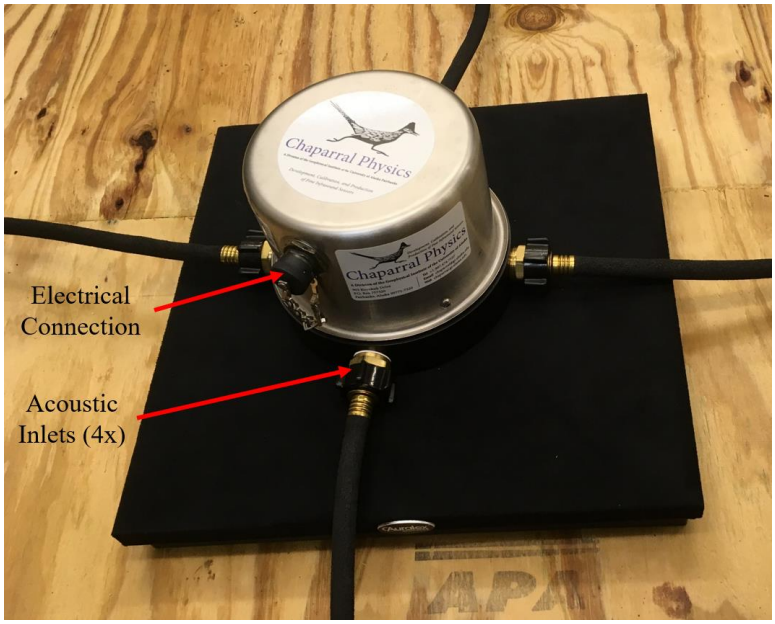

Figure 8: Picture of the Chaparral Model 24 microphone mounted on a vibration isolation pad. Arrows indicate the locations of the electrical connection for power and signal as well as one of the four acoustic inlets, which have soaker hoses attached in the picture.

The Chaparral microphones has a nominal sensitivity of 400 mV/Pa and are calibrated by the manufacturer before shipping using a calibration value traceable to the Los Alamos National Laboratory calibration chamber. The sensor has a differential output with a self-noise below 0.63µPa^2/Hz at 1 Hz (-62dB Pa^2/Hz, rel to 1 Pa), less than 3 mPa RMS from 0.1 to 40 Hz, and less than 0.8 mPa RMS 0.5 to 2 Hz. The typical frequency response relative to the sensitivity at 1 Hz between 0.1 and 200 Hz for the Chaparral Model 24 microphones is shown in Figure 9. A 12 volt DC signal is required to power the sensor, which is supplied via a 90 W, single-channel adjustable DC power supply (APS-1303, AKTAKOM) that can be adjusted between 0-30 V. For a single microphone there is a 0.3 amp draw with the 12 VDC signal. The output signal is

recorded using a dynamic signal analyzer (USB-4432, National Instruments) and a commercial software package (2015 Labview Sound and Vibration Package, National Instruments). A more detailed description of the data acquisition and processing is provided in a later subsection.

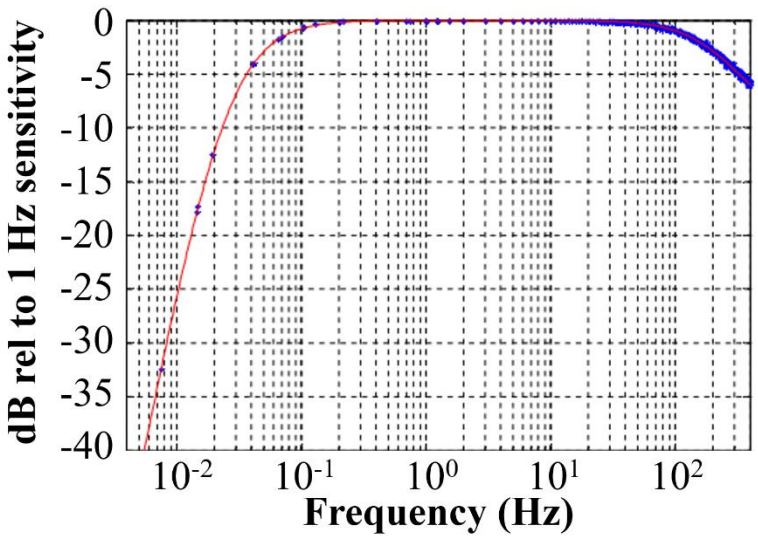

Figure 9: Typical frequency response of a Chaparral Physics Model 24 microphone, which shows a relatively flat response between 0.1 and 200 Hz.

2.1.2 Windscreens

Infrasonic measurements taken outdoors are highly affected by wind, making windscreens a vital part of any infrasonic experimental setup. There have been numerous methods researched to create an effective windscreen for infrasonic measurements including pipe arrays (Daniels, 1959; Burridge, 1971; Alcoverro, 1998), a barrier (Hedlin & Raspet, 2003), an open-mesh enclosure (Bruel, 1960; Anderson & Kettler, 1948; Ballard & Izquierdo, 1968), and recently a closed-cell foam enclosure (Shams et al., 2005, 2013, 2014; Zuckerwar & Shams, 2011). Pipe arrays, which are a series of hoses with many ports to spatially average out any random noise including wind, are the most

widely used by researchers. They utilize the fact that infrasonic signals are coherent over distances of a few wavelengths, which a 10 Hz signal has a wavelength of 34 m. A series of radial pipes (or soaker hoses) are extended from a single microphone, which results in a spatial averaging that eliminates the non-coherent wind noise while preserving the coherent infrasonic signal of interest. In early testing two 8 ft length segments of 0.175 inch PVC pipe were connected together at 7 different locations around a circular hub as shown in Figure 10. This setup was used with the low-cost microphones (Infra20, Infiltec), which had the clear hose (acoustic inlet) attached to the center circular hub as shown. Due to extremely poor performance, the PVC pipes were replaced with 25 ft long soaker hoses. The soaker hoses significantly increase spatially averaging since the walls are porous allowing acoustic waves to transmit through the walls. Note that the soaker hoses used with the Chaparral microphones were increased to 50 ft lengths, but looped back to the microphone resulting in a total diameter of 50 ft for the windscreens. Pictures of each of the windscreen configurations tested at Oklahoma State University (OSU) as well as the closed-cell foam setup from NASA Langley Research Center are shown in Figure 10. The NASA designed windscreens can reduced hurricane force winds without any attenuation of the desired infrasonic signals. Consequently, it is the long-term goal of this research to adapt these designs to the OSU infrasonic array.

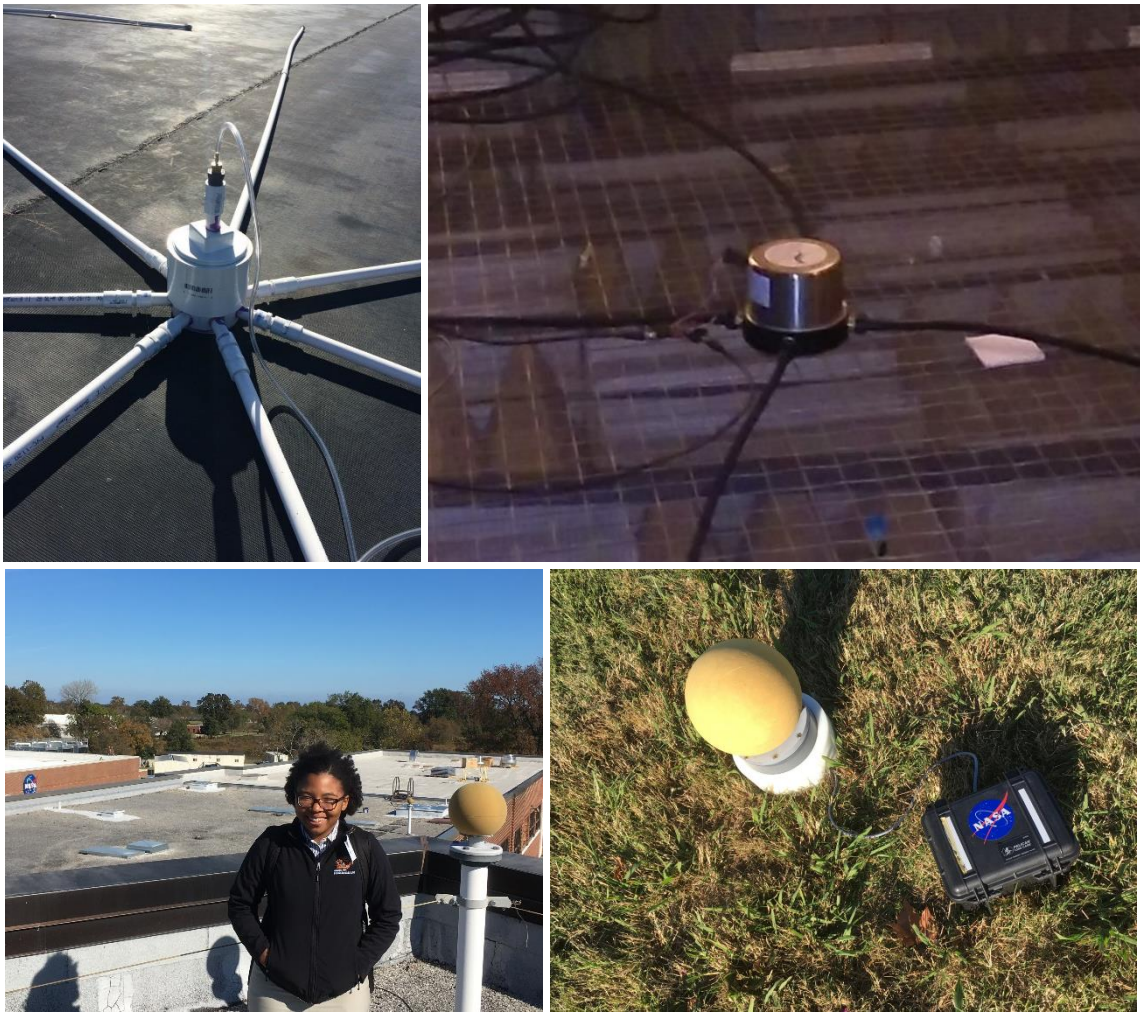

Figure 10: (top left) Original windscreen design used with the low-cost microphones and consisted of PVC pipes attached to a central hub. (top right) Soaker hoses attached to the Chaparral Model 24 microphone. (bottom row) Pictures of the NASA designed closed-cell foam windscreens deployed at NASA Langley Research Center.

2.1.3 Data Acquisition

Different data acquisition systems were utilized for each microphone. As stated earlier, the low-cost microphones (Infra20, Infiltec) used Amaseis software to record the measured signals. The program must be running in order for the microphone to operate. The sample rate was fixed at around 50 samples per second. Initially the recorded signal is displayed on the main screen (see Figure 11), which then the desired signal must be

selected and extracted (see Figure 12) in order to be saved as a SAC file. A MATLAB program (Beaudecel, 2016) was used to convert these SAC files into MATLAB readable arrays. Then a program created for this project processed and graphed the power spectrum with RMS averaging as many times as the user desires.

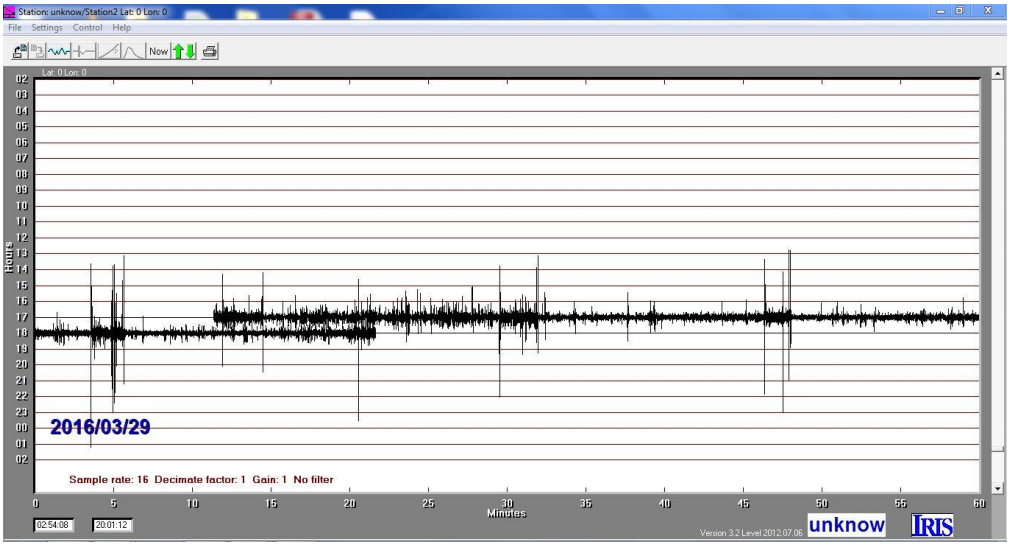

Figure 11: Main screen within Amaseis data acquisition software used for recording from the low-cost microphones. Displays acquired signals from the previous 24 hours.

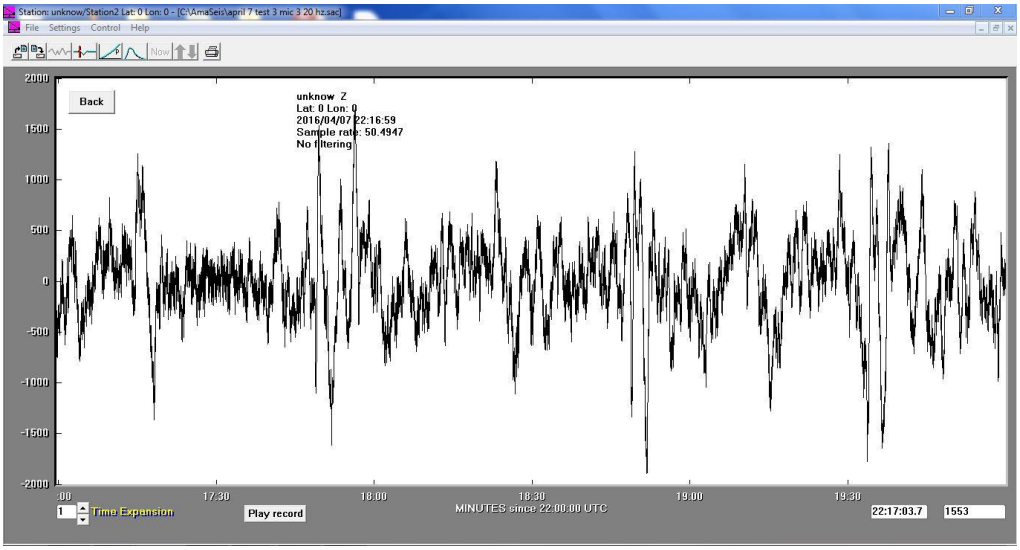

Figure 12: Example of an extracted signal from the Amaseis software.

The output from the Chaparral Model 24 microphone is an analogy voltage signal, which gives greater flexibility for the user in selecting a data acquisition system. As stated earlier, our setup used a dynamic signal analyzer (USB-4432, National Instruments) shown in Figure 13 to convert the analog voltage from the microphone to a digital signal, which was then recorded with a commercial software package (2015 Labview Sound and Vibration, National Instruments). The data acquisition software interface is shown in Figure 14. Specific data processing and analysis details will be discussed later in this chapter.

Figure 13: National Instruments image of their NI USB-4432, which is used to acquire the signals from the Chaparral microphones.

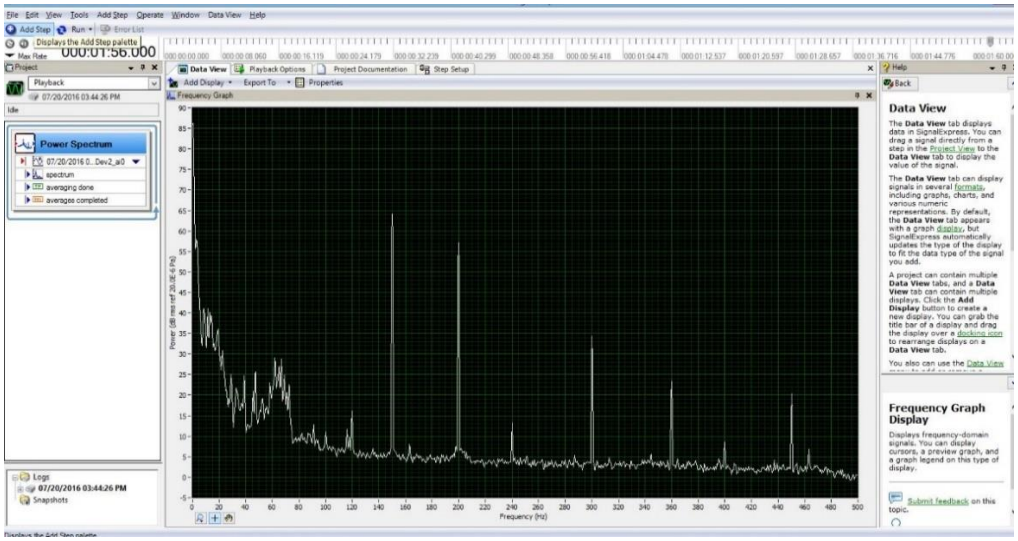

Figure 14: Interface of NI LabView Sound and Vibration used to acquire Chaparral signals.

2.1.4 Roof Deployment

Given that most atmospheric infrasound signals of interest are expectedly generated, a long term infrasonic system needed to be deployed for continuous monitoring. This system needs to record the various events that occur regularly and emit infrasound into the atmosphere as well as rare (singular) events. While the initial deployment only has a signal microphone, currently plans are to expand the system to have at least two additional microphones to measure the bearing angle of received signals. In addition, the long-term plans are to deploy additional 3-microphone arrays, which will enable precise localization of given signals. However, results for the current work only use the initial microphone.

The location chosen for this long term deployment needed enough space to accommodate the 50 foot radius formed by the soaker hose windscreens as well as positioned such that it would not be bothered by animals or curious people. After considering multiple sites, the roof of the OSU Fabrication Laboratory (Fab Lab) was chosen because (i) it is a clean roof with no HVAC equipment, (ii) the system would be relatively out of the way, and (iii) the roof top access would significantly limit the systems interactions with people, animals, and vehicles that could damage it. The original planned location was at the OSU Unmanned Aircraft Flight Station, which is roughly 12 miles East of the main OSU campus. However, there were several concerns about ensuring that the system was regularly monitoring and inspected for damage, especially from the lawn mowing crew.

Conversely, the roof of the Fab Lab is on the North edge of campus, which allows students to easily inspect the setup on a regularly basis. In addition, there is sufficient space to add the 2 additional microphones to create the desired array. The Fab Lab roof (GPS location: 36.134422, -97.081814) was ultimately chosen for the first site due to the lack of HVAC, its flatness, and the easy access to dedicated space for the project. The microphone is mounted to the roof with two cables (1 signal, 1 power) running along the roof, through an access panel, and into the building where the DC power supply and a data acquisition system (shown in Figure 15) are located.

Figure 15: Data acquisition system for Fab Lab roof top deployment including the DC power supply, digital signal analyzer, and computer.

For the long term deployment the microphone needs to sit in an enclosure that will minimize sudden temperature fluctuations and keep the microphone sufficiently elevated that it does not sit in standing water. Thus a platform for the microphone was designed and fabricated to weigh down the microphone so it is not move or be destroyed in high winds, protect the microphone from the sun radiation, and limits the influence of

structural vibrations. A picture of the final platform setup is shown in Figure 16, and a zoomed out view of the overall assembly with the soaker hoses is shown in Figure 17.

Figure 16: (left) Final platform design with microphone mounted (right) Final roof top system with hoses attached and dome covering microphone.

As shown the dome contains the microphone and the vibration isolation pad. The soaker hoses run out of the dome via holes that were drilled into the dome. An additional hole was drilled for the power and signal cables. The microphone sits on top of a small plank of wood covered in velvet that is epoxied on top of a dense sheet of foam that provides vibration isolation. The foam pad sits on a rubber sheet that is glued to a 0.75 inch thick sheet of plywood. The dome, which encloses the microphone and vibration isolation pad, is secured directly to the 0.75 inch thick plywood sheet. Under the 0.75 inch plywood base is a 35 pound steel plate, which is sandwiched between the base plate and a second 0.75 inch plywood sheet. The wood-steel "sandwich" is secured via screws, while the rubber pad, vibration isolation foam and smaller wooden plank are connected via multipurpose adhesive. The microphone itself was secured with Velcro strips that are glued to its bottom and the velvet covered wooden plank. The steel plate provides weight

to the overall system, and should prevent movement of the assembly for wind speeds in excess of 100 mph.

Figure 17: (left) Final configuration for the roof top microphone deployment with soaker hoses spread out in an ‘X’ shape. (right) Aerial view of the roof top deployment.

Direct burial UV BNC cables (BNC 1DB-100, Premium Phantom) were used to connect the microphone to the computer and DC power supply. These cables are made for outdoor use and exposure to UV light, but to increase the factor of safety the cables were run through blue flexible conduit for added protection. The soaker hoses were connected to the microphone through the dome and folded once with the end of the hose brought back near the dome to make the system have a nominal radius of 25 feet. These hoses were weighed down by 2×4 boards with lengths of either 3 or 4 ft with U-clamps used to secure the hoses to the boards. As of this writing, the Chaparral (Model 24; serial number 162644) microphone has been continuously recording since September 2, 2016.

This system will provide infrasonic data from natural and anthropomorphic occurrences that happen regularly such as small earthquakes, plane take offs and

landings, and storms systems. The times of these events will be recorded and correlated with the corresponding signals recorded by the microphone.

2.1.5 Triangulation 2nd and 3rd Deployment

To confidently be able to say that specific recordings correspond to the events at a given time, an array of microphones is needed. This array will enable the user to determine the direction of the signal and with several arrays the exact location can be found (with a known confidence level). The abundance of events recorded from the roof top deployment, made it apparent that an array is needed as soon as possible. The second and third microphones should be between 40 and 80 meters from each other, which according to Bedard et al. (2004a) is the ideal spacing for acoustic localization. With this knowledge and the places where digging would not impinge on any existing buried pipes or wires, two sites were chosen to install the 2nd and 3rd systems. The locations of the 2nd and 3rd system are shown as diamonds on the map in Figure 18, and the current roof top microphone is shown as a red circle on the Fab Lab roof.

Figure 18: Locations of microphone deployments at the OSU Fabrication Laboratory. The red circle denotes the location of the current roof top microphone, and the diamonds represent the planned locations of the 2nd and 3rd microphones assemblies.

The future plans are to emulate the infrasonic microphone system deployed at NASA Langley Research Center, which uses a combination of compact sub-surface and spherical windscreens. The sub-surface configuration has the infrasonic microphone buried in hole with a panel of closed-cell foam at the surface, surrounding the enclosure is gravel to help with drainage around the microphone when it rains. The 2nd and 3rd microphone deployments will both have a 2 ft x 2 ft hole filled with concrete, which will secure a wooden frame. On top of this frame will have a platform built the same way as the roof deployment except without the steel plate that was added for weight. The wood base mounted to the frame will have in order mounted on top of it a rubber mat, vibration isolation pad, another piece of wood, and then the infrasonic microphone attached. The dome then covers the entire system and the BNC cables that power and carry the output

signal to the computer system will be buried underground and covered with conduit to prevent animal or human interference. Both the 2nd and 3rd system will be powered by the same DC power supply and recorded on the same data acquisition system currently used for the roof mounted microphone.

The bearing angle of the received signals will be determined by cross-correlating the signals recorded by the different microphones to find the different time shifts between the different microphones. The bearing angle is then found using the speed of sound in air, the known distances between the microphones, and the measured time shifts.

2.2 Infrasonic Source Production

To develop the infrasonic array as well as test localization codes, a trusted/known infrasonic source is needed. This proves to be a very difficult task as producing a "loud" infrasonic signal in a controlled fashion requires a displacement of a large volume of air. In the experiments that are described here a subwoofer and a pulsed gas-combustion (propane) torch were used as infrasound sources.

2.2.1 Subwoofer

The use of a subwoofer is especially difficult due to the frequency limitations based on the size of the speaker. To produce a loud infrasonic source a large speaker would be necessary. For this testing two separate 12 inch speakers were used at different times. The first was a basic 12 inch Sony subwoofer speaker, which has a frequency response limit of roughly 20 to 60 Hz. The other speaker used was a Kicker CompVR,

which has a rated frequency range of 25 to 500 Hz. The Kicker speaker performed better during testing and produced signals below 25 Hz. These signals were not “loud”, but were detectable during laboratory testing. To produce the required signals each speaker was connected to a function generator. The Kicker speaker (shown in Figure 19) used an amplifier in addition to a function generator.

Figure 19: Two subwoofer speakers were used for laboratory testing; (left) a 12-inch Sony subwoofer and (right) a Kicker Comp VR.

Initial desktop tests were performed with the Sony speaker with the low-cost (Infra20, Infiltec) microphones. A square wave was inputted into the speaker at an amplitude of 5 volts and a variable frequency that was below 20 Hz. Tests were run for one minute at a time while the microphone was varied in distance from the source. The results of these tests were then compared with an analytical solution found Kinsler et al. (2000), which is graphically shown in Figure 20. This analysis describes how an oscillating cylinder (subwoofer) produces sound and analytically describes how the resulting pressure wave travels from the speaker. The results of the experiments aligned fairly well with the analytical solution described in the book, with the discrepancies

mostly due to the poor quality (extremely low sensitivity) of the low-cost microphones that limited the distance from the source. The measured signals from 0.5 and 1.0 Hz square wave inputs are shown in Figure 21 and Figure 22, respectively.

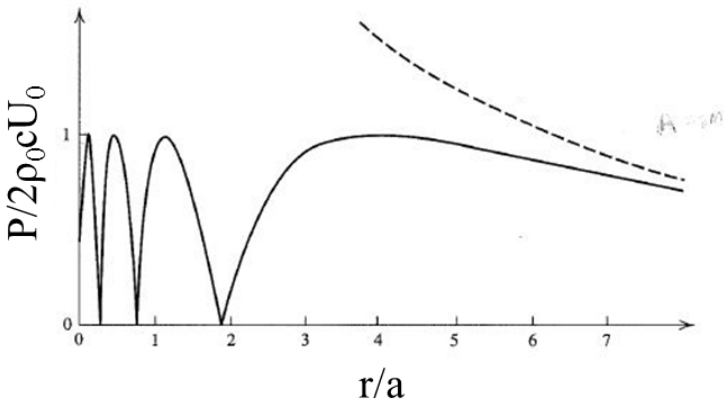

Figure 20: Graphical representation from Kinsler et al. (2000) of the analytical solution to sound pressure distribution generated from an oscillating piston.

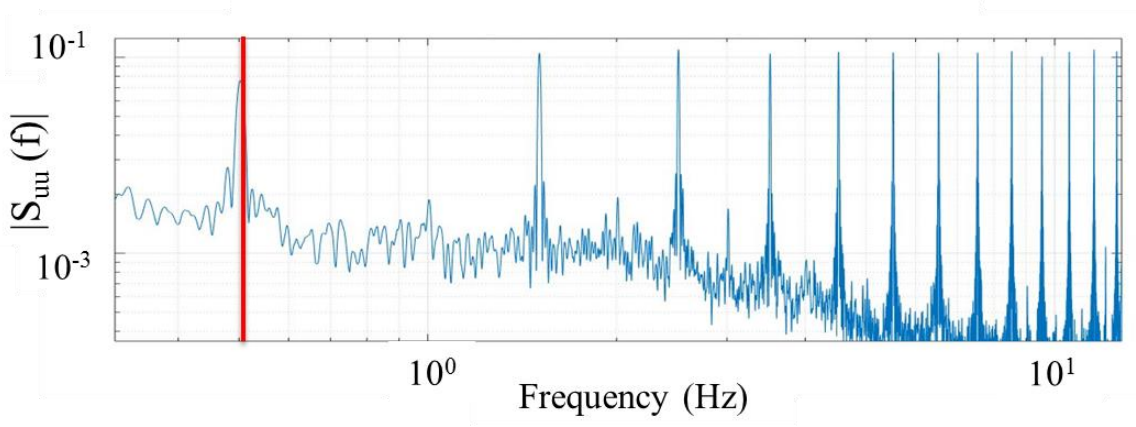

Figure 21: Measured sound pressure levels from a square wave at 0.5 Hz measured with the low-cost microphones. The microphone had to be placed within inches of the subwoofer.

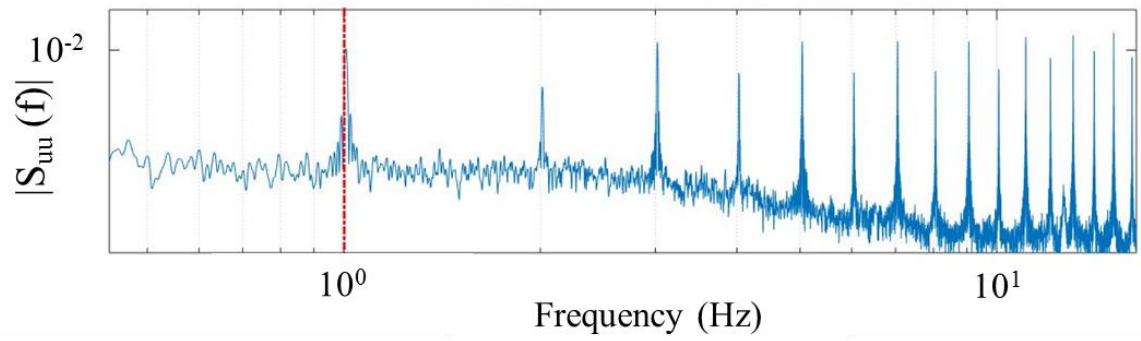

Figure 22: Measured sound pressure levels from a square wave at 1.0 Hz measured with the low-cost microphones. The microphone had to be placed within inches of the subwoofer.

In Figure 20, the pressure fluctuates when measured right next to the oscillating cylinder corresponds to the "near field." When measured sufficiently far from the source, the sound pressure should asymptote to the dotted line. This limit is an exponential function proportional to the inverse of the radial distance of measurement. At this distance and beyond, the subwoofer can be treated as a point source. Calculations performed using the equation: $^{r_1}/_{a} = {}^{a}/_{\lambda} - {}^{\lambda}/_{4a}$, determine at what radial distance *r* the measurements must be taken based on the radius of the speaker face *a* and λ is the wavelength, which is equal to the speed of sound in air divided by the operating frequency. The calculations suggest that all of the experiments were performed in the far-field. The normalized spectral peak as a function of radial distance is provide in Figure 23 and displays how well the subwoofers behaved like a point source. The frequencies with deviations from the 1/*r* line indicate the need for improved instrumentation. The low-cost (Infra20, Infiltec) microphone was unable to measure any signal beyond one foot from the subwoofer, further reiterating the need for an improved instrumentation. Tests with the Kicker subwoofer will be described in later sections.

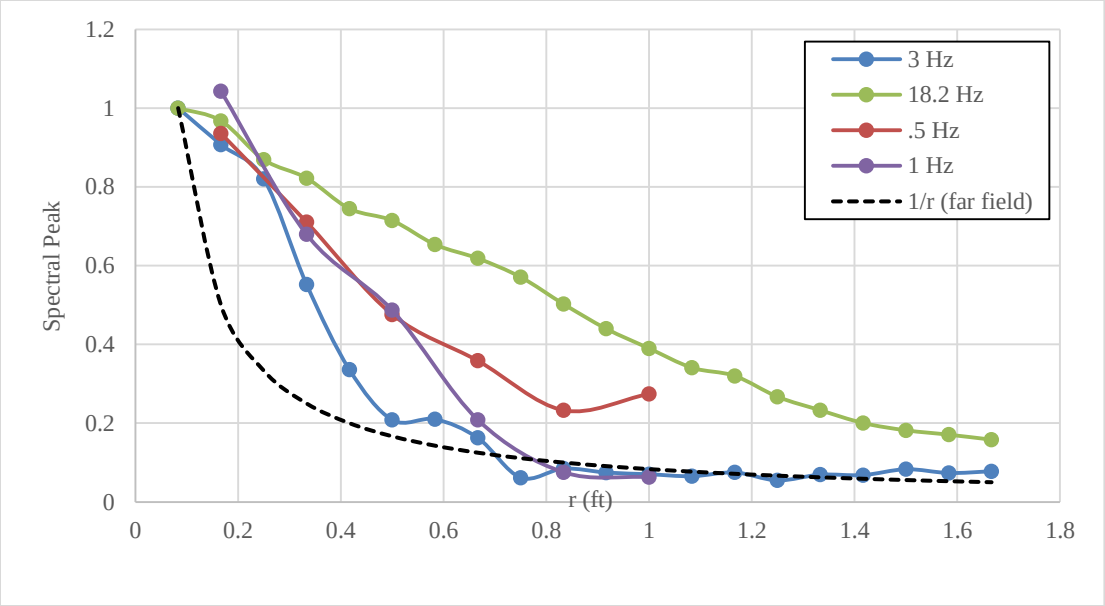

Figure 23: Normalized spectral peak as a function of distance from the subwoofer. Measurements were acquired with the low-cost microphones.

2.2.2 Pulsed gas-combustion torch (propane torch wand)

A novel idea was recently proposed by Smith & Gabrielson (2015), which notes that an infrasonic signal can be produced by the rapid increase and decrease of a volume of air via heating and cooling of the flame of a pulsed propane torch. The torch is held "on" (large flame) for a specified period of time and then turned "off" (pilot light/small flame) for the same period of time to create a square wave. The frequency is determined by dividing 1 by the sum of the period of time on and off. Initial tests were performed manually, but the frequency range and accuracy were significantly limited. Human and mechanical limitations of the torch made manual operation of the torch at frequencies above 1 Hz impossible. Thus a mechanically controlled oscillating propane torch (shown in Figure 24) was built by a mechanical engineering senior design team (Bertrand et al., 2016). This torch operates at frequencies up to 20 Hz.

Figure 24: Pulsed gas-combustion torch in operation at the Fab Lab.

Tests were run with the pulsed gas-combustion torch to gauge its effectiveness at producing signals at the desired frequency and amplitude. The tests were mostly successful as can be seen in resulting spectrum shown in Figure 25. The signal produced by the pulses of the propane torch are expected to be similar to a square wave, which would have a peak at the fundamental frequency (5 Hz for the test shown) and additional spikes at all odd integer multiples of the fundamental frequency (i.e. 15, 25, 35… Hz). However, there are also strong peaks at the even harmonics, which suggests that it is not well approximated as a square wave. Other tests were run with the oscillating propane torch, however due to the low amplitude of the signals produced these tests did not produce favorable results. In the future it might be beneficial to run more tests utilizing the torch with the infrasonic sensors at closer distances.

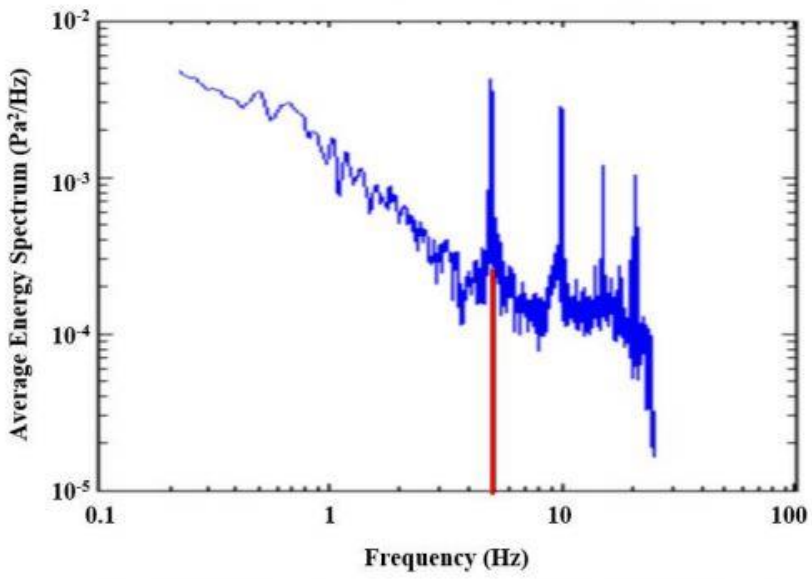

Figure 25: Results from tests at 5 Hz with oscillating propane torch. The red line indicates where the fundamental frequency (5 Hz).

2.3 Data Processing and Analysis

As stated earlier the two main programs used to record from the microphones were Amaseis and Labview Sound and Vibration 2015 (National Instruments). When using Amaseis the signal was extracted and then imported into a MATLAB program that created a power spectrum from the sound pressure time traces and then RMS averages were produced from those spectra. A screenshot of this program along with a sample spectrum file is given in Figure 26 and Figure 27, respectively.

```
Editor - C:\AmaSeis\fullcode_intervals.m
fullcode_intervals.m | DLTdv5.m | rdsacupdate.m
1   %Created by Arnesha Threatt on 07/14/2015
2   %%
3
4   %Program takes .sac files recorded in Amaseis program and creates
5   %a spectrum for each file and an average spectrum for all of the files
6
7   x2=10;    %Number of different runs
8   test=1;    %Test number
9
10  rdsacupdate %Calls rdsac program that uploads .sac file to matlab
11
12  t=t*24*60*60;   %Converts the time collected in the rdsac program from days to seconds
13  d=d/1000; %converts from counts to pascals
14
15  figure
16  plot(t,d);
17  hold on;
18  plot(t,d);
19  hold off
20
21  p=length(t);
22  L=floor(p/x2);
```

Figure 26: Screenshot of MATLAB code used to process power spectra from acoustic pressure time traces.

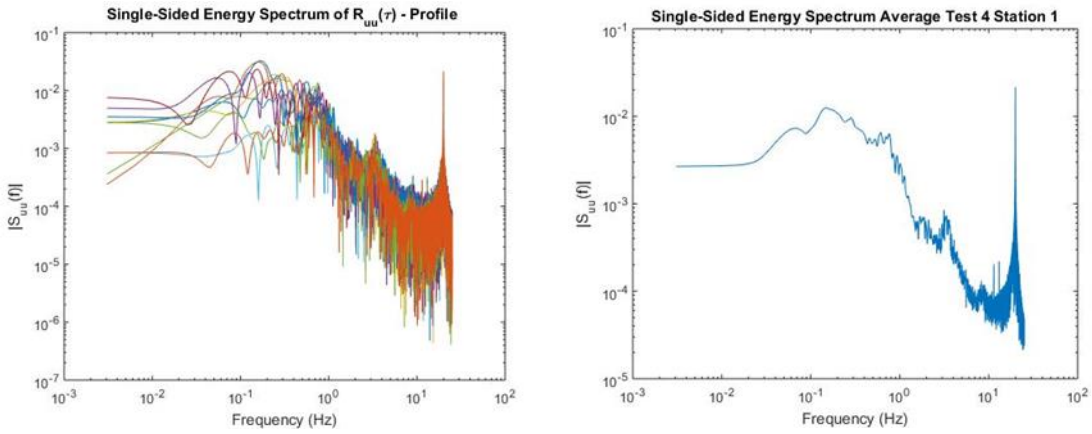

Figure 27: (left) All of the individual spectra used to generate (right) the RMS averaged spectrum.

The LabView Sound and Vibration Package (National Instruments) created a power spectrum from the recorded data as well as the RMS averaged spectrum. The spectra were then exported to files in excel. Eventually a MATLAB code was created that takes the files directly from NI Sound and Vibration format and creates an RMS averaged spectrum. To determine whether events were recorded, a spectrum is created at times when events are not present then these are compared with events to determine the

prominent frequencies emitted above background levels by those events and possibly find a frequency signature for the given event.

Originally the Chaparral Model 24 microphone recorded at a sample rate of 1,000 samples per second and the samples-to-read was set to 1,000 as well. It was also decided that roof system would record and save data in hour increments. Later it was decided to increase the samples-to-read to 5,000 to improve the resolution of the signal at the frequencies below 20 Hz. It was also decided that the data would be saved in 20 minute increments instead of an hour to reduce the file sizes and make them easier to handle and process within MATLAB.

CHAPTER III

3. LABORATORY & FIELD TESTING

3.1 Windscreen transmission lab testing

To gauge the effectiveness of the windscreens (soaker hoses) used with the Chaparral Model 24 infrasonic microphones, controlled experiments were performed. These tests were performed in the anechoic chamber at OSU shown in Figure 28 and Figure 31. This location was chosen because of its relative seclusion and availability, but the anechoic chamber is only anechoic down to roughly 200 Hz. All of the tests performed were below this frequency, thus subject to noise from the environment.

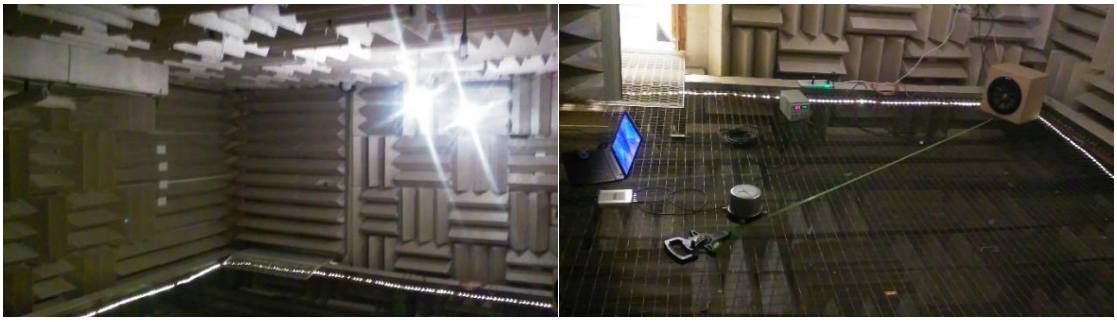

Figure 28: Oklahoma State University anechoic chamber (left) before the experiment was set up and (right) during testing.

In practice it is impossible to remove infrasonic noise all together from the measurements taken, it can only be reduced. To compensate for the background noise in the anechoic chamber, recordings of the ambient noise in the chamber were taken (i.e. when sound source is turned off). There were a total of 6 background measurements taken. The first was taken with no soaker hoses attached to the microphone, before the tests in which the soaker hoses were not utilized. The second was taken with the soaker hoses, before the tests in which the soaker hoses were utilized. The third and fourth measurements were exactly the same as the first and second but taken after all of the other experiments were performed to ensure that no significant change in the background had occurred during testing. All of the tests were performed on the weekend (Saturday) to limit the amount of noise from construction work and students in the building. The fifth and sixth measurements were ran with only the fan on, to know what frequency signature the fan produced and what it looked like with and without the soaker hoses.

An infrasonic sound source had to be used to determine whether the windscreens were effective at suppressing wind noise without attenuating coherent signals. Thus the Kicker subwoofer setup described earlier was used for testing. However, to prove that the windscreens were effective the outdoor environment (wind noise) had to be simulated as well. This was achieved with a Lasko 20-inch box fan placed inside of the anechoic chamber and run on it highest speed during the tests that required “wind noise.” The acoustic signature of these fans were determined by running them at the highest speed without and with the soaker hoses attached to the microphone. These results are shown in Figure 29 and Figure 30, respectively. Both results have three strong peaks with the first peak at ~87 Hz. As shown in Figure 31, the microphone was placed 9 feet from the front

of the subwoofer. The fan, when in operation, was placed 6.5 feet from the microphone and 7 feet from the subwoofer.

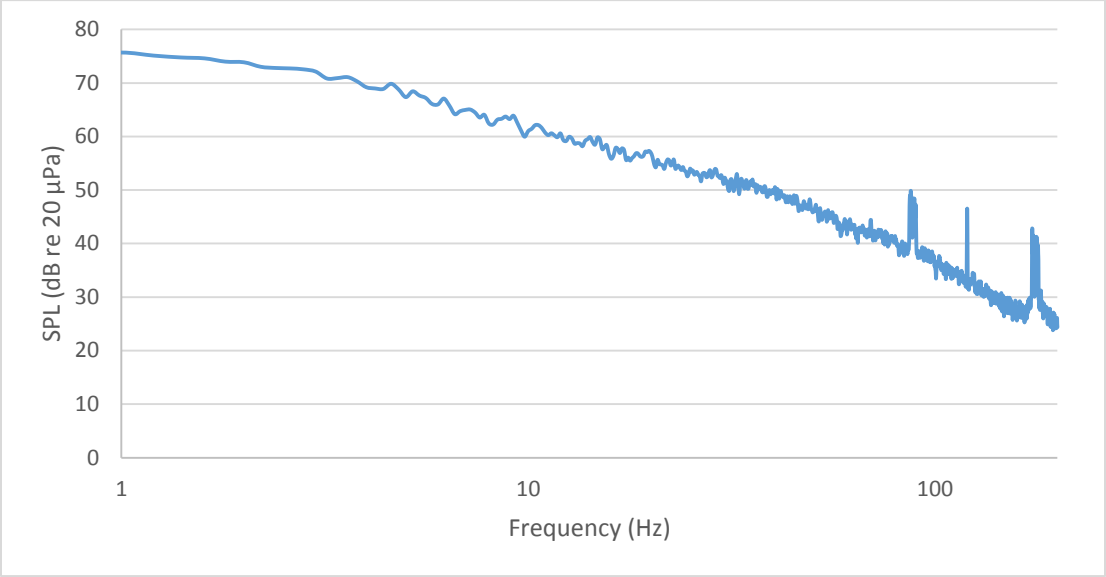

Figure 29: Results from spectral analysis of noise emitted from the box fan with no windscreen (soaker hoses) attached to the Chaparral microphone.

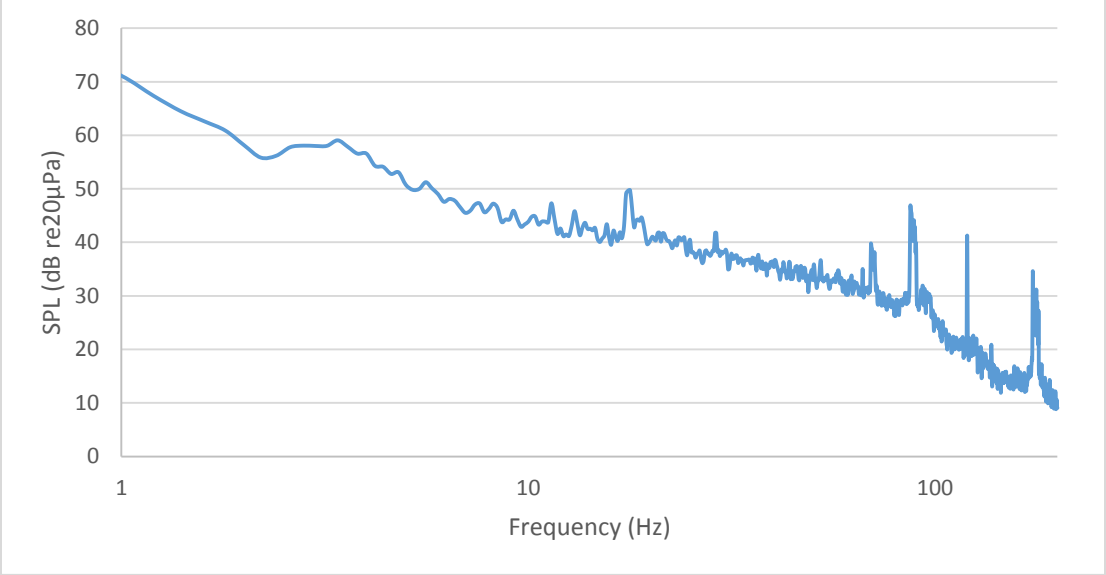

Figure 30: Results from spectral analysis of noise emitted from the box fan with the windscreen (soaker hoses) attached to the Chaparral microphone.

Figure 31: Infrasonic setup inside of anechoic chamber with soaker hoses attached to the Chaparral microphone, subwoofer, and the box fan.

Four different tests were run with this setup. These tests include every possible setup that the microphone could encounter in the field. The signal was emitted for every test but factors used in measuring the signal were changed. The different tests include: (i) Microphone with no soaker hoses attached and the fan turned off, (ii) microphone with no soaker hoses and the fan turned on, (iii) microphone with soaker hoses attached and the fan turned off, and (iv) the microphone with soaker hoses attached and the fan turned on. The tests were run with the infrasonic signal at seven different frequencies; 10, 15, 20, 50, 100, 150, and 200 Hz, all at the same amplitude. We expected the experiments to produce the lowest sound from the times when the soaker hoses were attached to the microphone. We expected the order from highest to lowest to be: 1. Microphone with fan no soaker hoses, 2. Microphone with fan and soaker hoses, 3. Microphone no fan and no soaker hoses, 4. Microphone no fan with soaker hoses. The results of the experiments are shown in Figure 32 to Figure 40.

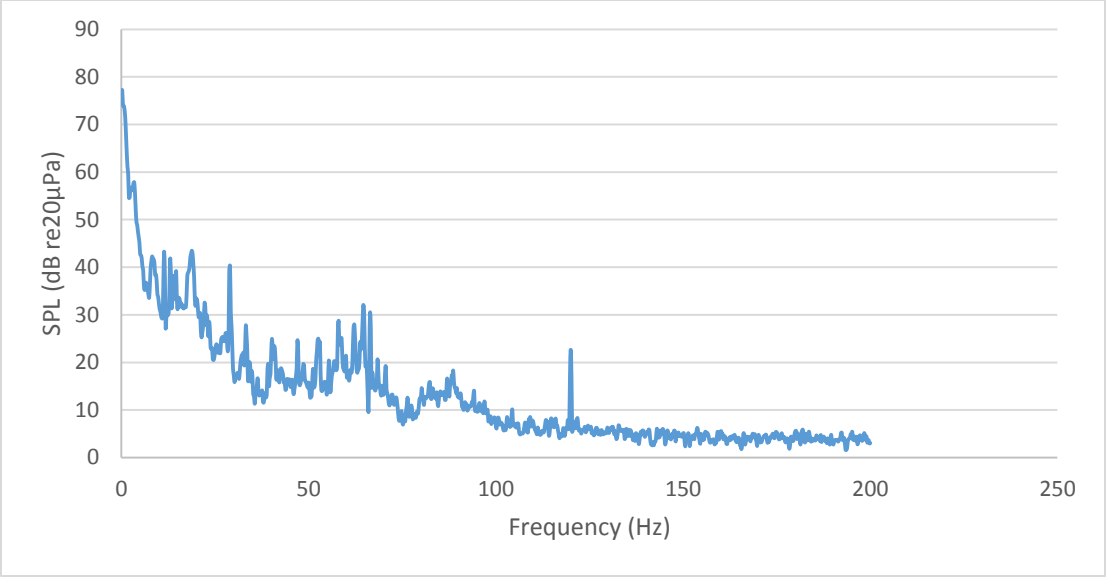

Figure 32: Ambient noise in anechoic chamber measured without windscreen.

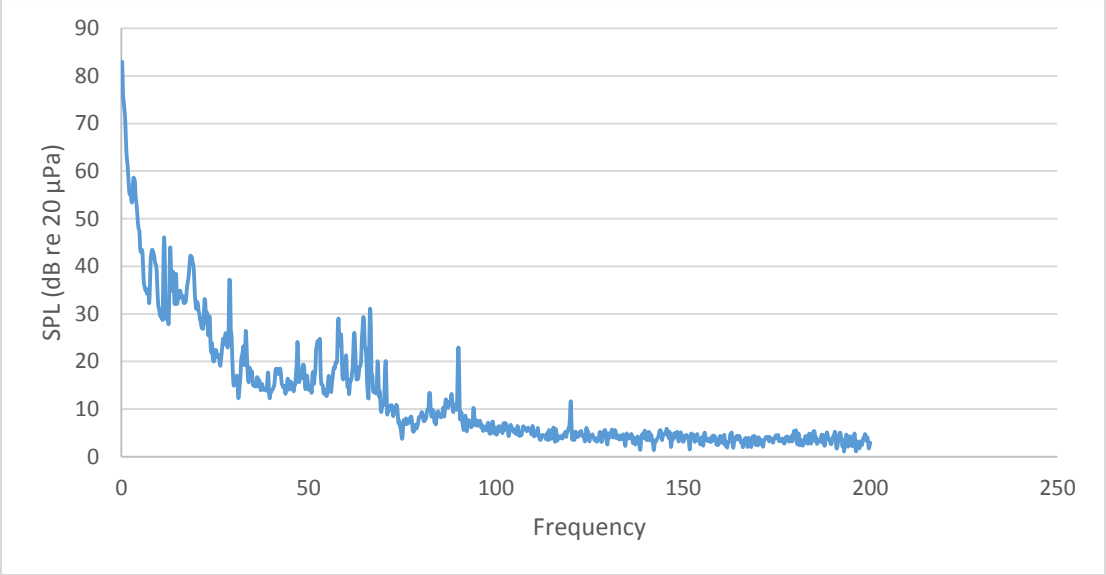

Figure 33: Ambient noise in anechoic chamber measured with windscreen.

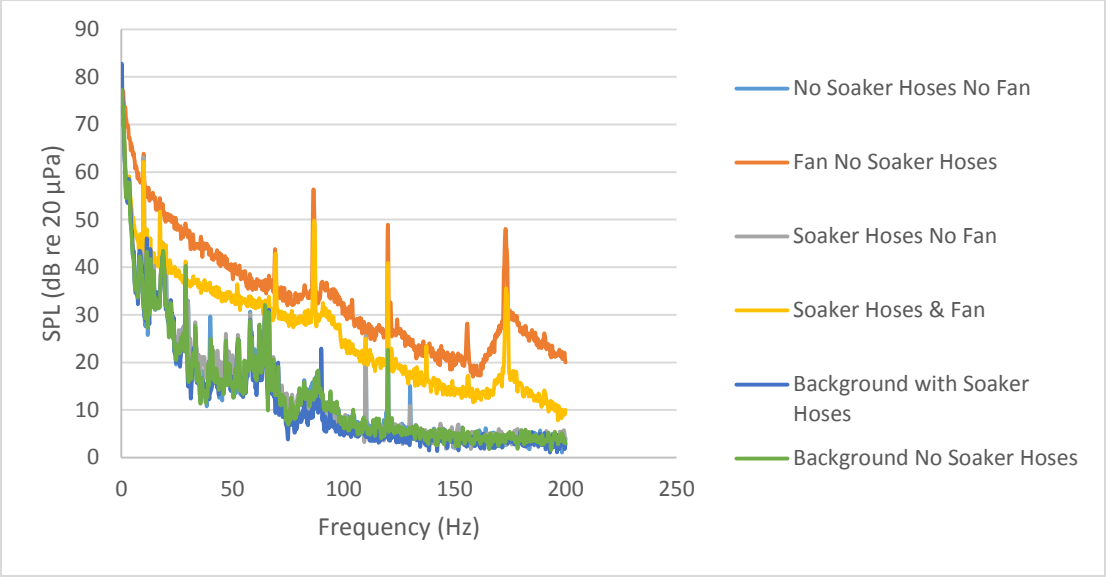

Figure 34: Comparison of various configurations tested with a source frequency of 10 Hz.

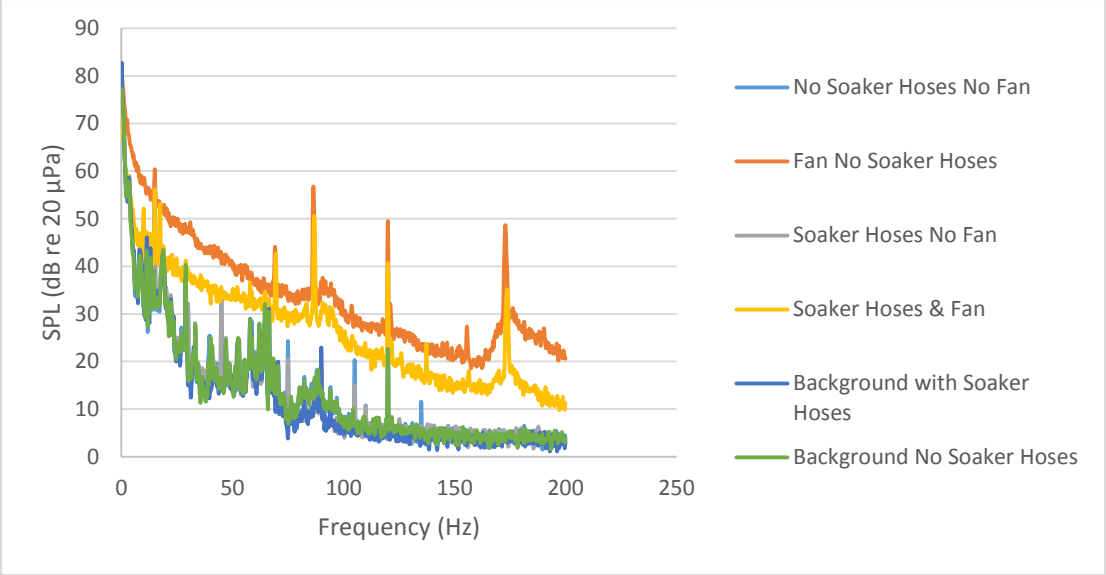

Figure 35: Comparison of various configurations tested with a source frequency of 15 Hz.

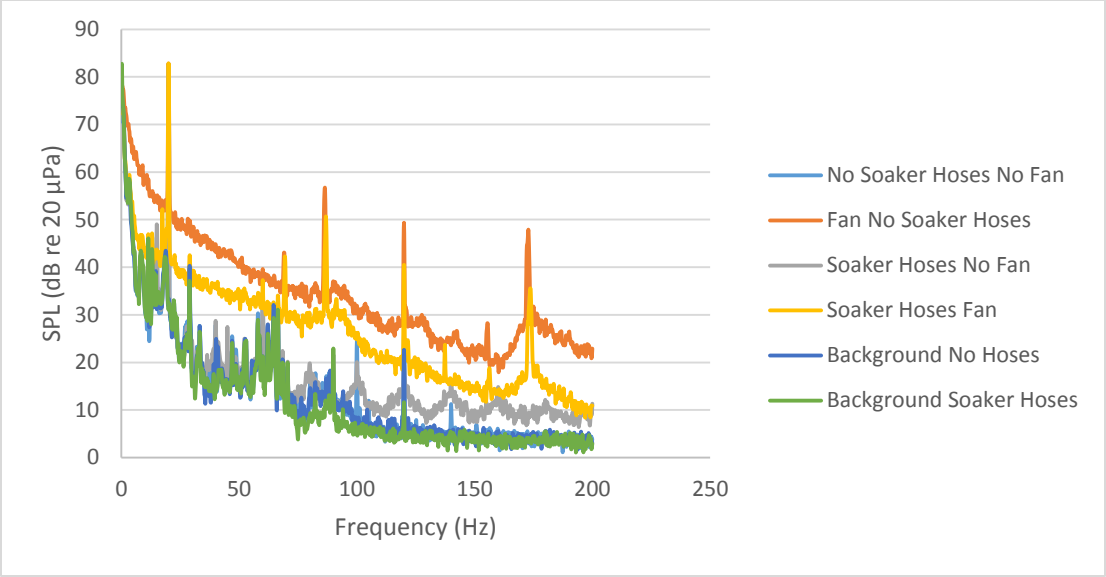

Figure 36: Comparison of various configurations tested with a source frequency of 20 Hz.

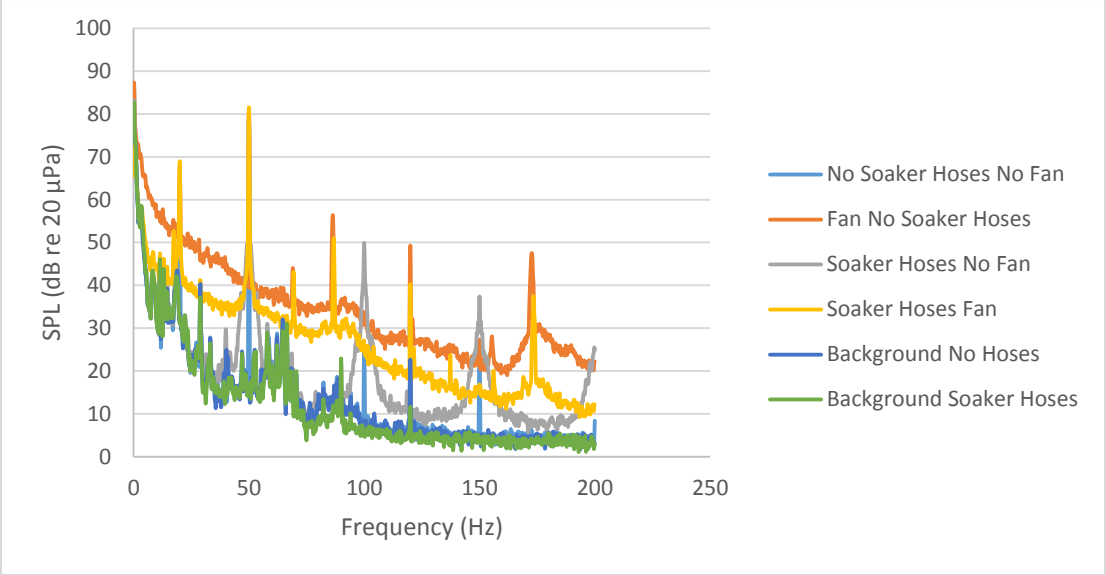

Figure 37: Comparison of various configurations tested with a source frequency of 50 Hz.

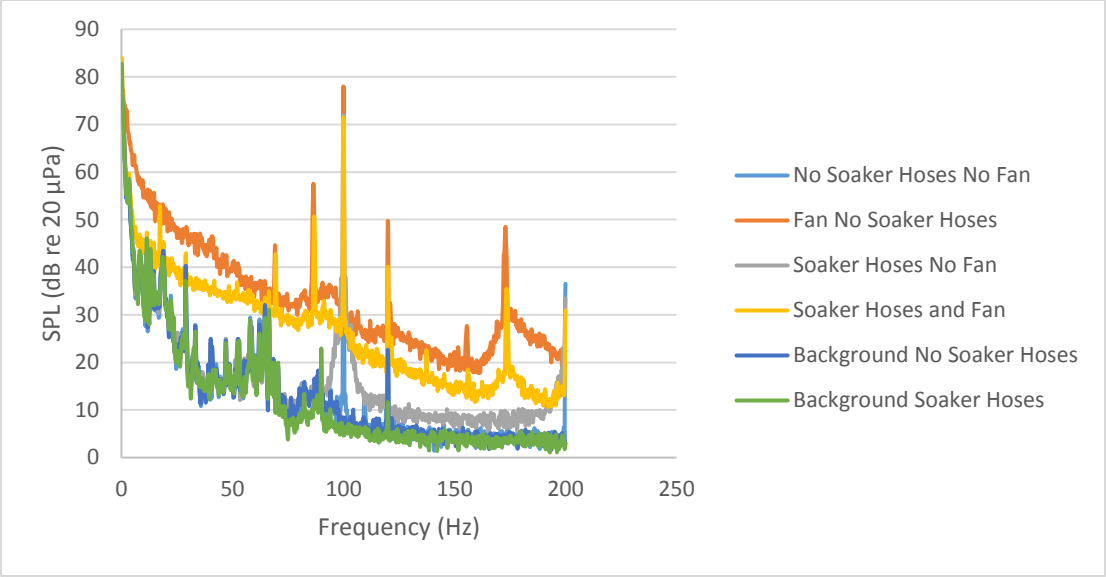

Figure 38: Comparison of various configurations tested with a source frequency of 100 Hz.

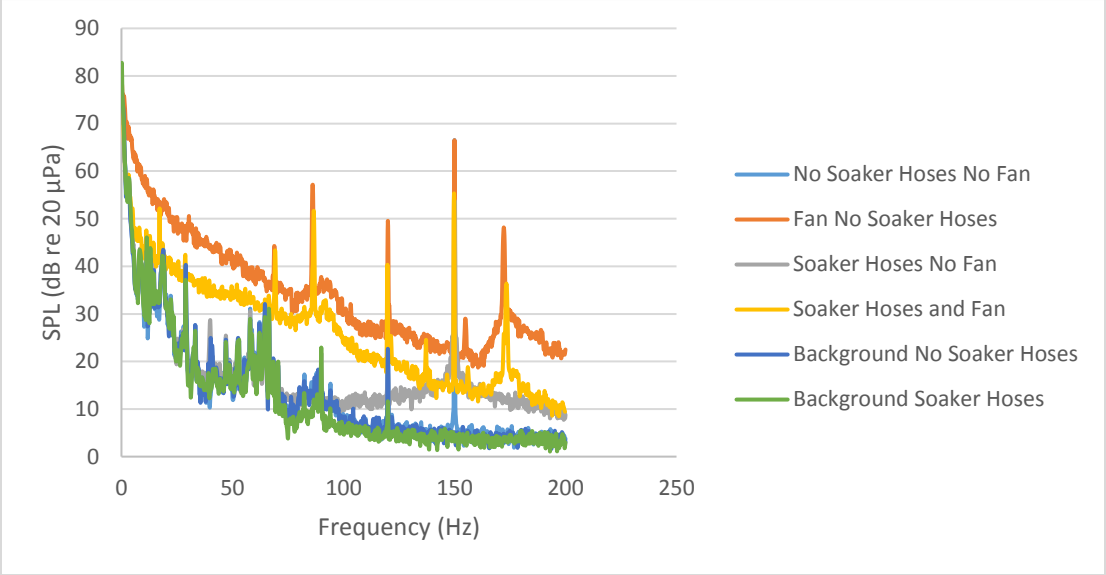

Figure 39: Comparison of various configurations tested with a source frequency of 150 Hz.

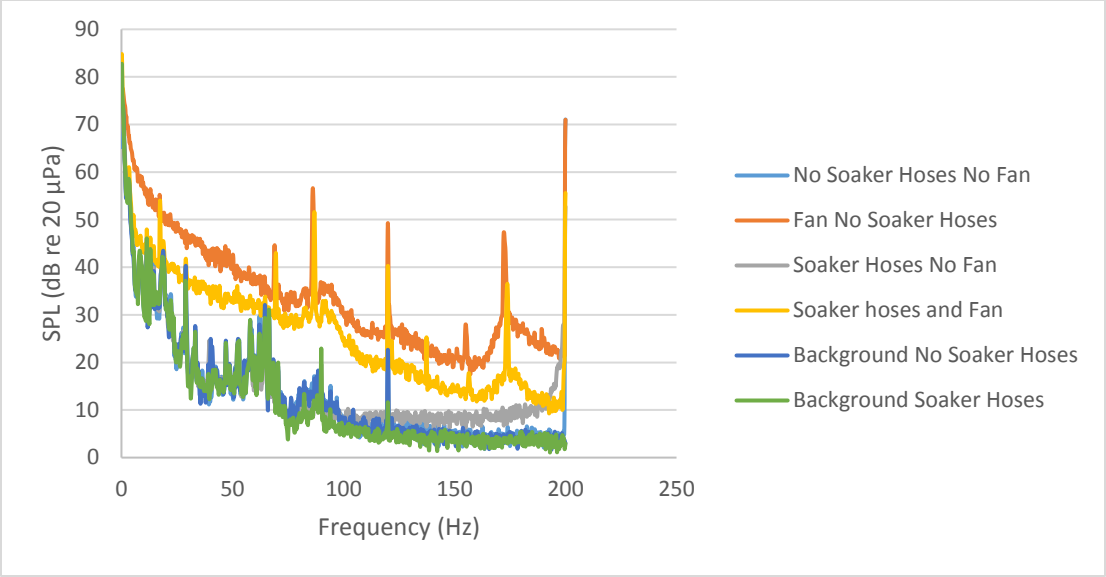

Figure 40: Comparison of various configurations tested with a source frequency of 200 Hz.

As seen in the figures the results are just as expected. The soaker hoses when the fan is on leads to a significant drop in dB level for the noise floor. This leads to the conclusion that the soaker hoses do in fact reduce noise and should be used during all testing. Figure 41 was created to distinguish exactly how much the soaker hoses reduce the noise floor as well as assessing if the source signal is being attenuated. Here the reduction in dB between the signals with the fan running with and without soaker hoses is plotted versus the signal frequency. The blue line only assess the reduction at the source frequency, while the orange line is the average reduction observed over the entire frequency range measured. The graph shows the reduction at the testing frequency increases with frequency, while the average stays fairly consistent at around 7.8 dB reduction.

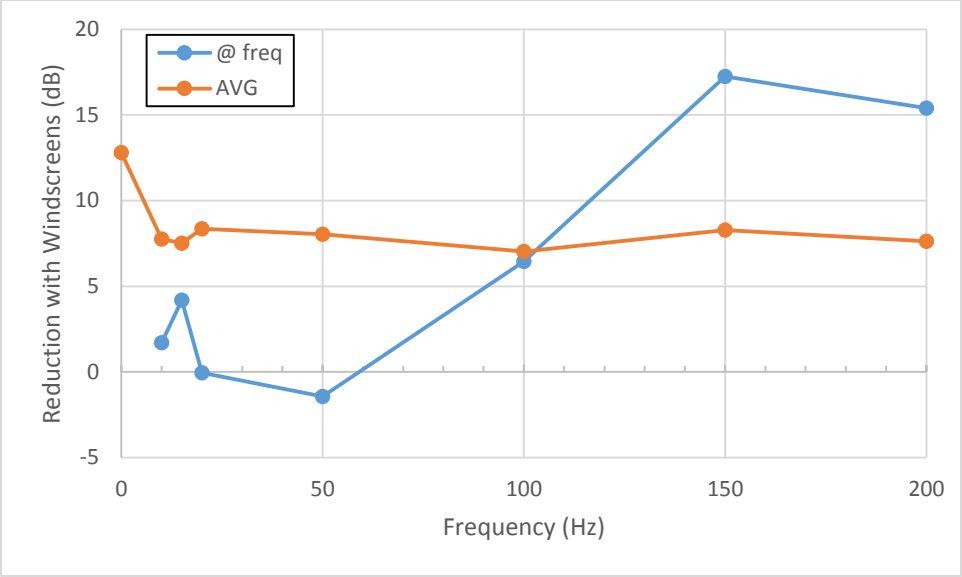

Figure 41: Reduction of amplitude of signal at different source frequencies compared with the average broadband signal reduction.

It is helpful to describe the ideal results to help interpret these results. The perfect wind screen would show the blue line (reduction of desired signal) flat at 0 dB while the orange line (broadband reduction) would be as large as possible. The results of the windscreen used shows that below 50 Hz the reduction with the attenuation of the desired signal is virtually nonexistent. Conversely, the source signals above 100 Hz are attenuated even more than the broadband reduction. This is because the wavelengths are starting to be small compared to the radius of the soaker hose configuration. Consequently, the windscreens will produce excellent results at frequencies below 50 Hz (as desired), but data above ~100 Hz should be used with caution noting that the actual amplitude is likely significantly higher than measured.

3.2 Microphone Comparison

Tests were performed in the anechoic chamber to compare the Chaparral Model 24 microphone, Infiltec Infra20 microphone, and a G.R.A.S half inch pre-polarized pressure microphone (Type 40AD; Serial Number 145169). These tests were designed to determine the sensitivity of the Infra20 microphone and gauge the performance of the new acquired Chaparral microphones. The tests used a similar setup as the one described in the windscreen evaluation. The microphones were all placed at a distance of 9 ft from the source. The G.R.A.S microphone used the same recording and processing tools as the Chaparral Model 24 (Labview Sound & Vibration and NI DAQ 2194) while the Infra20 utilized the Amaseis program. These tests were performed the same day as the windscreen tests, right after they were completed.

The G.R.A.S microphone has a frequency response of 10 to 20,000 Hz, while the Infra20 and Chaparral Model 24 sensors have lower frequency ranges because they are designed specifically for infrasonic measurements. The Infra20 frequency range is 0.1 to 20 Hz and the model 24 from Chaparral has a frequency range of 0.1 to 200 Hz. Due to the limits in overlapping frequency range from these three microphones only two tests (10 and 20 Hz) were successfully performed with all three microphones. Spectra from these tests are provided in Figure 42 (10 Hz) and Figure 43 (20 Hz).

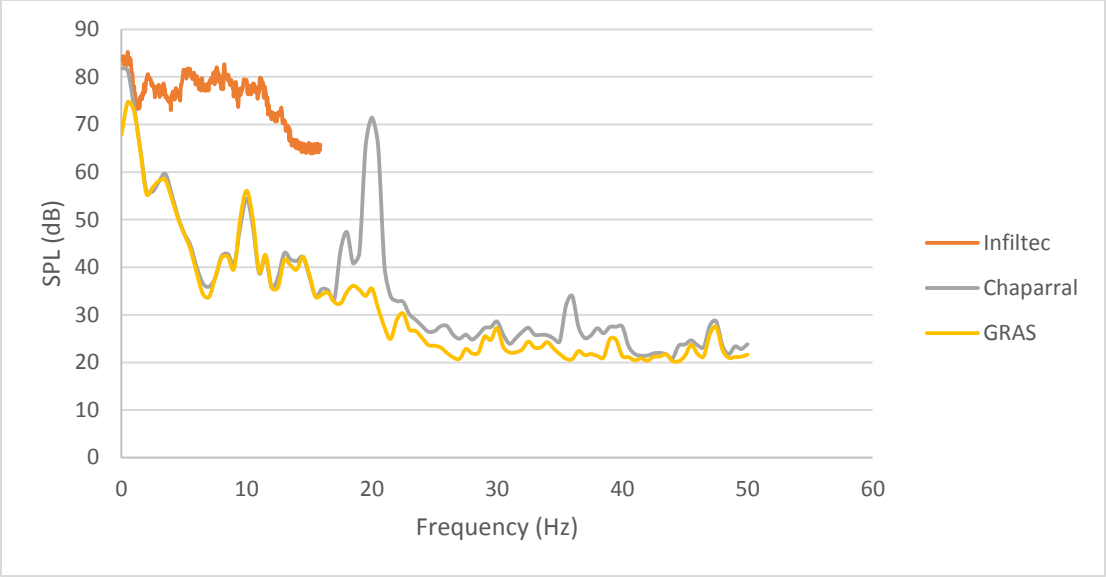

Figure 42: Microphone comparison with a source signal of 10 Hz.

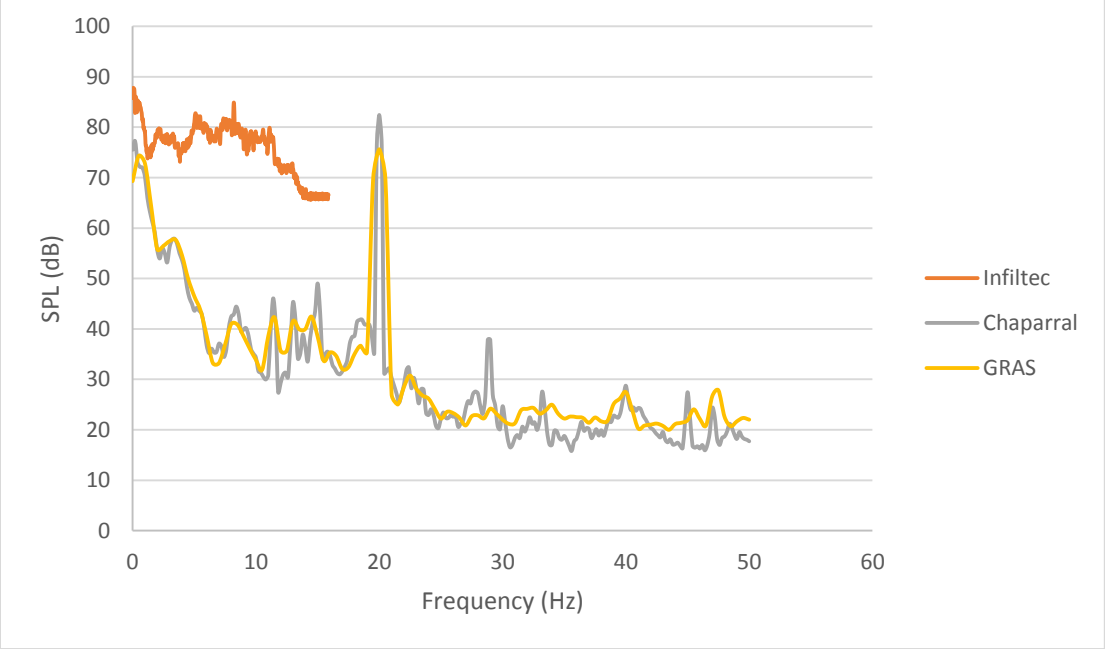

Figure 43: Microphone comparison with a source signal of 20 Hz

These results show that the Infiltec Infra20 microphone has an extremely high noise floor. It appears as if the signals would only really be detected by the Infra20 microphone if the SPL was above ~80 dB. This would explain why during earlier tests, signals were

undetectable beyond roughly a foot. Due to the measurement being taken from nine feet away for these tests the SPL was not loud enough to overcome the noise floor of the Infra20. There does appear to be a spike in all the graphs at 0.5 Hz that produces a SPL of roughly 85 dB.

The Chaparral Model 24 and G.R.A.S microphones produced similar results for both tests. The Chaparral microphone produced a larger peak at 20 Hz and had more clear peaks at higher frequencies than the G.R.A.S sensor. The Chaparral sensor also produced a spike at roughly 20 Hz in the 10 Hz graph that the G.R.A.S sensor does not appear to show at all. This has happened before with tests run with both microphones and will be discussed later on in this document.

CHAPTER IV

4. ATMOSPHERIC MONITORING

4.1 CLOUD-MAP 2016 Field Demonstration

As stated earlier, the National Science Foundation funded CLOUD-MAP project's main goal is to improve weather forecasting via the use of several integrated unmanned aircraft systems (UAS). Part of this project includes utilizing infrasonic technology to collect data from storms. The first CLOUD-MAP field demonstration was performed the week of June 27- July 1 with data collected June 27-30. Only some of the data collected was considered reliable due to errors with the data acquisition. Table 1 describes when reliable data was collected and the conditions during the collection.

Table 1: Time during CLOUD-MAP 2016 Field Demonstration when reliable data was collected.

Date	Time (CDT)	Temp (°F)	Wind Direction	Avg Wind Speed (mph)	Max Wind Speed (mph)
06/27	5:30pm- Midnight	72-91	East	3.2	18.5
06/28	Midnight- 3:00am	70-94	East	4.8	21.0
06/30	7:30- 9:00am	72-92	Southwest	6.3	22.1
06/30	10:30am-1:00pm				

All the data was collected at the OSU Unmanned Aircraft Flight Station, located at 4015 N3460 Rd, Glencoe, OK 74032. The Chaparral Model 24 (serial number: 162642) microphone recorded the signals roughly 50 feet from the runway at a GPS location of 36.1628, -96.8354 (36°09’46.1”N, 96°50’07.4”W). The microphone setup was very similar the roof deployment setup with only small differences. These differences include an upside down kiddie pool to regulate the microphone’s temperature instead of the dome, a laptop (Panasonic CS-19 Toughbook) was used for data acquisition instead of the desktop computer, a 24 gallon Rubbermaid 1172 ActionPacker Lockable Storage Box held all of the electronic equipment, and the soaker hoses used as windscreen were stretched to their full lengths instead of being looped back to the microphone. The sample rate was also different for the demonstration. The microphone utilized a sample rate of 1,000 samples per second and the samples to read option was set at 2,000. Data was recorded in 5 to 10 minute increments as well.

4.1.1 Earthquake Data

Earthquakes have been known to produce infrasonic signals (Bedard, 1998). Due to the times of the reliable data several earthquakes were inadvertently recorded by the infrasonic system. The Incorporated Research Institutions for Seismology (IRIS) IEB (http://ds.iris.edu/ieb) and OU Oklahoma Geological Survey (OGS) (www.ou.edu/content/ogs.html) databases were used to generate a list of earthquakes that occurred during the field demonstration. Table 2 provides a list of the earthquakes recorded during the field demonstration that were over 2.3 magnitude and within 210 km of the microphone.

Table 2: List of recorded earthquakes during CLOUD-MAP 2016 Field Demonstration.

Time		Mag	Distance	Depth	Location		OGS
(UTC)	(CDT)		(km)	(km)	Latitude	Longitude	ID
6/28 2:50 AM	6/27 9:50 PM	3.1	203	5.88	36.50566	-99.05647	24119
6/28 3:25 AM	6/27 10:25 PM	3.7	174	5.34	36.70126	-98.66034	24113
6/28 3:58 AM	6/27 10:58 PM	2.4	203	5.00	36.50724	-99.05363	24120
6/28 5:16 AM	6/28 12:16 AM	2.3	4	6.01	36.12917	-96.81333	24118

The first earthquake recorded was a M3.1 located 203 km (143 miles) from the microphone. The spectrum (Figure 44) before and during the earthquake as well as a background spectrum is shown for each of the earthquakes that occurred. There was a broadband signal above the background 10 minutes before the earthquake, which then becomes discrete tones once the earthquake occurs. In the broadband signal before the earthquake the dominate peaks during the earthquake could still be seen, which suggests that these signals are related. Bedard (1998) postulated about the possibility of using infrasonic signals to detect precursors to earthquakes, which this preliminary data seems to support.

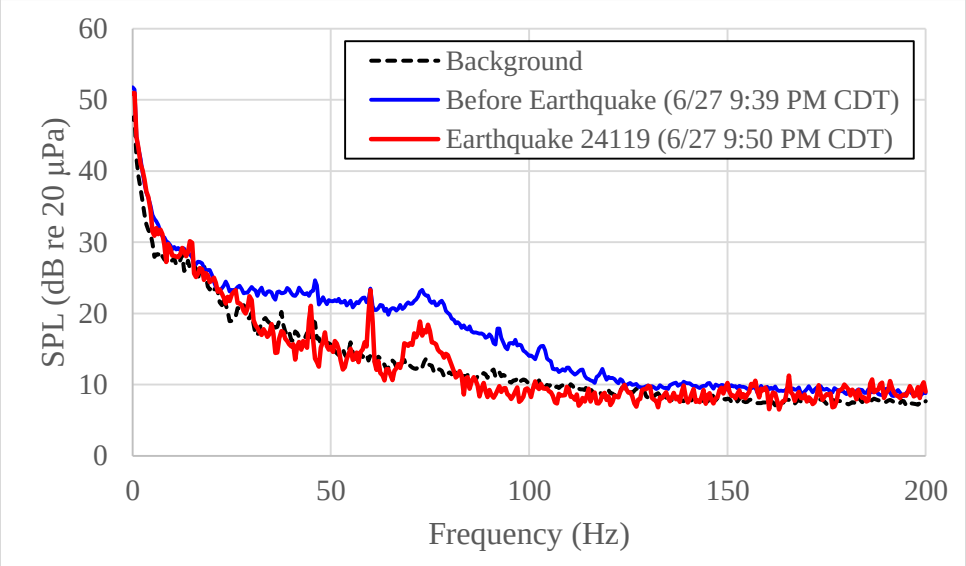

Figure 44: Earthquake on June 27 at 9:50 PM. It was M3.1 and located 203 km from the microphone.

The next earthquake was a 3.7 magnitude that occurred 174 km (108 miles) from the microphone. This was the largest recorded earthquake recorded during the demonstration week, which has a strong spike in the spectrum shown in Figure 45. The third earthquake (Figure 46) recorded was a 2.4 magnitude and occurred at a distance of 203 km (143 miles) from the microphone. It is notable to mention that this earthquake occurred around the same location as the first earthquake. The final earthquake (Figure 47) recorded during the demonstration week was a 2.3 magnitude, occurring 4 km (2.5 miles) from the microphone. Due to the close location of this earthquake the signal during the earthquake has large magnitudes at the lower frequencies. This may be due to the vibrations felt by the microphone during the quake.

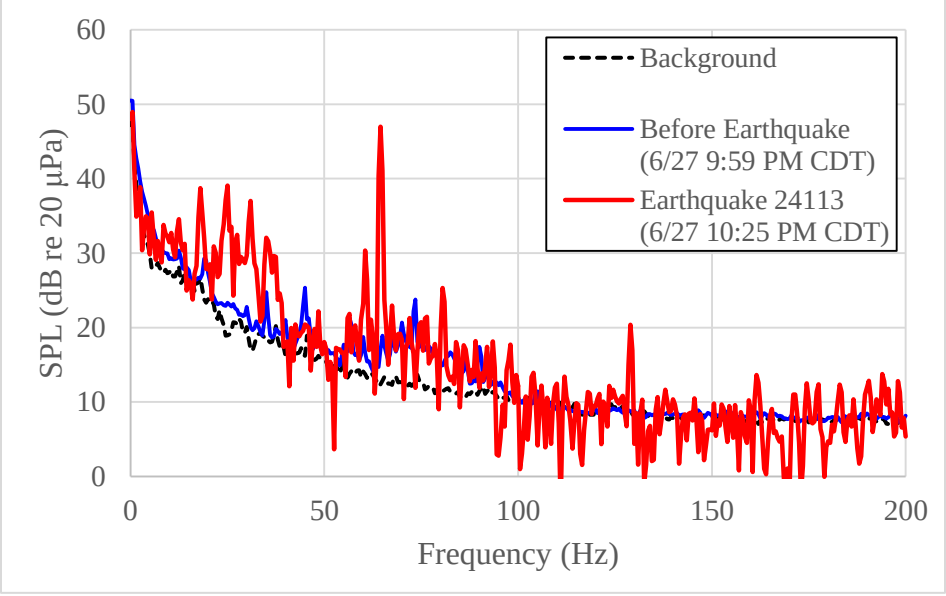

Figure 45: Earthquake on June 27 at 10:25 PM. It was M3.7 and located 174 km from the microphone.

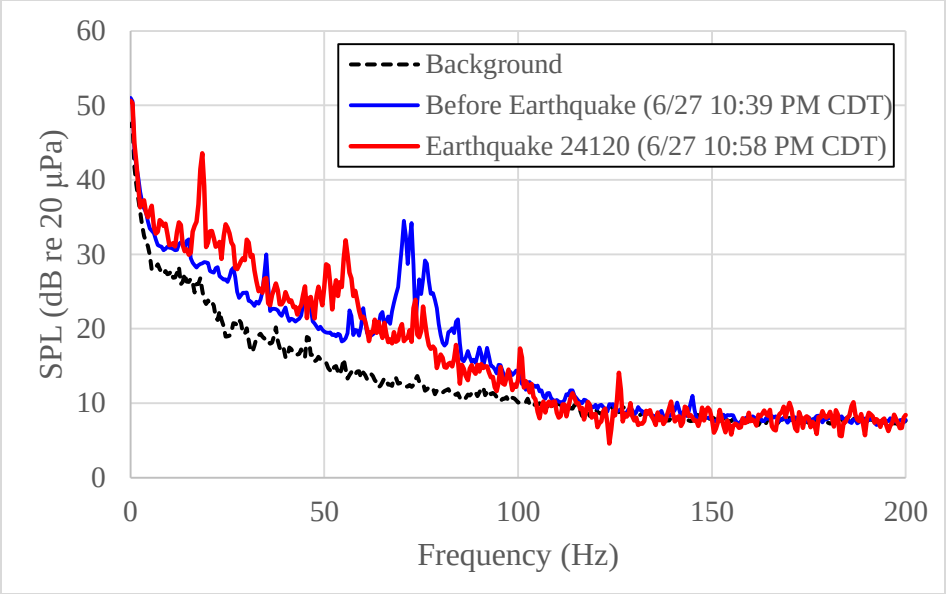

Figure 46: Earthquake on June 27 at 10:58 PM. It was M2.4 and located 203 km from the microphone.

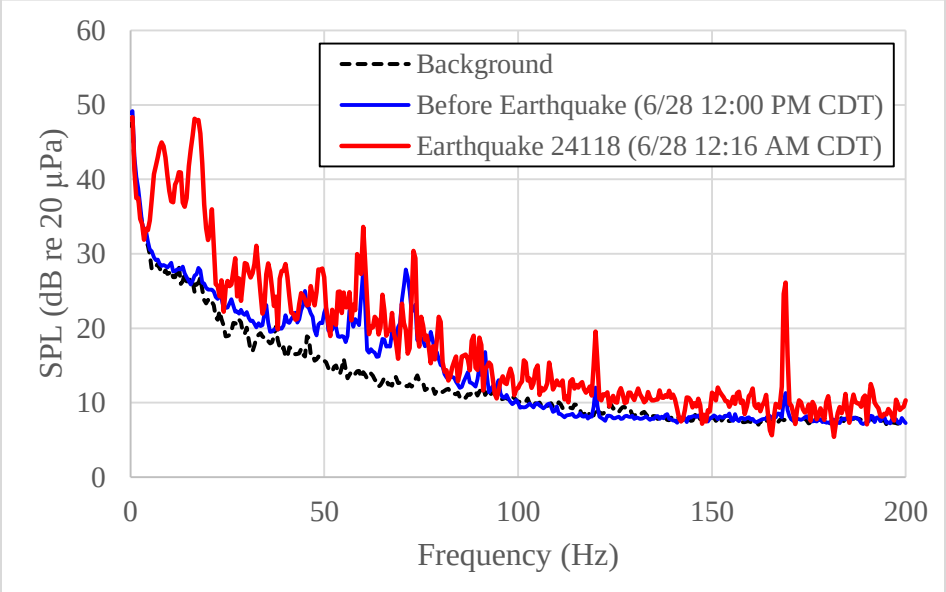

Figure 47: Earthquake on June 28 at 12:16 AM. It was M2.3 and located 4 km from the microphone.

Consistently throughout all of the earthquakes recorded, the signal recorded 10 minutes before the earthquake produced a broadband signal that has distinct peaks

between 50 and 100 Hz. There is consistently a spike around 73.5 Hz. More research is needed to determine if this was a unique feature of this cluster of earthquakes or is a typical trend.

4.2 Background Spectrum

All sound pressure measurements have some level of noise associated with them. Infrasonic measurements tend to have more noise than measurements recorded at higher frequencies. In order to distinguish between the signals emitted by different events and this noise, it is informative to determine the spectrum from regular days. These data are best shown in the frequency domain. The next few sections will show the background spectrum from a typical night, a typical day, and a full day average one hour spectrum.

4.2.1 Typical Night Spectrum

The typical night spectrum was found by taking the data from several different nights and averaging them. The days chosen were September 13, 14, 15, 18, and the 23. These dates were selected because of their relative calmness, implied by the lack of a significant event recorded on these dates (i.e. no storms, small amount of earthquakes, etc).

Data are typically recorded in twenty minute intervals, which means that there are three data sets per hour. The data set from each twenty-minute interval was averaged with the data set from the same time on a different day. The three averaged data sets from the selected hour was then averaged to generate an hourly average. The averages from

midnight to 5:00 AM were then averaged together to create a typical night spectrum. The hours of midnight to 5:00 AM were chosen because majority of the people are asleep by midnight and wake up around 6:00 AM . This means that many of the man-made causes of infrasound throughout the day are not being produced. The typical night spectrum is shown in figure 48.

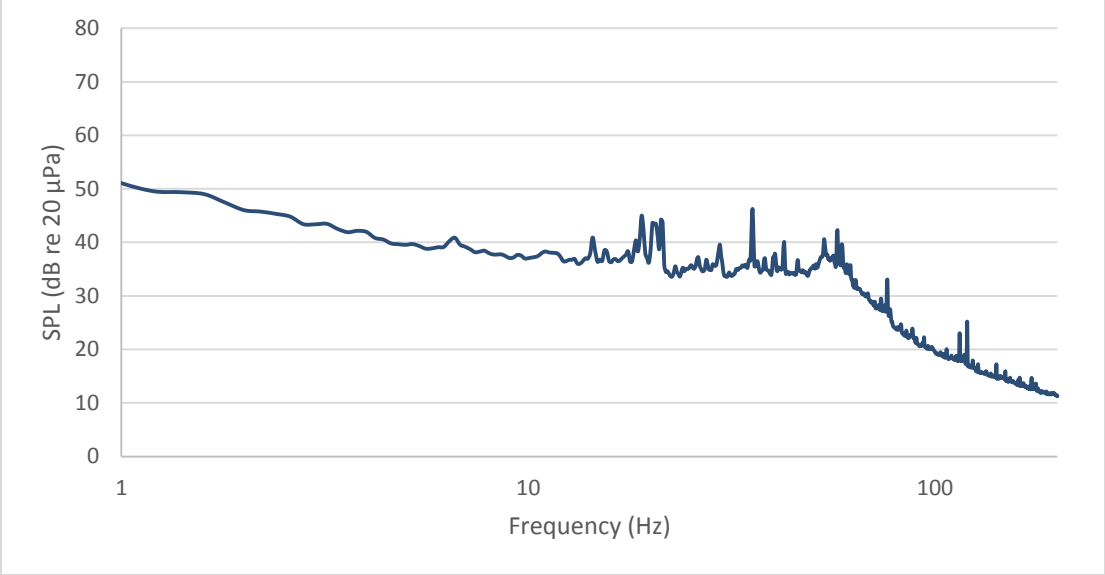

Figure 48: Average spectrum for a "typical" night, which was produced from averaging 5 calm nights between midnight and 5:00 AM.

4.2.2 Typical day Spectrum

The typical day spectrum, shown in Figure 49, was found using the exact same method used for the typical night spectrum though over a different period of time. The hours averaged were 8:00 AM to 6:00 PM, which are the hours of a typical work day.

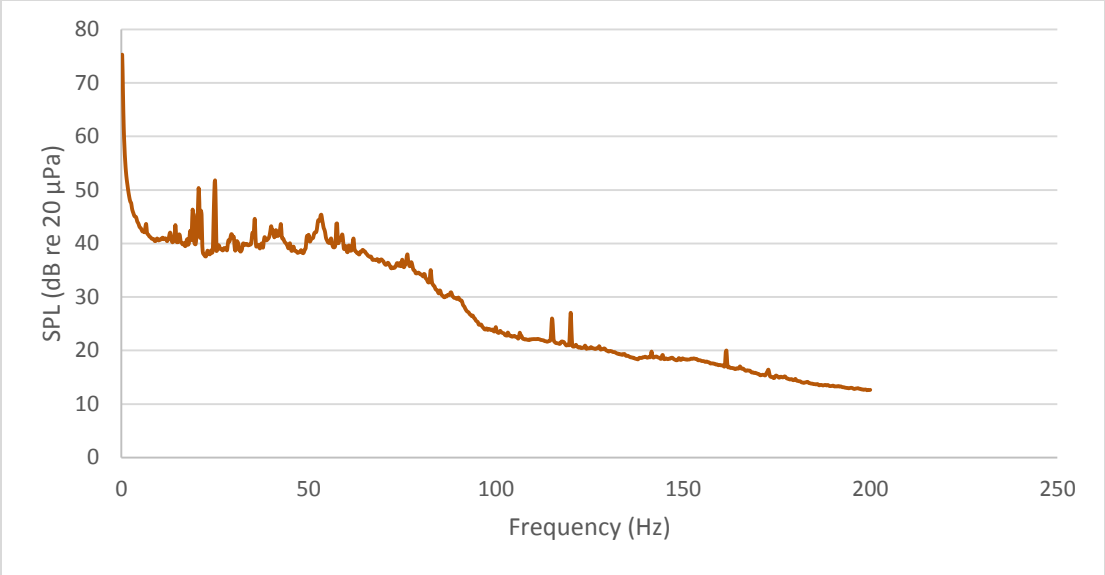

Figure 49: Average spectrum for a "typical" day, which was produced from averaging 5 calm days between 8:00 AM and 6:00 PM.

To compare the difference between the background noise during the day and at night, the two spectra were plotted together in Figure 50. As can be seen the typical day spectrum is louder than the typical night spectrum by about 4.3 dB on average. The largest difference between the two spectra is from the 60 to 100 Hz.

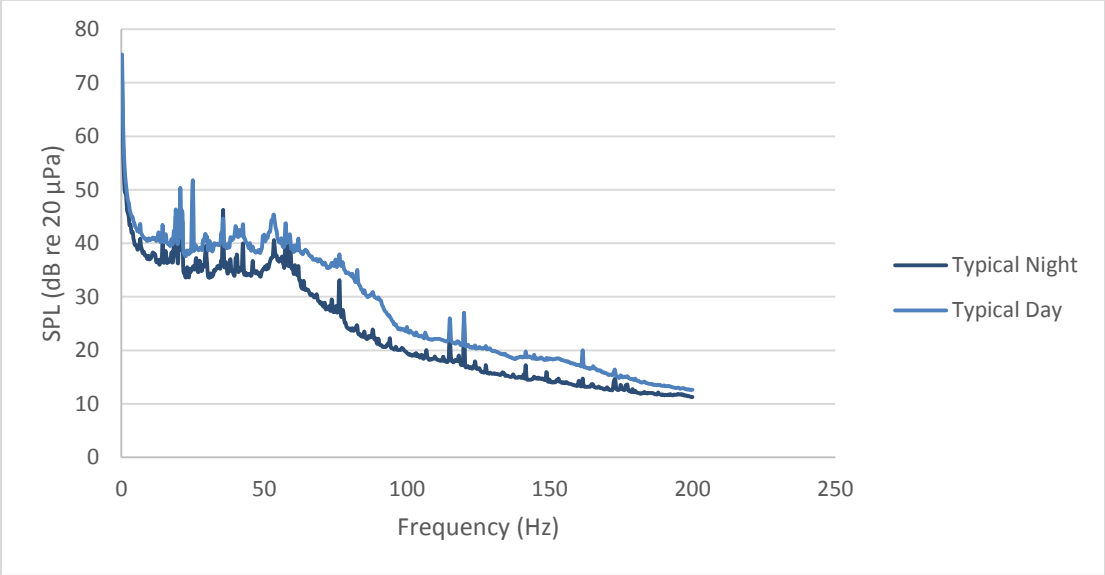

Figure 50: Typical day spectrum compared with the typical night spectrum.

4.2.3 Full day 1-Hour Average Spectrum

As stated earlier, 1-hour average spectra were created for each hour of the day. To minimize the amount of graphs shown, only the 1-hour spectrum from Midnight (Figure 51), 5:00 AM (Figure 52), noon (Figure 53), and 5:00 PM (Figure 54) are shown. The full day 1-hour average spectra from the other times are provided in the appendix. These graphs will be used heavily in the next sections as references to what the frequency content looks like when the event that is being focused on is not present.

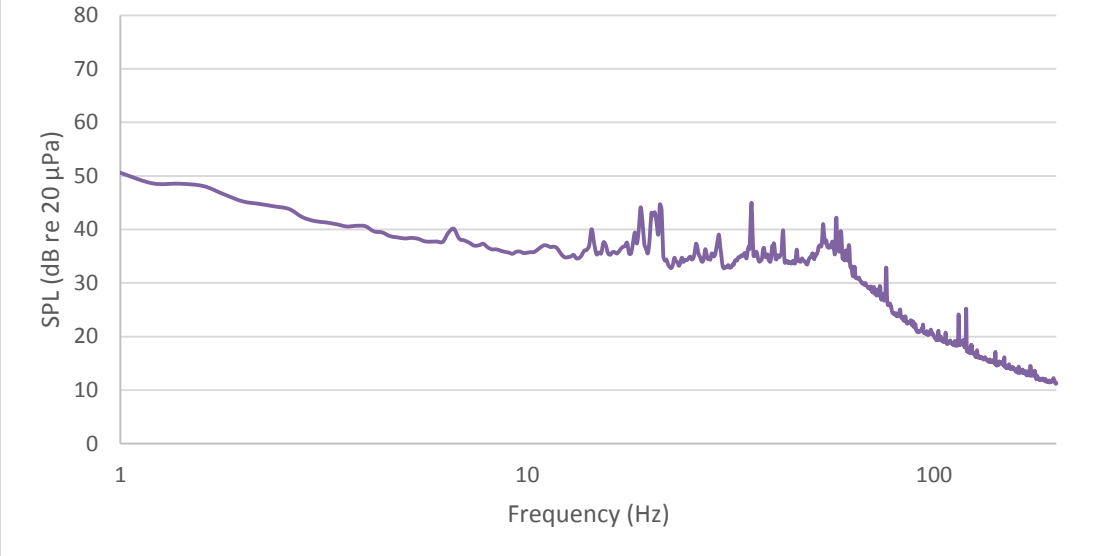

Figure 51: One-hour average spectrum from midnight.

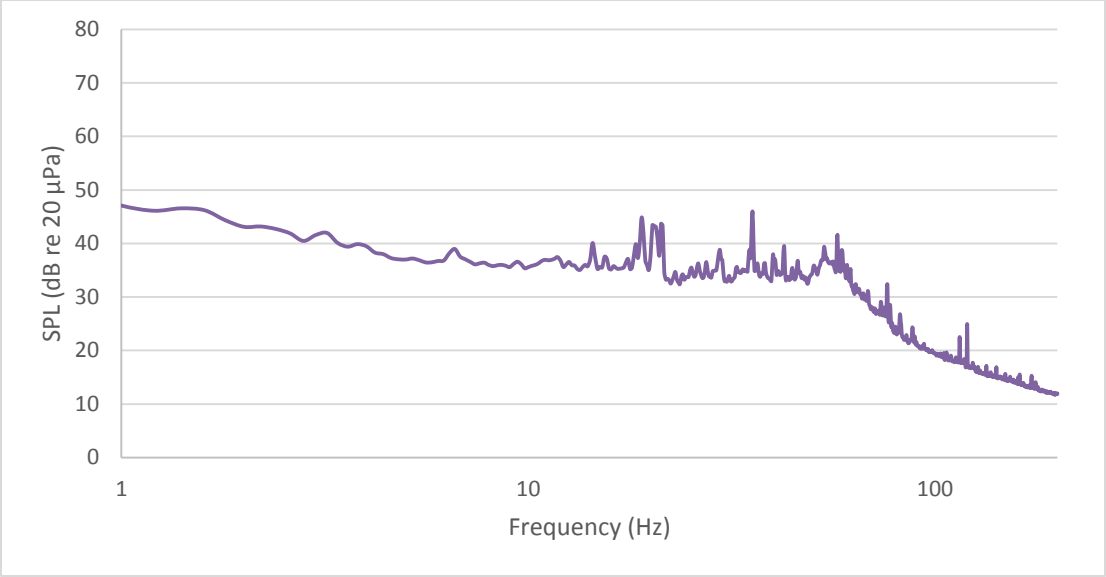

Figure 52: One-hour average spectrum from 5:00 AM.

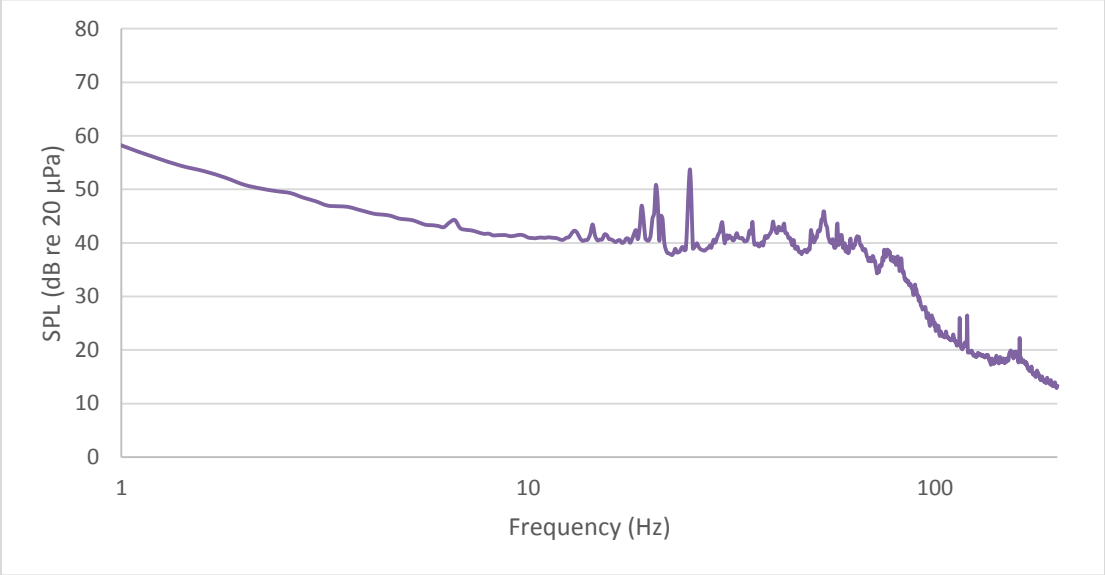

Figure 53: One-hour average spectrum from noon.

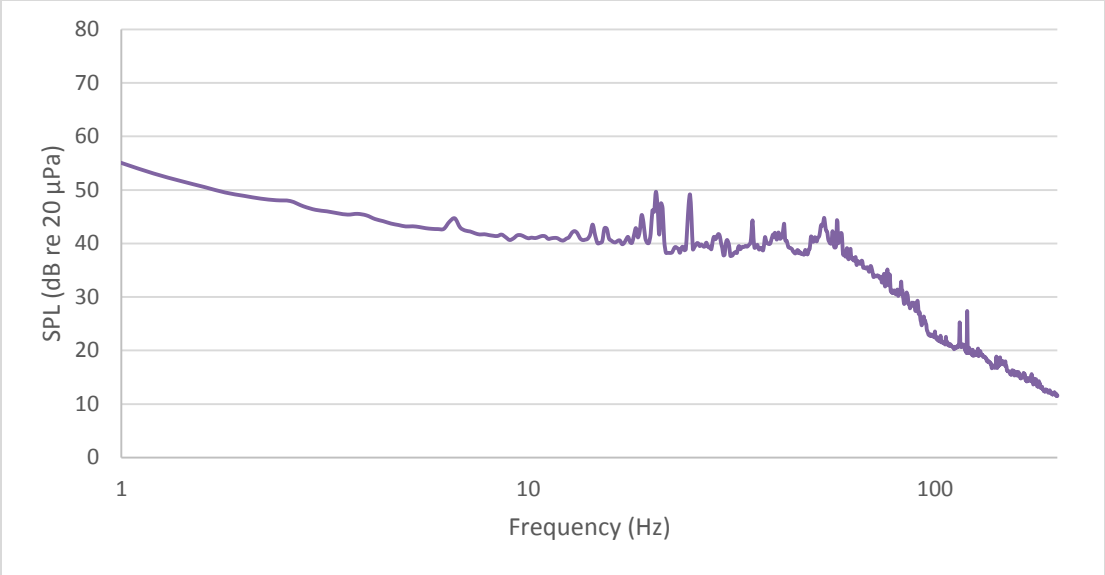

Figure 54: One-hour average spectrum from 5:00 PM

4.3 Events Recorded from Roof System

The roof system has recorded numerous events since its deployment on September 2, 2016. These events include earthquakes, fireworks, planes, and several storms. The events recorded will be described in the next few sections.

4.3.1 Earthquakes

The roof system has recorded 400+ earthquakes since its deployment on September 2, 2016. This includes earthquakes within a radius of roughly 110 miles. Earthquakes with magnitudes above 3.0 and recorded in the month of September were considered in this document. The roof setup was completed the day before Oklahoma's largest recorded earthquake. This M5.7 earthquake occurred at GPS location: 36.42591, -96.92931, approximately 23 miles from the OSU infrasonic system. The time trace of the raw sound pressure is shown Figure 55.

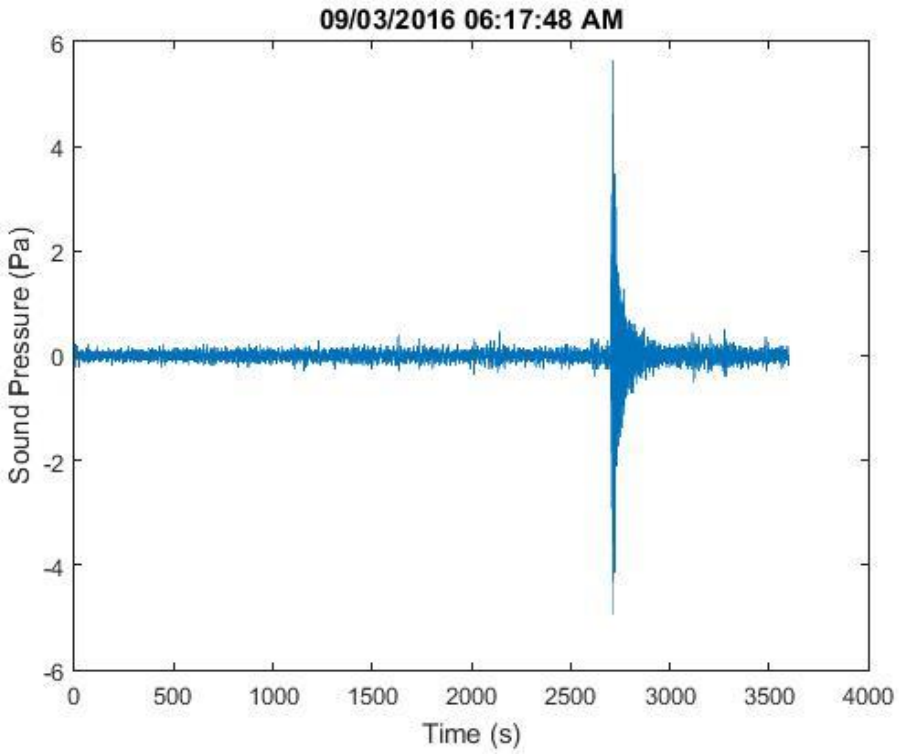

Figure 55: Sound pressure versus time on September 3, 2016 from 6:17 AM to 7:17 AM. The large spike is due to the M5.7 earthquake that hit ~23 miles from the microphone.

As can be seen in the graph at roughly 7:02 AM on September 3, 2016, the earthquake occurs. It is believed that this large spike on the graph is associated more with the shaking of the microphone than the actual sound the earthquake produced. Using the speed of sound in air and the origin location of the microphone the time that the sound should reach the microphone can be found. The equation used to find the time of the earthquake recording is: $time\ shift = c/distance$, where c is the speed of sound in air (343.2 m/s, 1,126 ft/s, or 768 mph). The time the sound from this earthquake reached the microphone was around 7:04 AM. The sound pressure time trace and sound pressure spectrum are shown for both 7:02 AM and 7:04 AM in Figure 56 and Figure 57, respectively.

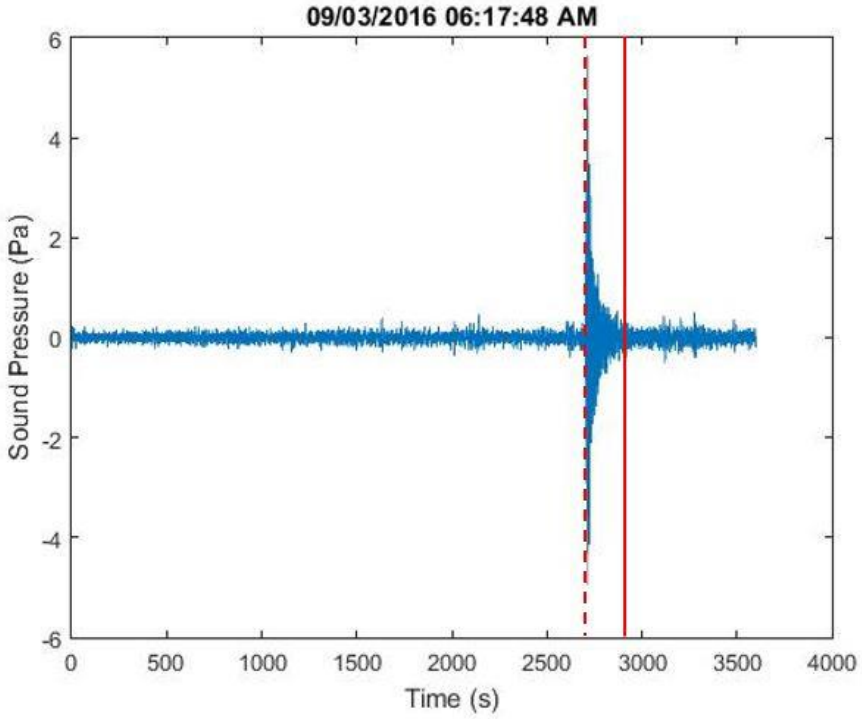

Figure 56: Time trace of the sound pressure on September 3, 2016 from 6:17 AM to 7:17 AM. The dotted line corresponds to the M5.6 earthquake initial shaking while the solid line notes the time when the acoustic waves from the earthquake should reach the microphone.

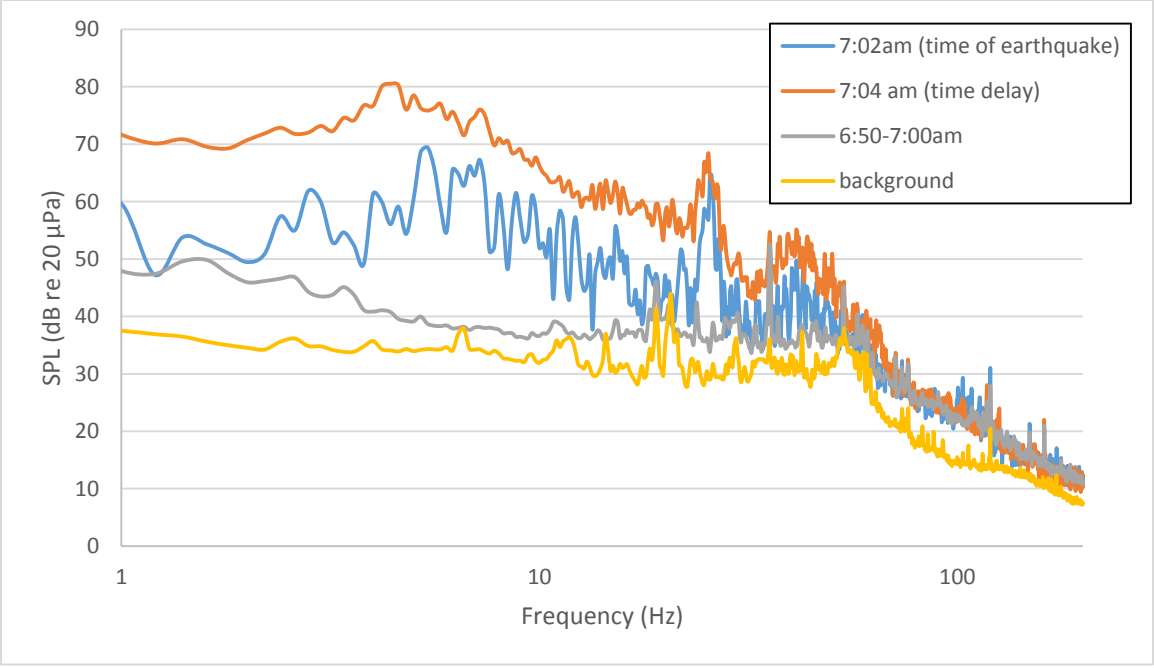

Figure 57: Spectrum from the M5.6 earthquake on September 3, 2016 at 7:02 AM.

Figure 57 shows the spectrum from the origin time, the time the sound reaches the microphone, the 10 minute average before the earthquake, and the background spectrum. The time delay spectrum has a larger SPL than the origin time of the earthquake, but has peaks in the same places (5, 25, and 44 Hz). This indicates that the sound does reach the microphone later and that the sound from the earthquake produced a louder signal than the shaking caused by the quake. This affected the way the rest of the earthquakes were processed. Several other earthquakes were recorded during this month and provided interesting frequency content. A table of the earthquakes processed is shown in Table 3 with the earthquakes that are presented in the current work highlighted in red.

Table 3: Table of processed spectrum from earthquakes.

Date	Time (CDT)	Mag	Latitude	Longitude	Distance (mi)	New Time (CDT)	IRIS ID
9/27	1:10:00 AM	3	36.51	-97.25	27.54	1:12 AM	5194530
9/26	6:30:52 PM	3.7	36.79	-98.26	79.68	6:37 PM	5194490
9/26	10:47:03 PM	3.2	36.09	-97.44	20.27	10:49 PM	5194453
9/24	5:41:30 PM	3.6	35.98	-97.2	12.54	5:42 PM	5194320
9/22	1:42:18 AM	3.2	36.43	-96.92	22.29	1:44 AM	5194042
9/21	1:18:48 AM	3.4	35.87	-97.24	20.27	1:20 AM	5193931
9/20	1:40:07 PM	3.1	36.93	-97.91	71.65	1:46 PM	5193863
9/20	12:59:11 AM	3.9	36.92	-97.89	70.4	1:04 AM	5193804
9/18	1:30:34 PM	3.1	36.28	-97.52	26.46	1:32 PM	5193678
9/17	1:08:08 AM	3.2	36.86	-98.34	86.08	1:15 AM	5193546
9/16	1:01:28 PM	3	36.78	-98.56	93.6	1:08 PM	5193688
9/14	12:13:45 PM	3.7	36.45	-98.76	96.17	12:21 PM	5193263
9/13	12:45:18 PM	3.3	36.78	-97.82	60.6	12:50 PM	5193140
9/13	10:09:14 AM	3	36.78	-97.82	60.6	10:14 AM	5193111
9/13	7:16:25 AM	3.1	35.02	-97.88	89.02	7:23 AM	5193146
9/12	9:15:21 PM	3.4	36.25	-98.42	75.21	9:21 PM	5193059
9/12	9:05:48 PM	3.6	36.24	-98.43	75.7	9:11 PM	5193058
9/10	11:57:16 PM	3.1	36.42	-96.91	21.9	11:59 PM	5192870
9/9	5:51:28 PM	3.1	36.09	-96.74	19.37	5:53 PM	5192788
9/8	9:06:29 PM	5.3	35.52	-97.38	45.55	9:10 PM	5192725

9/8	7:21:33 PM	3	36.38	-97.32	21.53	7:23 PM	5192722
9/8	4:34:43 PM	3	36.17	-97.06	2.74	4:34 PM	5192707
9/8	4:29:29 PM	3.6	36.28	-97.52	26.46	4:31 PM	5192706
9/6	9:26:50 PM	3.5	36.43	-96.9	22.77	9:28 PM	5192519
9/6	1:33:49 PM	3.5	36.94	-97.91	72.17	1:39 PM	5192485
9/6	12:49:45 PM	3.7	36.94	-97.93	72.89	12:55 PM	5192490
9/6	12:48:34 PM	3.9	36.94	-97.91	72.17	12:54 PM	5192482
9/4	3:03:06 PM	3.2	36.05	-96.78	17.86	3:05 PM	5192319
9/3	11:20:28 PM	3.5	36.32	-96.98	14	11:21 PM	5192277
9/3	10:55:46 PM	3.2	36.04	-96.79	17.58	10:57 PM	5192275
9/3	10:15:56 PM	3.1	36.41	-96.92	21.04	10:18 PM	5192273
9/3	10:55:46 PM	3.2	36.04	-96.79	17.58	10:57 PM	5192275
9/3	10:31:40 AM	3.2	36.42	-96.9	22.15	10:33 AM	5192235
9/3	10:25:00 AM	3.1	36.41	-96.9	21.54	10:27 AM	5192236
9/3	9:56:31 AM	2.6	36.42	-96.87	22.97	9:58 AM	5192248
9/3	9:47:04 AM	3.2	36.42	-96.88	22.69	9:49 AM	5192234
9/3	7:58:39 AM	3.6	36.39	-96.97	18.7	8:00 AM	5192226
9/3	7:57:36 AM	2.9	36.43	-96.89	23.02	7:59 AM	5192227
9/3	7:16:22 AM	3.4	36.41	-96.86	22.68	7:18 AM	5192230
9/3	7:02:44 AM	5.6	36.43	-96.93	22.07	7:04 AM	5192223

Figure 58 to Figure 62 shows example spectra from a sampling of earthquakes to give a sense of typical earthquake spectrum. The first earthquake shown occurred on September 3 at 7:57 AM and had a magnitude of 2.9 (telatively close to the location of the 5.6 magnitude earthquake that occurred at 7:02 AM).

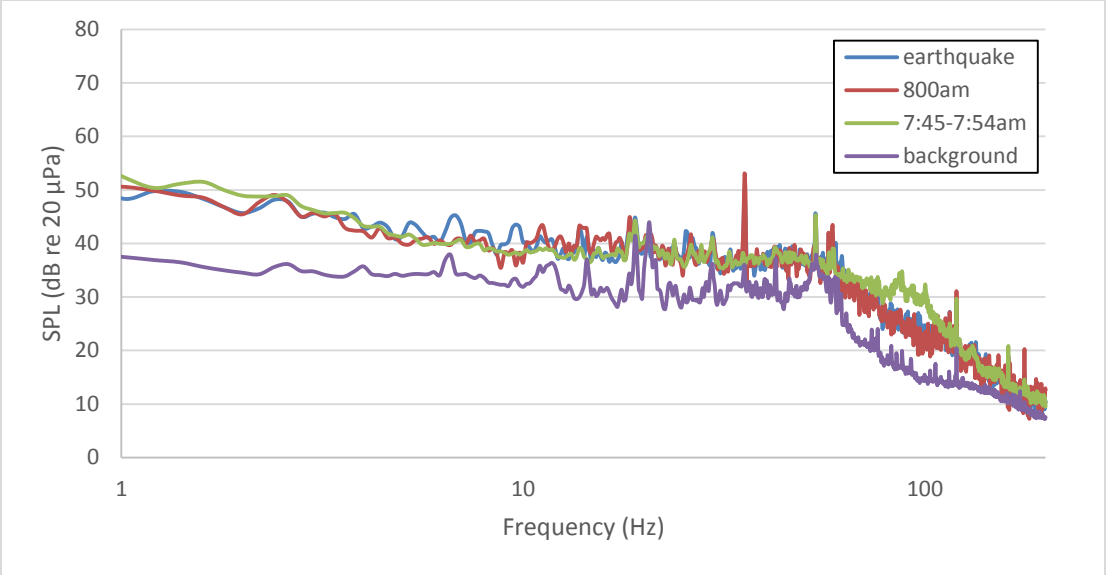

Figure 58: 7:57 am, Sept 3, Mag 2.9. GPS location: 36.43, -96.89 (approx.. 18.7 miles from mic)

The 10-minute average spectrum from before the earthquake demonstrates similar behavior (at a higher frequency) to that of the earthquakes recorded during the CLOUD-MAP demonstration week. Throughout all of the earthquakes shown there are peaks between 50 to 100 Hz. It usually happens within the 10-minute average spectrum, but as the following graphs illustrate these spikes do occur at the origin and destination time.

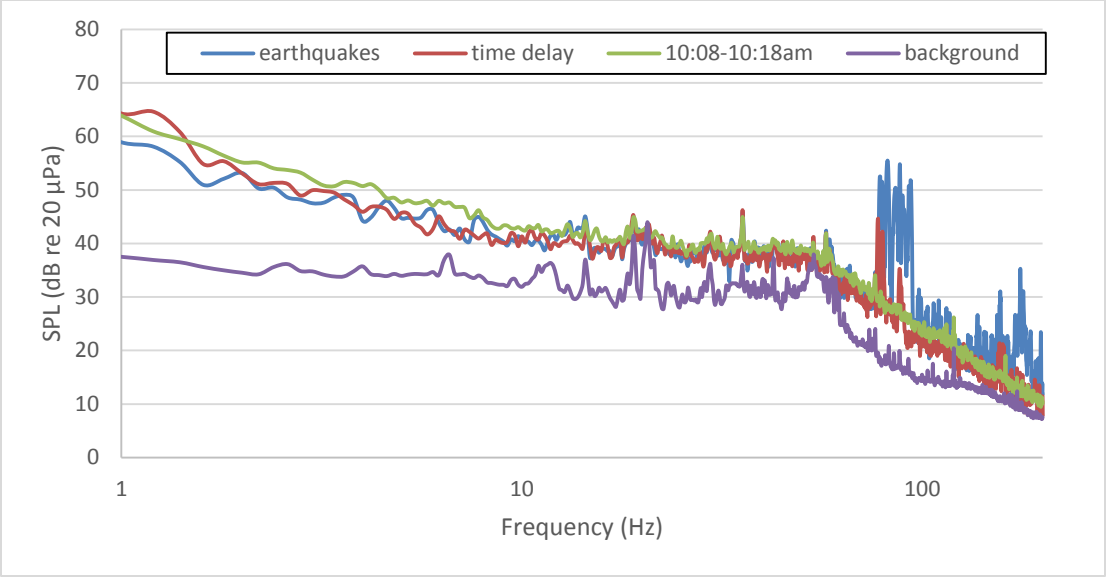

Figure 59: 10:25 am, Sept 3, Mag 3.1, GPS location: 36.41, -96.9 (approx. 22 miles from mic)

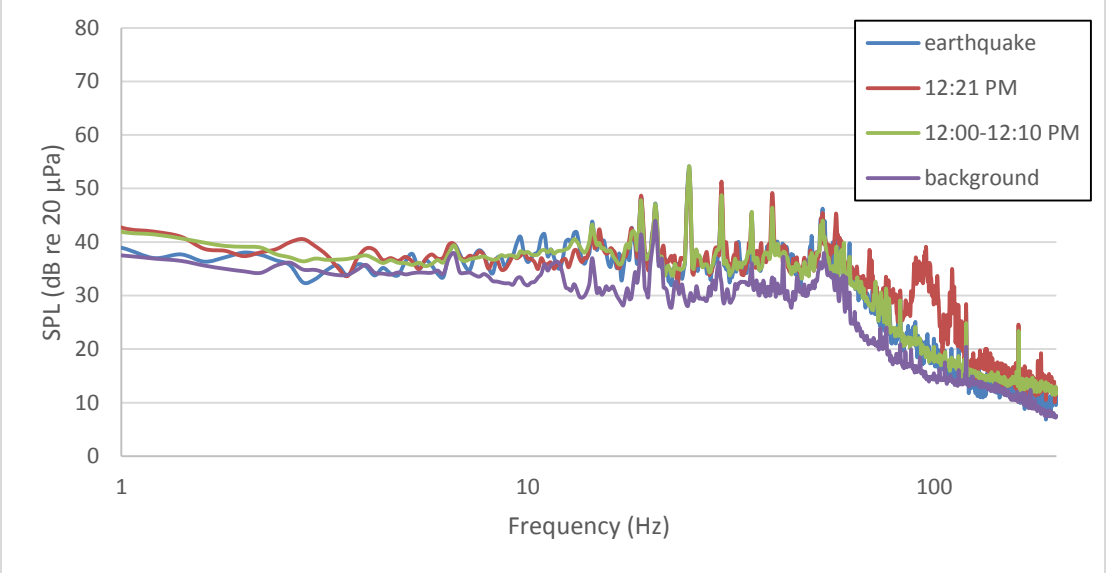

Figure 60: 12:13 pm, Sept 14, Mag 3.7, GPS location: 36.45, -98.76 (approx. 96 miles from mic)

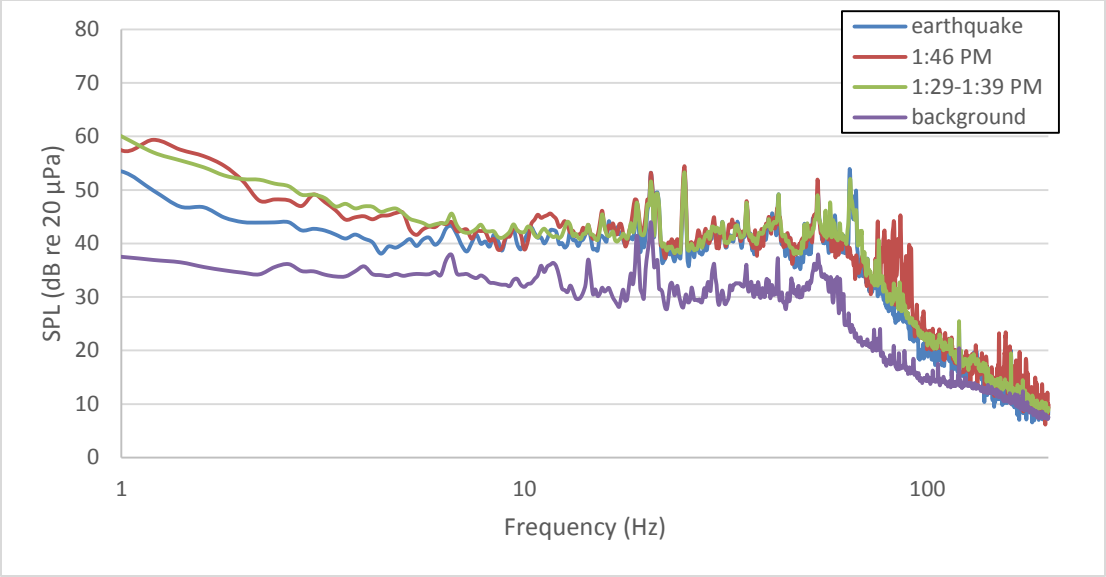

Figure 61: 1:40 pm, Sep 20, Mag. 3.1, GPS location: 36.93, -97.91 (approx. 72 miles from mic).

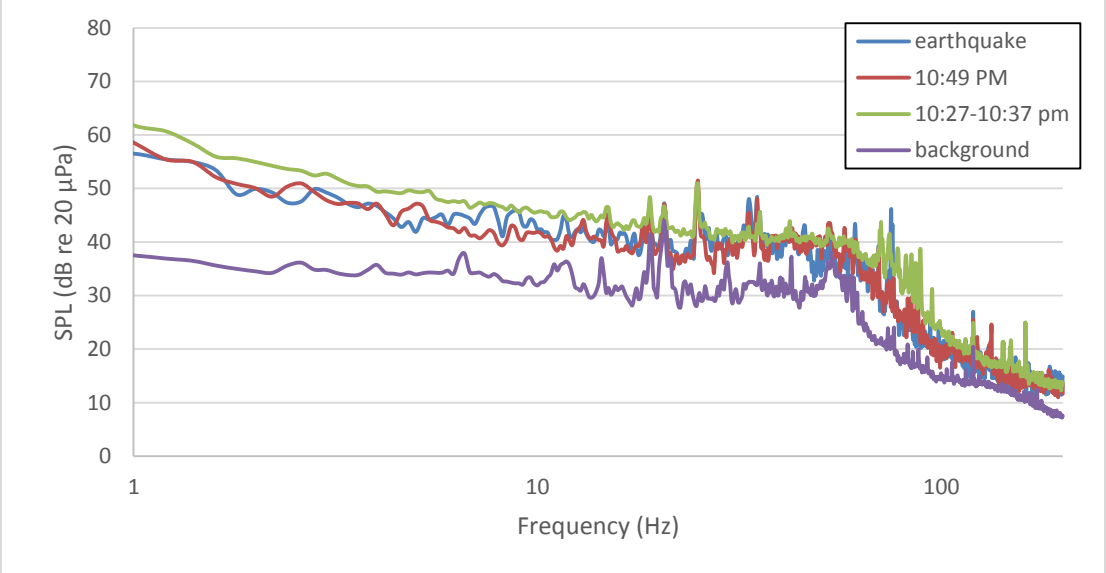

Figure 62: 10:47 am, Sept 26, Mag 3.2, GPS Location: 36.09, -97.44 (approx 20 miles from mic)

The spikes shown in these spectrum consistently appear in roughly half of the data that was processed. The spikes from the earthquakes recorded at the OSU Unmanned Aircraft Flight Station have similar spikes for all of the recorded earthquakes. This could be due

to the large difference in noise level while recording. The UAS flight station is in a relatively secluded area, where the bulk of the noise is from farming equipment, while the roof setup is near the campus of Oklahoma State University and records noise from occurrences inside the building, on the roads nearby, and at the airport a few miles away. However, the consistent spikes in earthquakes of larger magnitude near the roof setup leads one to suspect that there is a similar mechanism responsible for the earthquakes.

The locations of the earthquakes processed from the month of September can be seen in Figure 63 (taken from the IRIS earthquake Browser). There are several clusters of earthquakes in various places on this map. These clusters can be seen along with the location of the roof system in Figure 64. In this map the red house marker indicates where the roof top infrasonic system is located. The arrow points at the location of the M5.6 earthquake. This is right around the cluster of earthquakes at GPS location of: 36.43, -96.9. To determine whether there was a correlation between the location of the earthquake and its frequency content, the spectrum from each cluster of earthquakes were averaged together.

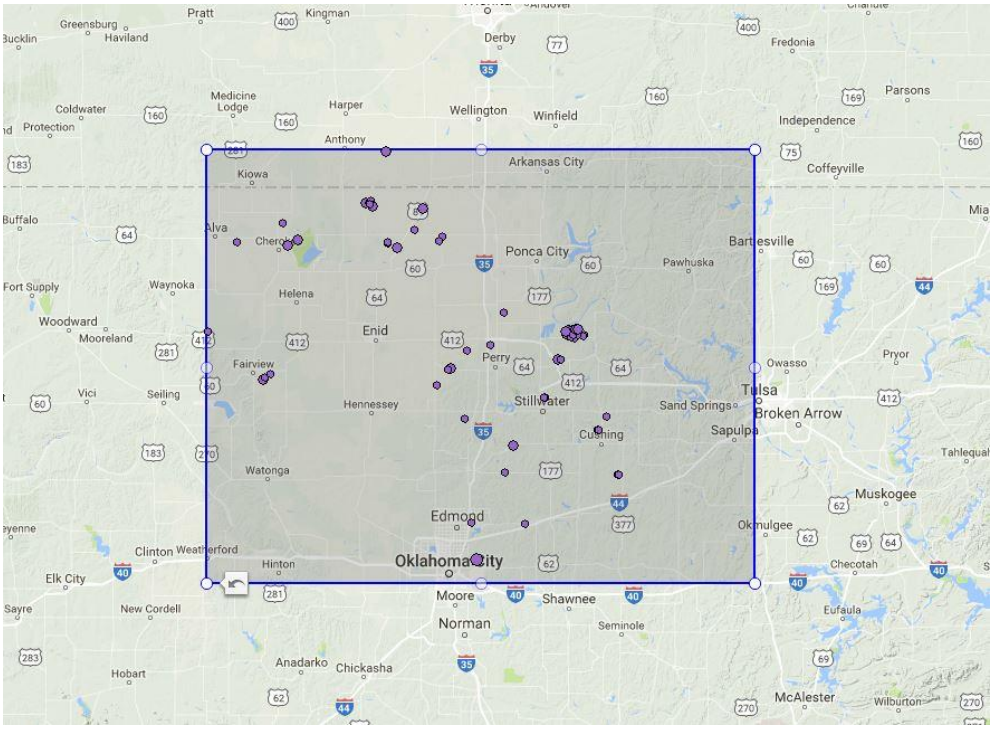

Figure 63: Locations of earthquakes recorded with the infrasonic microphone in the month of September 2016.

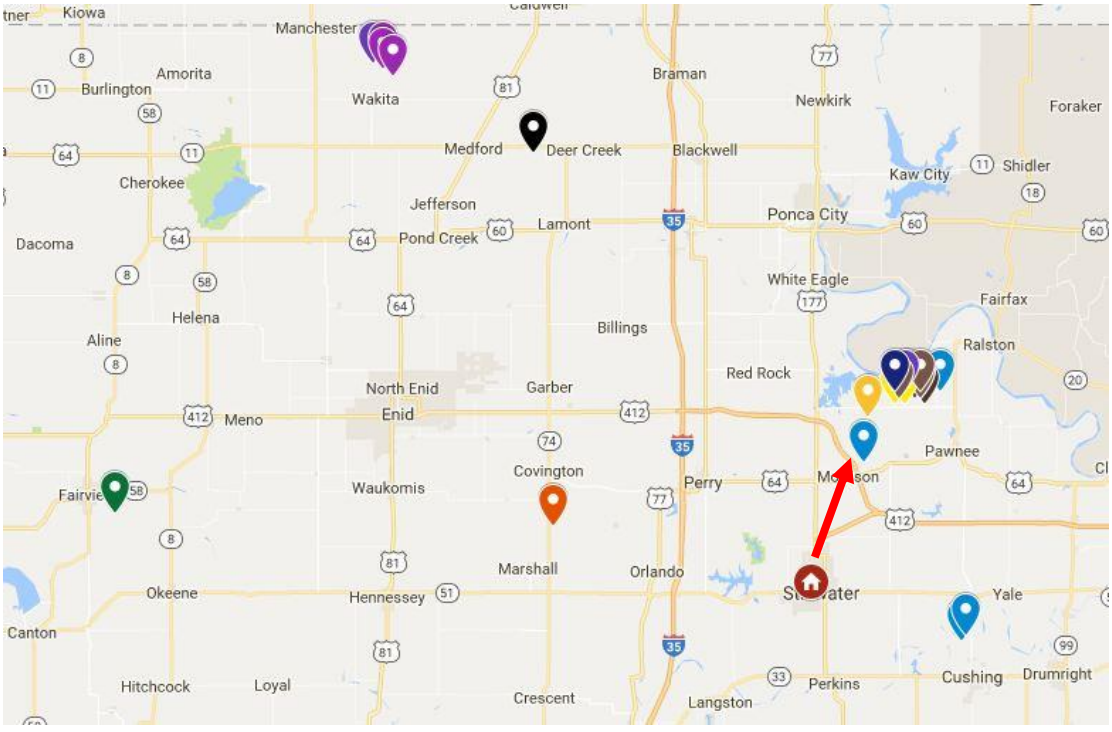

Figure 64: Locations of clusters of earthquakes. The red house indicates location of microphone.

Figure 65 shows the average from the area near where the 5.6 magnitude earthquake occurred, while Figure 66 shows the average from the area on the map where the purple indicators are clustered. These averages were found using every earthquake that occurred in the area described in the table above. While this does weaken the spikes that could normally be seen in the spectrum, there is still a significant bump in the 10 minute average in the first graph from 80 to 110 Hz and a bump in the second graph around 85 Hz in the destination time spectrum. This further implies that the earthquakes at both locations could be caused by singular source.

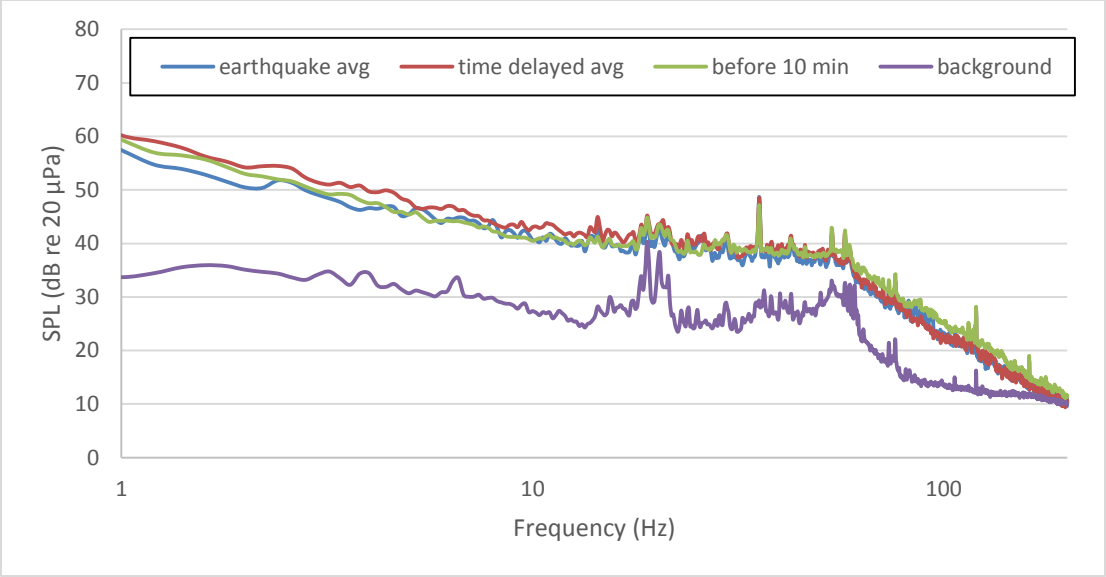

Figure 65: Average spectrum from earthquakes at GPS location: 36.42, -96.9.

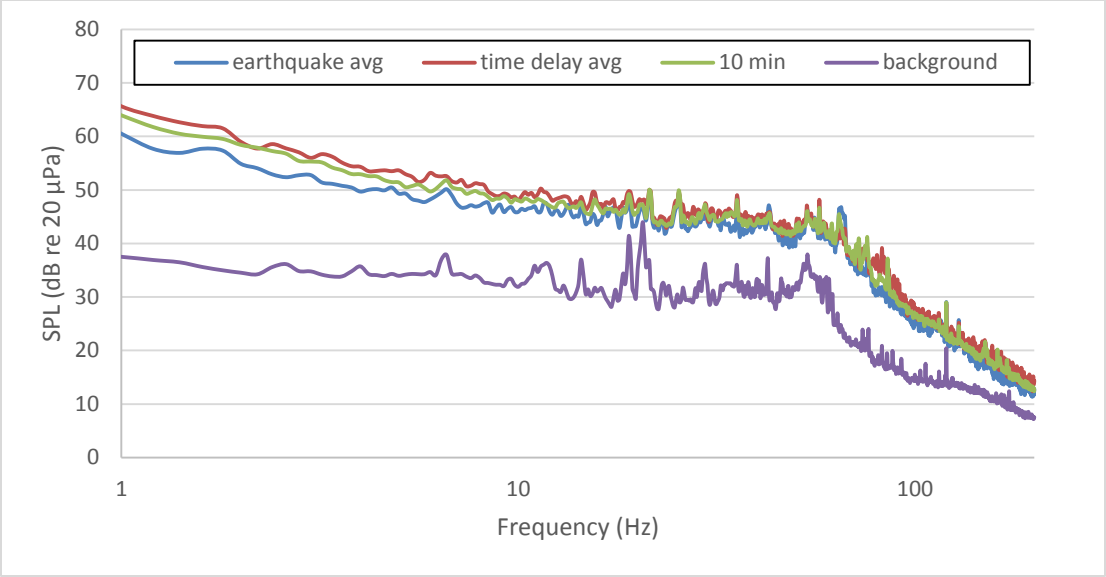

Figure 66: Average spectrum from earthquakes at GPS location: 36.94, -97.91.

4.3.2 Storms

Several thunderstorms have been recorded since the deployment of the roof system. These storms all produced a significant amount of rain, thunder, and lightning. Only one of the storms produced tornadoes. These tornadoes formed and hit areas in several Kansas counties. These counties however are towards the interior of Kansas, which is slightly out of range of events normally recorded by the microphone. It might be possible that these tornadoes were in fact recorded by the roof detection system, but with no other tornado data to compare the measurements to, there is no way to know for certain. Figure 67 to Figure 74 show the sound pressure spectra from the storms recorded on September 9, 2016; September 17, 2016; October 6, 2016; October 26, 2016; and November 2, 2016. In addition pictures of the radar during the most recent storms are also provided.

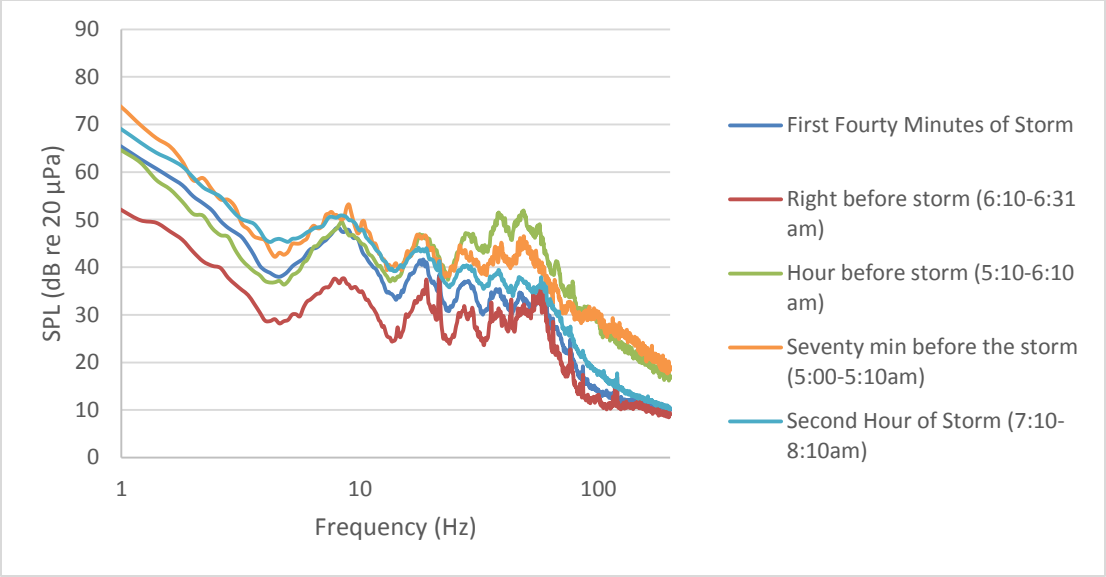

Figure 67: Pressure spectra from storm on September 9, 2016.

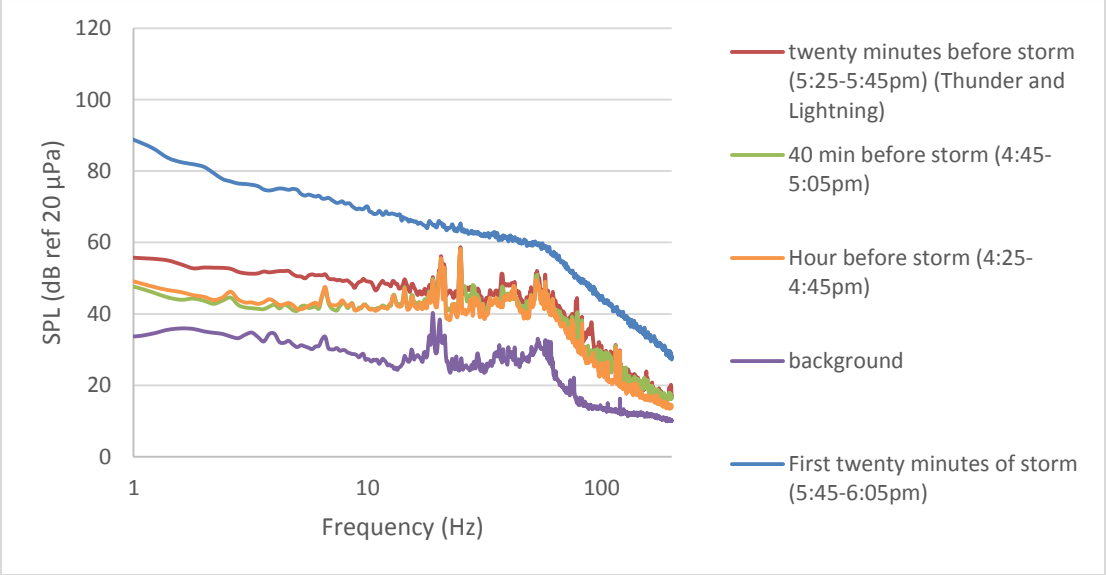

Figure 68: Pressure spectra from storm on September 17, 2016.

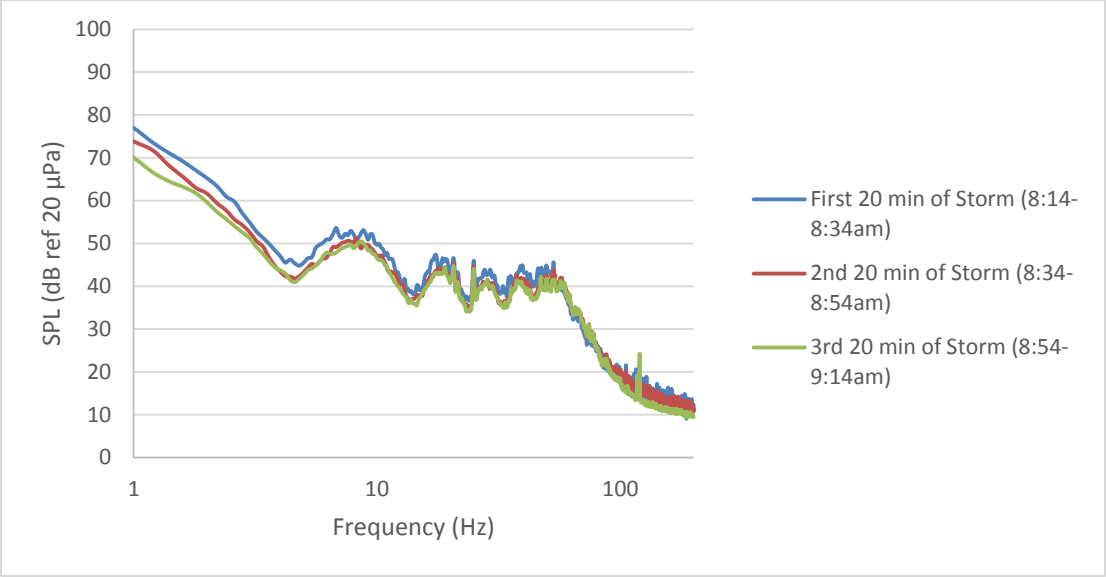

Figure 69: Pressure spectra from storm on October 6, 2016.

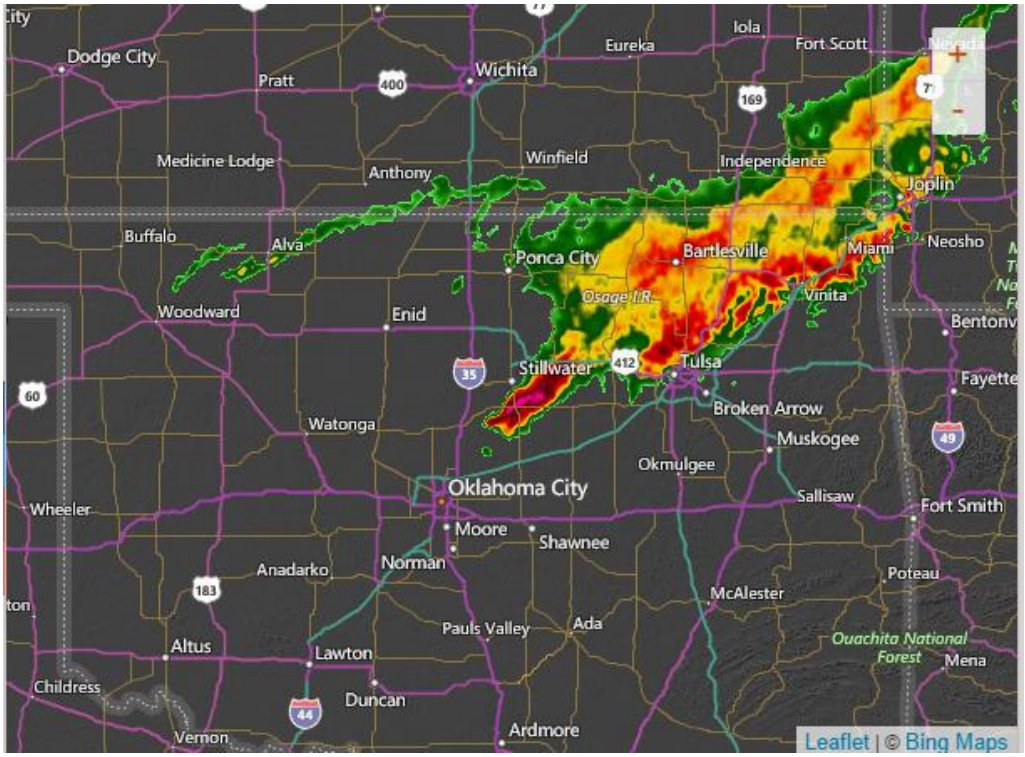

Figure 70: Radar from after storm on October 26, 2016.

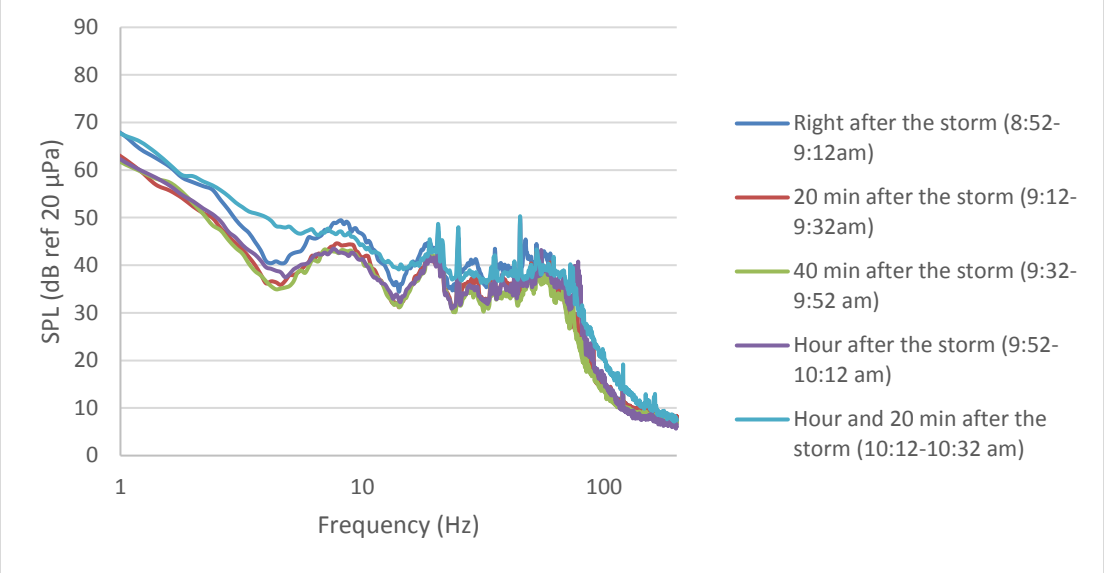

Figure 71: Pressure spectra from storm on October 26, 2016.

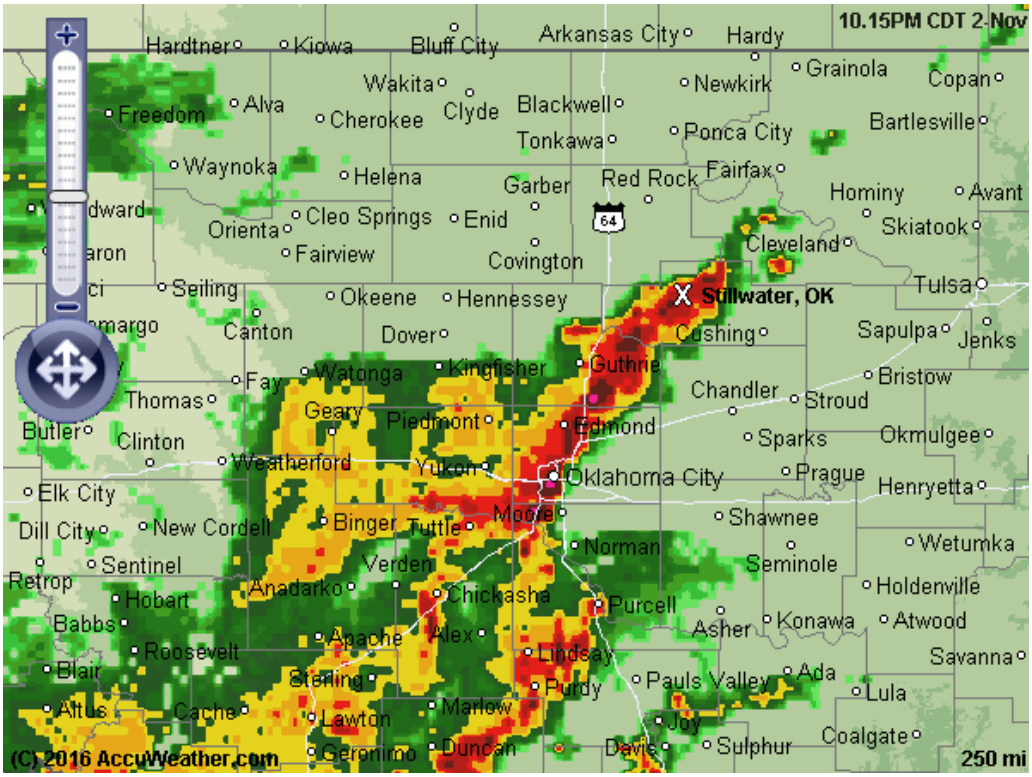

Figure 72: Radar from Storm on November 2, 2016

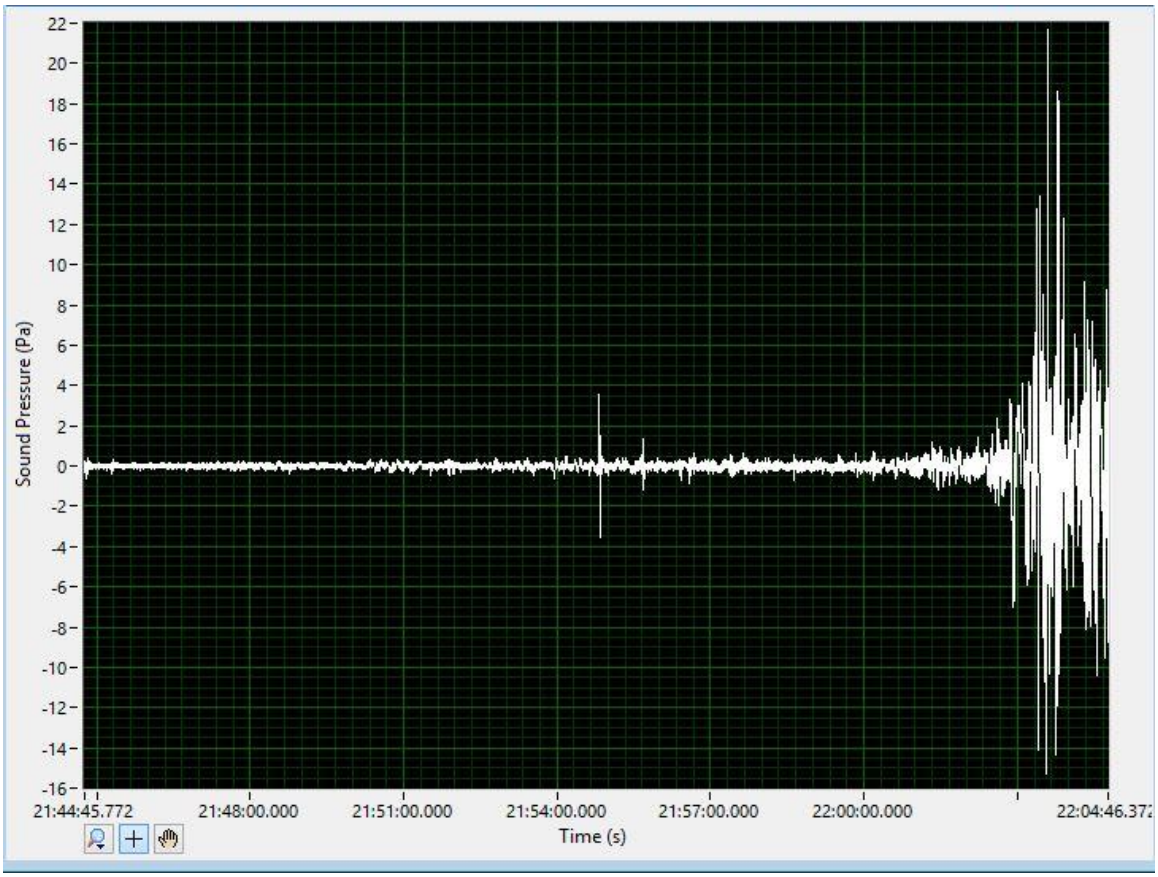

Figure 73: Sound pressure versus time from beginning of storm on November 2, 2016 (9:44-10:04 PM).

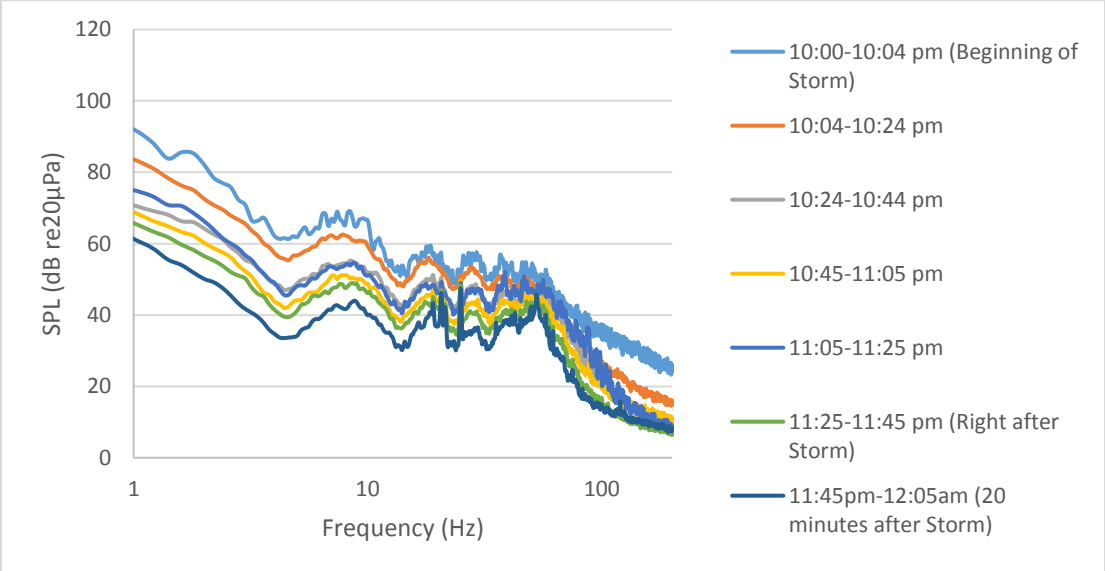

Figure 74: Pressure spectra from storm on November 2, 2016.

The time of the storm as described by the graphs is defined as the time it starts raining in Stillwater, Oklahoma. The time after or right before the storm describe the times right after it stops raining or right before the rain started. The storms from the month of September shows data from before and during the storm. The storm from October 6, 2016 shows data from during the storm and the storm from October 26, 2016 shows data from after the storm only. The storm from October 26, 2016 only recorded data from after the storm due to technical difficulties.

The data from four of the five storms show oscillations in the frequency domain, which are multiples of 10 (i.e. 10, 20, 30, 40, 50, 60, and 70 Hz). These oscillations have shown up at most an hour and ten minutes before the storm reaches Stillwater and have remained a little over an hour after the storm has left Stillwater. This implies that storms have a distinct signature and can be tracked. These similarities also imply that these storms could possibly be predicted to hit certain areas an hour before the storm reaches the area where the microphone is recording from.

There are also specific differences between the spectra derived from each storm. The storm recorded on September 9, 2016 produces the loudest signals an hour before the storm and the next loudest is the signal recorded seventy minutes before the storm. The next three signals are in the order expected with the signal getting louder the closer the signal gets to the microphone. It is also useful to note that this storm produced oscillations to higher frequencies than the other storms, reaching a frequency of 70 Hz.

The storm recorded on September 17, 2016 is the only storm that does not exhibit oscillatory behavior in the frequency content. This may be due to the ability of this storm to produce severe weather (tornado) or due to some other occurrences in the physics of this specific storm. More research must be done to determine what is actually making the signals from these storms to determine why some storms exhibit different spectral content than others. This storm however did show the signal getting louder as the storm approaches the microphone, which implies the microphone is tracking the storm just as in the September 9, 2016 storm. Another interesting thing about this storm is the behavior of the signal once the storm reached the microphone. The noise level becomes very high limiting the ability to see any distinct frequency content from the storm. Originally it was believed that this was due to the heavy rain hitting the dome, but after further investigation it is now believed to be due to high winds. Soaker hose windscreens are typically only useful at wind speeds below 2.5 m/s.

The storm on October 6, 2016 produced several storms in Kansas after passing through Stillwater, Oklahoma. The cloudy overcast weather persisted throughout the day however the only times to clearly have produced the oscillating signals that have been investigated thus far is at the times shown above. This may be due to the inconsistency of the storm on October 6, 2016 and its constant changing behavior. Despite this, the signals on the morning of October 6 produced the same oscillations as the storm on September 9th, with the signal getting quieter as it persists.

The storm on October 26, 2016 produces the oscillating signature the longest time after the storm has passed, at an hour and 20 min. This signal persisted hours after the storm passed the microphone.

The storm on November 2, 2016 produced very interesting results. The roof system did not pick up this storm before it reached the microphone as in other storm recordings. Figure 73 shows a large spike towards the end of the recording around 10:00 PM when the storm began. The oscillating frequencies do not appear until these large spikes occur in the sound pressure files. In the future it would be beneficial to have radar from each storm day to compare with the spectra found from the recordings.

4.3.3 Fireworks Recordings

Every year on Independence Day in Stillwater, Oklahoma a large fireworks show is put on. In 2016 this fireworks show was delayed to Labor Day, September 2, 2016. Because of the potential for "large booms" from the fireworks, several recordings were taken. One from our long term system roughly 1.5 miles away and a temporary system set up for just the night at the Oklahoma State Unmanned Systems Research Institute (GPS location: 36.150625, -97.063499) roughly 1.9 miles away.

The Model 24 Chaparral microphone (serial number: 162642) was used similarly to the roof setup without the platform/dome. The 50 foot soaker hoses were again rolled out and turned halfway back towards the microphone. Recording begun roughly 45 minutes before the fireworks show began. This was to get an accurate idea of the ambient/background noise. A few sound pressure times traces and spectra graphs of the ambient noise in the atmosphere are shown in Figure 75 to Figure 77.

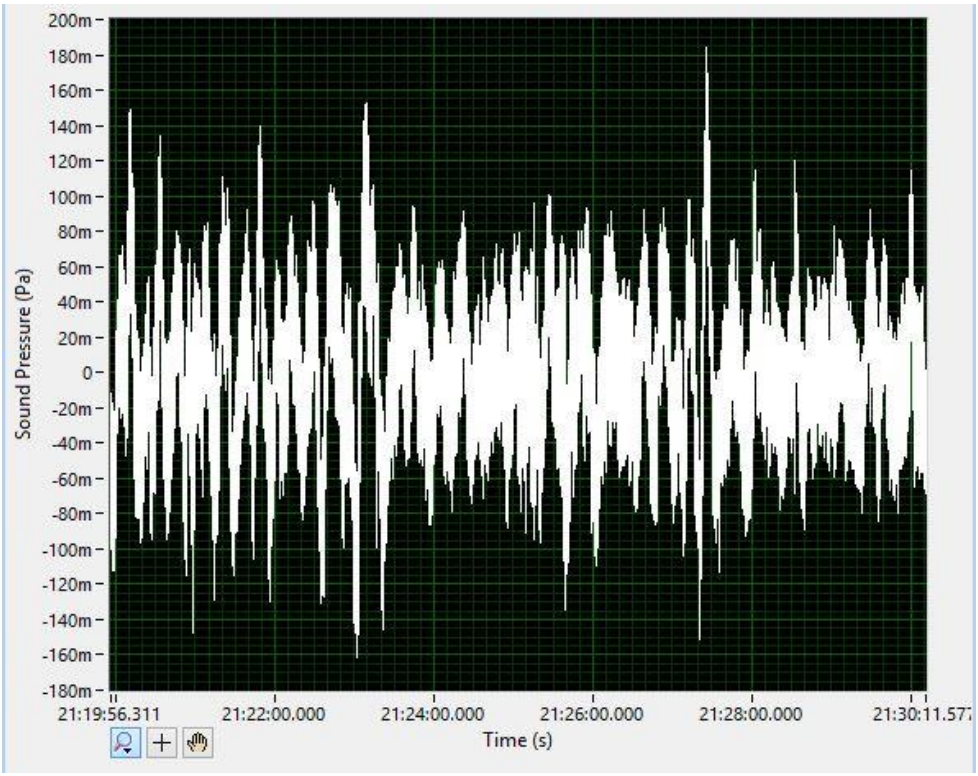

Figure 75: Sound Pressure vs. Time Graph Ambient Noise before fireworks 9:20-9:30 pm.

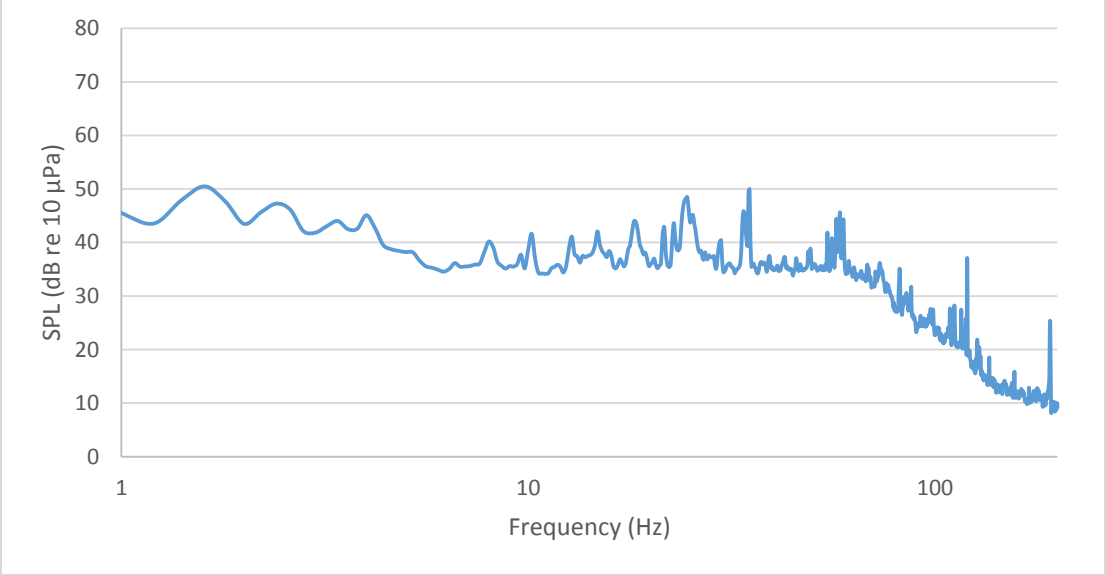

Figure 76: Spectrum from background noise before fireworks (9:20-9:30 pm).

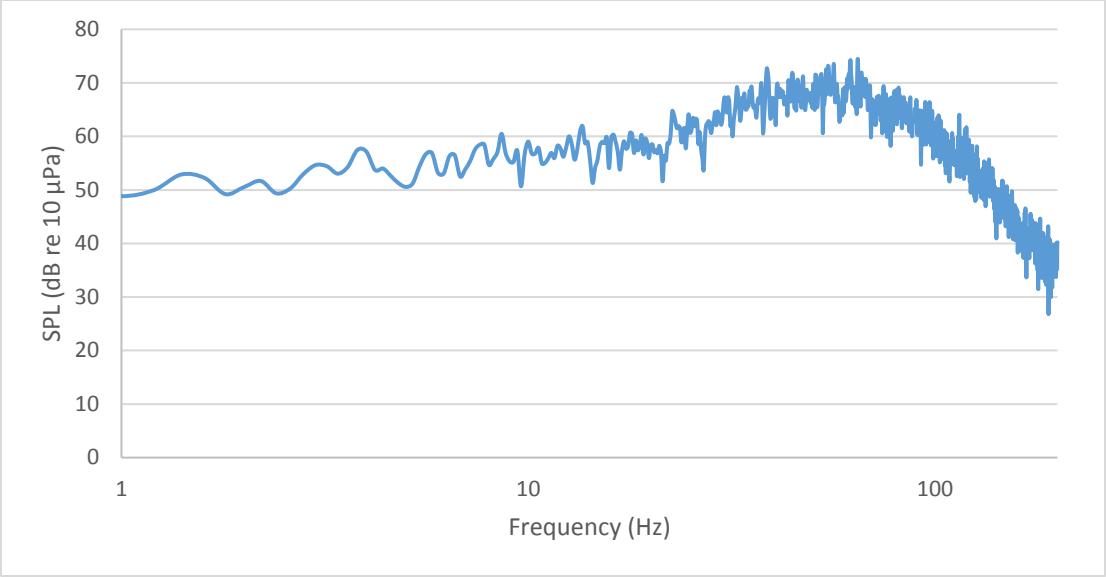

Figure 77: Spectrum from loudest part of fireworks (9:56-9:57pm).

For the recordings samples were taken at a sample rate of 1,000 Hz and the samples to read value was set at 5,000. This was done to minimize the amount of memory required for each file and to ensure that events that have strong frequency content below 10 Hz have enough data to provide clear peaks. As can be seen the sound produced from the fireworks produced a broadband signal that reached roughly 74 dB with the peak at ~ 60 Hz. This data will be used as a comparison between recordings from other interesting events.

Data was also collected from plane take offs and landings from nearby regional Stillwater airport (SWO). However, there was no consistent signal associated with the noise from the planes. This is more than likely due to the different flight paths taken out of and into the Stillwater airport. More work is needed to find a consistent signal from the aircrafts that fly over the microphone.

CHAPTER V

5. FUTURE WORK

There is two different types of work that will need to be done on this project in the future. The first type is the expansion of the array, and the other type is on the data processing algorithms. To know the location of recorded signals an increase in the number infrasonic systems is needed. Utilizing the three microphone system that is currently being implemented, a direction of the recorded signal can be acquired. However, for a more accurate estimation multiple arrays are necessary. The distance of these arrays from one another is yet to be determined but there should be at least 2 more arrays added to the system for accurate localization.

The improvements in processing of the data is a multifaceted task. One of the tasks necessary is the in depth analysis of events to compare with the recorded data. This would be helpful for similar events that demonstrate different data behavior including storms and earthquakes. The in depth analysis of the storms includes Doppler radar data, information on the potential of the storm to produce tornadoes, and other atmospheric data from the storm itself. Some of this data may be found by members of other teams of this project and some may be found by an outside source. In the future this data combined with the geophysical data can possibly be used to identify an “acoustic signature” of a tornado. The in depth analysis of the earthquakes would mainly include the utilization of

multiple arrays to get a location of the sound source. This would eliminate the possibility that the signal being read is not from the earthquake. In depth analysis of the airplane data will be necessary as well.

Another improvement to the data processing would be to implement a way to process a day's worth of data in a short period of time. Currently it can take around 2 to 3 hours to process a day's worth of data (72 files 20 minute files), and this is done manually by using the playback option in LabVIEW to replay the frequency vs sound pressure graph and then exporting that graph to excel. This can make it difficult to average for a specific week or month due to the large time commitment. The MATLAB file described earlier which creates spectrum and processes files quickly may be useful for this task.

The last task for improvements in data processing is the need for new background spectrum for each season. Due to the change in temperature and humidity as the seasons change the sounds from the background should be different, hence the need for seasonal spectra.

CHAPTER VI

6. CONCLUSIONS

In conclusion, many natural and man-made occurrences emit infrasonic frequencies including earthquakes, tornadoes, and supersonic aircrafts. More may be learned about these events by investigating these sounds and early prediction of these events may be possible through this gained knowledge. This project's main motivation is the possibility of using infrasound to improve tornado warnings and the eventual partnering with data collected by sensors on UAVs. The data collected by Bedard demonstrates the ability to track the path of a storm, which further implies that infrasound is a viable option for tornado detection.

Initial experiments were performed to create infrasonic sources and measure those sources with infrasonic sensors. A subwoofer and a pulsed gas-combustion torch were the infrasonic sources chosen, which differ from the sources used by other researchers in the past (e.g. MOAS, TRW). However, these sources demonstrated the ability to produce lower amplitude infrasound. More tests were performed to confirm the belief that the Chaparral Model 24 microphone with soaker hoses as a windscreen would perform the best in field testing.

The experimental setup which utilizes the Chaparral Model 24 microphone was used during the first CLOUD-MAP demonstration week. This setup was then installed on the roof of the Fabrication Laboratory at Oklahoma State University as a long term monitoring system. Several interesting events were recorded as a result including a fireworks display, earthquakes, and storms. This data was then compared to averages of the data on calm days. The data presented from the earthquakes clearly show a pattern in the frequency band of 50-100 Hz. These peaks mostly occur in the ten minute window before the earthquake occurs. More recordings with the 2nd and 3rd system setups would be beneficial in confirming the signals origin direction. The storm data presented clearly show oscillations at least an hour before thunderstorms reach the recording system. More storms with and without tornadoes will need to be recorded by the systems, 2nd and 3rd microphones included, in order to establish a pattern in the data from the storms. This data correlated with the data found from the UAVs will hopefully give insight into the physics of the atmosphere during severe weather.

REFERENCES

Abdullah, A. J. (1966) "The 'musical' sound emitted by a tornado," *Monthly Weather Review*, **94**(4), 213–220.

Ahuja, K. K., Stevens, J. C. & Walterick, R. E. (1993) "A giant simulator of sonic boom and aircraft noise," *15th AIAA Aeroacoustics Conference*, Long Beach, CA, American Institute of Aeronautics and Astronautics (dx.doi.org/10.2514/6.1993-4430).

Alcoverro, B. (1998) "Proposition d'un systeme de filtrage acoustique pour une station infrason IMS," CEA-DASE Scientific Report, No. 241, 1998.

Anderson, L. J. & Kettler, A.H. (1948) "Windscreen for microphones," U.S. Patent 2,520,706, filed Jan. 30, 1948.

Arnold, R. T., Bass, H. E. & Bolen, L. N. (1976) "Acoustic spectral analysis of three tornadoes," *Journal of the Acoustical Society of America*, **60**(3), 584-593.

Ash, R. L., Zardadkhan, I. & Zuckerwar, A. J. (2011) "The influence of pressure relaxation on the structure of an axial vortex," *Physics of Fluids*, **23**, 073101.

Ballard, H. N. & Izquierdo, M. (1968) "Multiple wind screen noise attenuation system," U.S. Patent 3,550,720, filed Sept. 24, 1968.

Bass, H. E., Sutherland, L. C., Zuckerwar, A. J., Blackstock, D. T. & Hester, D. M. (1995) "Atmospheric absorption of sound: Further developments," *Journal of the Acoustical Society of America*, **97**, 680–683.

Beaudecel, F. (2016) "RDSAC and MKSAC: Read and write SAC seismic data file," MATLAB Central File Exchange, last updated Aug 11, 2016.

Bedard, A. J. (1998) "Infrasonic and near infrasonic atmospheric sounding and imaging," *Proceedings of the Progress in Electromagnetics Research Symposium*, July 13-17, Nantes, France; 4th International Workshop on Radar Polarimetry.

Bedard, A.J. (2005) "Low-frequency atmospheric acoustic energy associated with vortices produced by thunderstorms," *Monthly Weather Review*, **133**(1), 241-263.

Bedard, A. J. Jr. & Georges, T. M. (2000) "Atmospheric Infrasound", *Physics Today*, **53**(3), 32-37.

Bedard, A. J., Bartram, B. W., Keane, A. N., Welsh, D. C. & Nishiyama, R. T. (2004a) "The infrasound network (ISNET): Background, design details, and display capabilities as an 88D adjunct tornado detection tool," *Proceedings of the 22nd Conference on Severe Local Storms*, October 4-8, 2004, Hyannis, MA (sponsored by the American Meteorological Society, Boston, MA).

Bedard, A. J., Bartram, B. W., Entwistle, B., Golden, J., Hodanish, S., Jones, R. M., Nishiyama, R. T., Keane, A. N., Mooney, L., Nicholls, M., Szoke, E. J., Thaler, E. & Welsh, D. C. (2004b) "Overview of the ISNET data set and conclusions and recommendations from a March 2004 workshop to review ISNET data," *Proceedings of the 22nd Conference on Severe Local Storms*, October 4-8, 2004, Hyannis, MA (sponsored by the American Meteorological Society, Boston, MA).

Bertrand, J., Likins, M., Nichols, J. & Niemeyer, M. (2016) "Early tornado detection," *Oklahoma State University MAE Senior Capstone Design Report*.

Bruel, P. V. (1960) "Aerodynamically induced noise of microphones and windscreens," B&K Technical Review, No. 2, Copenhagen, Denmark.

Burridge, R. (1971) "The acoustics of pipe arrays," *Geophysical Journal of the Royal Astronomical Society*, **26**, 53-69 (doi:10.1111/j.1365-246X.1971.tb03382.x).

Cook, R. K. (1962) "Strange sounds in the atmosphere, Part 1," *Sound: Its Uses and Control*, **1**(2), 12-16.

Daniels, B. (1959) “Noise reducing line microphone for frequencies below 1 Hz,” *Journal of the Acoustical Society of America*, **31**, 529-531.

Dean, L., Samaras, T. & Moran, D. (2015, unpublished) “Infrasonic acoustics and pressure measured during the El Reno, OK EF-3/EF-5 tornado 31-May-2013,” hosted on stormtrack.org; draft provided by Lanny Dean and posted: https://stormtrack.org/community/attachments/infrasonic-acoustics-measured-during-the-may-5-2013-el-reno-tornado-pdf.7437/

Dowling, D. R. & Sabra, K. G. (2015) “Acoustic Remote Sensing” *The Annual Review of Fluid Mechanics*, **47**, 221-243.

Elbing, B. R. & Gaeta, R. J. (2016) “Integration of Infrasonic Sensing with UAS” *8th Atmospheric and Space Environments Conference*, AIAA Aviation, AIAA2016-3581, Washington, DC (June 13-17) (doi:10.2514/6.2016-3581).

Farges, T. & Blanc, E. (2010) “Characteristics of infrasound from lightning and sprites near thunderstorm areas,” *Journal of Geophysical Research*, **115**, A00E31 (doi:10/1029/2009JA014700).

Frazier, W. G., Talmadge, C., Park, J., Waxler, R. & Assink, J. (2014) “Acoustic detection, tracking, and characterization of three tornadoes,” *Journal of the Acoustical Society of America*, **135**(4), 1742-1751.

Golden, P., Negraru, P. & Herrin, E. T. (2008) “Infrasound propagation in the zone of silence,” *Journal of the Acoustical Society of America*, **123**(5), 3920.

Hedlin, M. A. H. & Raspet, R. (2003) “Infrasonic wind-noise reduction by barriers and spatial filters,” *Journal of the Acoustical Society of America*, **114**, 2379-1386.

Kinsler, L.E., Frey, A. R., Coppens, A. B. & Sanders, J. V. (2000) *Fundamentals of Acoustics*, 4th Edition, John Wiley & Sons, New York.

Lorenz, R. D. & Christie, D. (2015) “Dust devil signatures in infrasound records of the International Monitoring System,” *Geophysical Research Letters*, **42**, 2009-2014 (doi:10.1002/2015GL063237).

NOAA (2002) “Infrasonic detection of tornadoes and tornadic storms,” *National Oceanic and Atmospheric Administration (NOAA) Technical Report*, accessed 11-30-16 (http://www.esrl.noaa.gov/psd/programs/infrasound/isnet/Infrasonic_Detection_of_Tornadoes.pdf)

Noble, J. M. & Tenney, S. M. (2004) “Detection of naturally occurring events from small aperture infrasound arrays,” *U.S. Army Research Laboratory Report*.

Park, J., Garcés, M. & Thigpen, B. (2009) “The rotary subwoofer: A controllable infrasound source” *Journal of the Acoustical Society of America*, **125**(4), 2006-2012 (doi: 10.1121/1.3082115).

Park, J. & Robertson, J. (2009) “A portable infrasound generator” *Journal of the Acoustical Society of America*, **125**(4), EL148-EL151 (doi: 10.1121/1.3093797).

Powell, A. (1959) "Similarity and turbulent jet noise,” *Journal of the Acoustical Society of America*, **31**, 812–813.

Rotunno, R. (2013) “The fluid dynamics of tornadoes,” *Annual Review of Fluid Mechanics*, **45**, 59-84 (doi:10.1146/annurev-fluid-011212-140639).

Schecter, D. A., Nicholls, M. E., Persing, J., Bedard, A. J., & Pielke, R. A. (2008) “Infrasound emitted by tornado-like vortices: Basic theory and a numerical comparison to the acoustic radiation of a single-cell thunderstorm,” *Journal of the Atmospheric Sciences*, **65**, 685-713 (doi: 10.1175/2007JAS2384.1).

Shams, Q. A., Zuckerwar, A. J. & Sealey, B. S. (2005) “Compact nonporous windscreen for infrasonic measurements,” *Journal of the Acoustical Society of America*, **118** (3), 1335-1340 (doi: 10.1121/1.992707).

Shams, Q. A., Zuckerwar, A. J., Burkett, C. G., Weistroffer, G. R. & Hugo, D. R. (2013) "Experimental investigation into infrasonic emissions from atmospheric turbulence," *Journal of the Acoustical Society of America*, **133**(3), 1269-1280 (doi: 10.1121/1.4776180).

Shams, Q. A., Zuckerwar, A. J. & Knight, H. K. (2014) "Development and installation of an infrasonic wake vortex detection system at Newport News International Airport" *WakeNet-Europe 2014*, Bretigny, France May 13-14.

Shields, F. D. (2005) "Low-frequency wind noise correlation in microphone arrays," *Journal of the Acoustical Society of America*, **117**, 3489–3496.

Smith, C. M. & Gabrielson, T. B. (2015) "Theoretical model and experimental validation of a gas-combustion infrasound source," *Journal of the Acoustics Society of America*, **137**(4), 2407 (doi: 10.1121/1.4920767).

Talmadge, C. & Waxler, R. (2016) "Infrasound from tornados: Theory, measurement, and prospects for their use in early warning systems" *Acoustics Today*, **12**(1), 43-51.

Threatt, A. & Elbing, B. R. (2015) "Acoustic localization with infrasonic signals," *American Physical Society (APS) – Division of Fluid Dynamics (DFD) Annual Meeting*, D7.06, Boston, MA (Nov. 22-24); abstract in *Bull. Am. Phys. Soc.* Vol. 60(21).

Threatt, A. & Elbing, B. R. (2016) "Characterization of atmospheric infrasound for improved weather monitoring," *American Physical Society (APS) – Division of Fluid Dynamics (DFD) Annual Meeting*, H4.04, Portland, OR (Nov. 20-22); abstract in *Bull. Am. Phys. Soc.* Vol. 61(20).

Waxler, R., Evers, L. G., Assink, J. & Blom, P. (2015) "The stratospheric arrival pair in infrasound propagation," *Journal of the Acoustical Society of America*, **137**(4), 1846-1856.

Wurman, J, D Dowell, Y Richardson, P Markowski, E Rasmussen, D Burgess, L Wicker & HB Bluestein (2012) “The second verification of the origins of rotation in tornadoes experiment: VORTEX2,” *Bulletin of the American Meteorological Society*, **93**(8), 1147-1170.

Zuckerwar, A. J. & Shams, Q. A. (2011) “Sub-surface windscreen for outdoor measurement of infrasound,” U.S. Patent 0132095 A1, filed June 9, 2011.

APPENDIX

The next few graphs shows the average spectrum to the hours not shown in section 4.2.3. This includes hours 1am-4am, 6am-11am, 1pm-4pm, and 6pm-11pm.

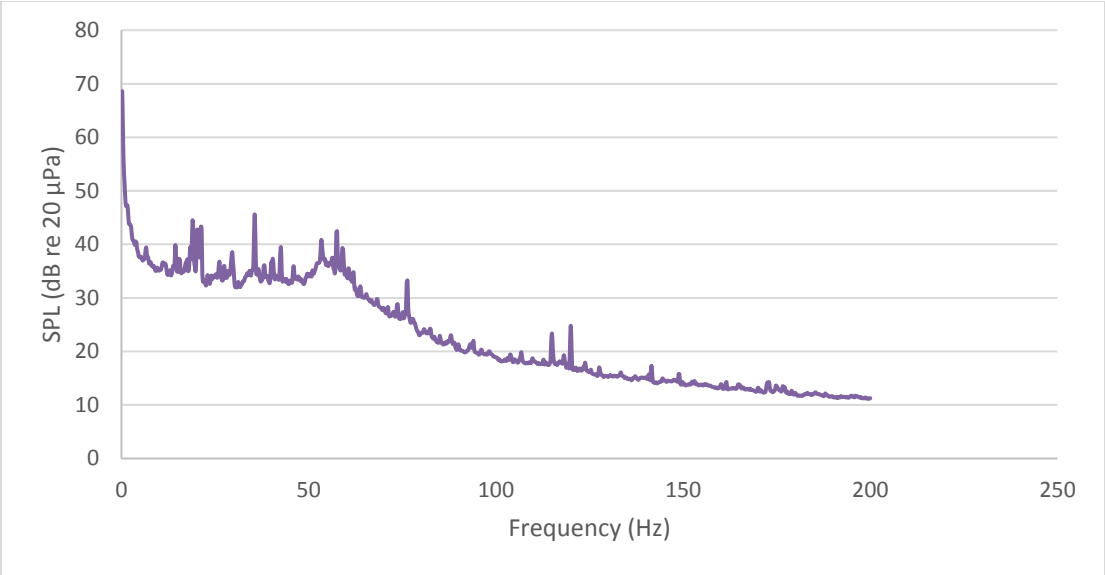

Figure 78: 1:00 AM

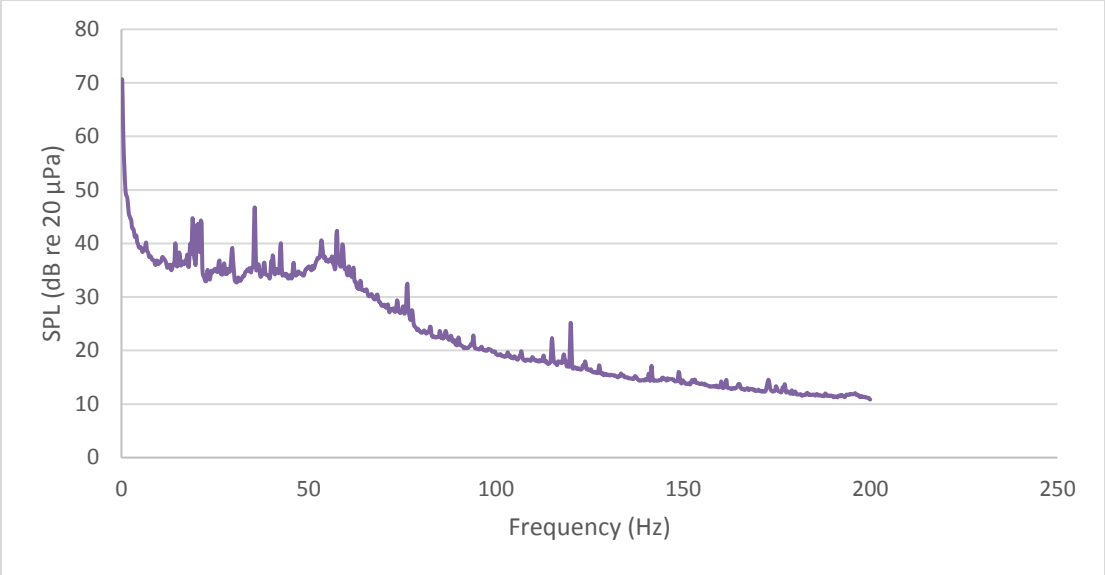

Figure 79: 2:00 AM

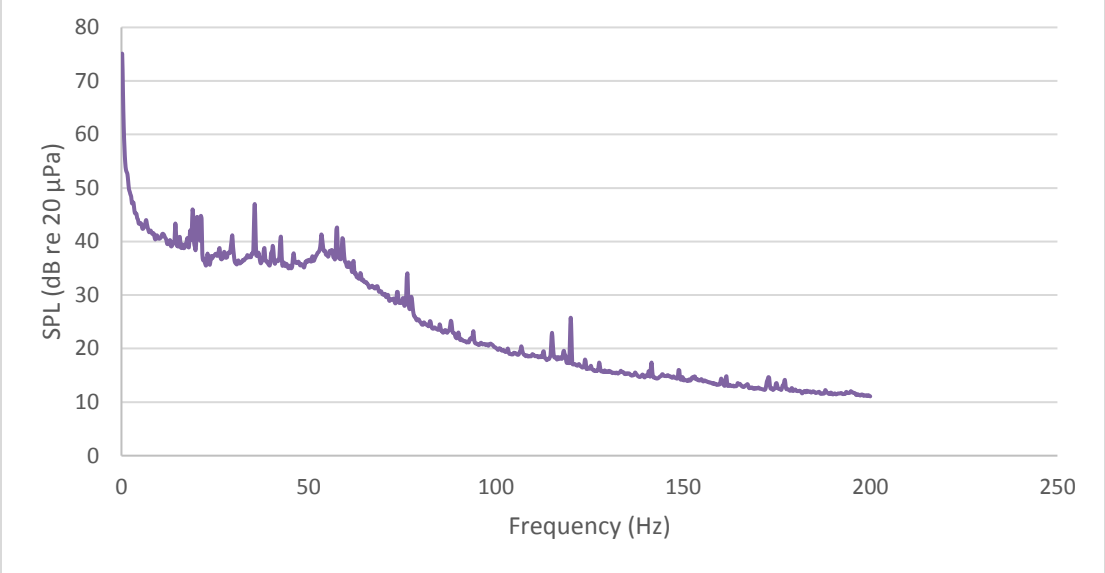

Figure 80: 3:00 AM

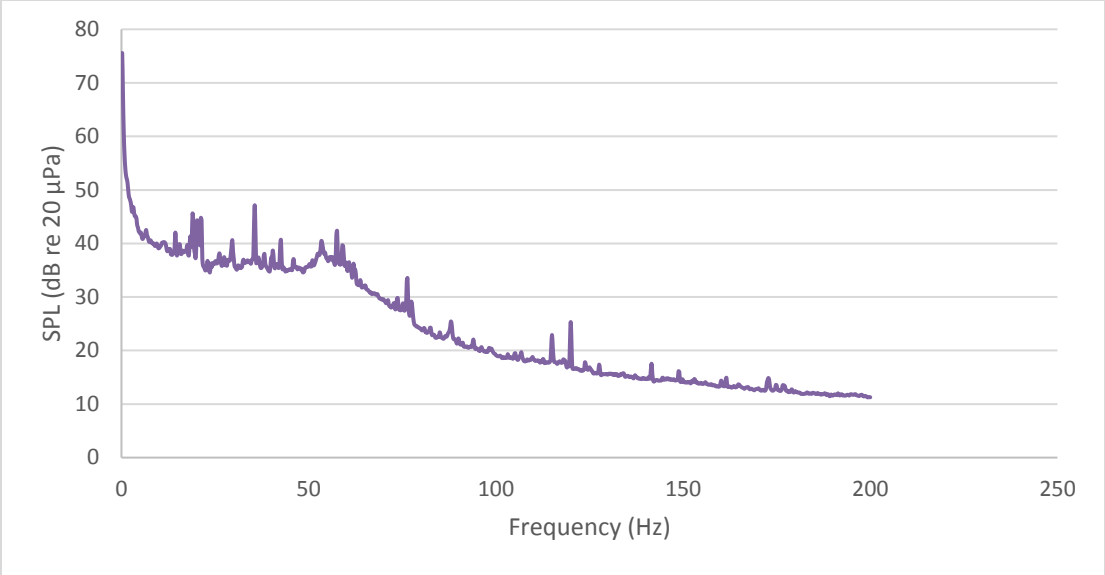

Figure 81: 4:00 AM

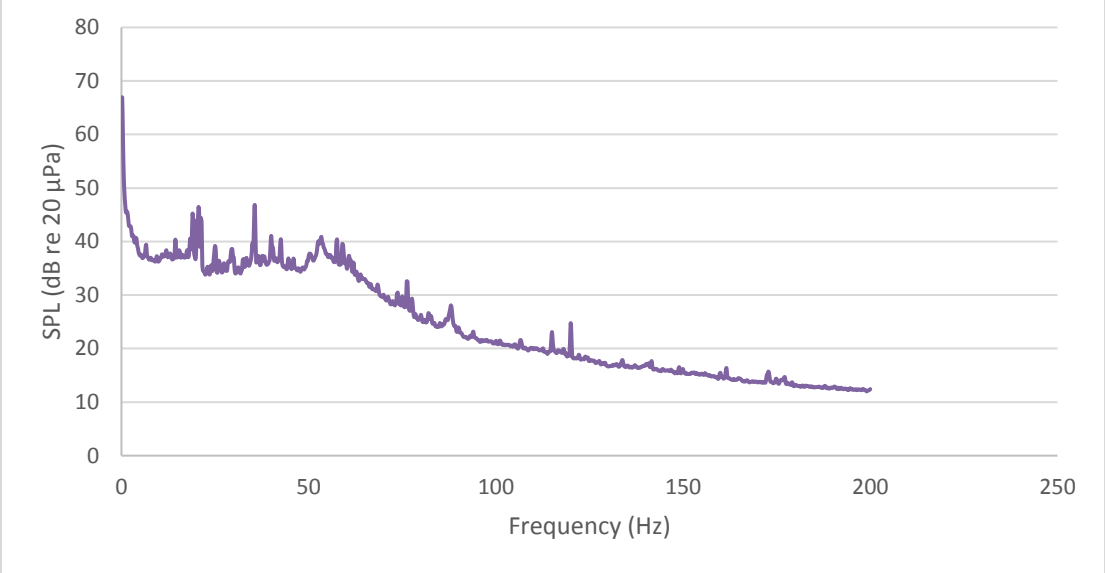

Figure 82: 6:00 AM

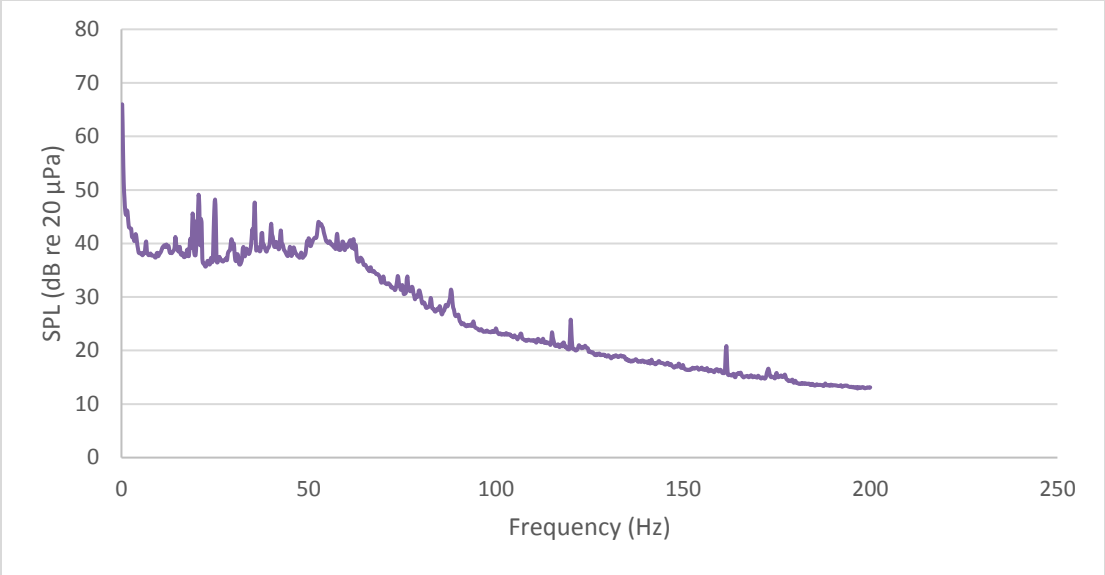

Figure 83: 7:00 AM

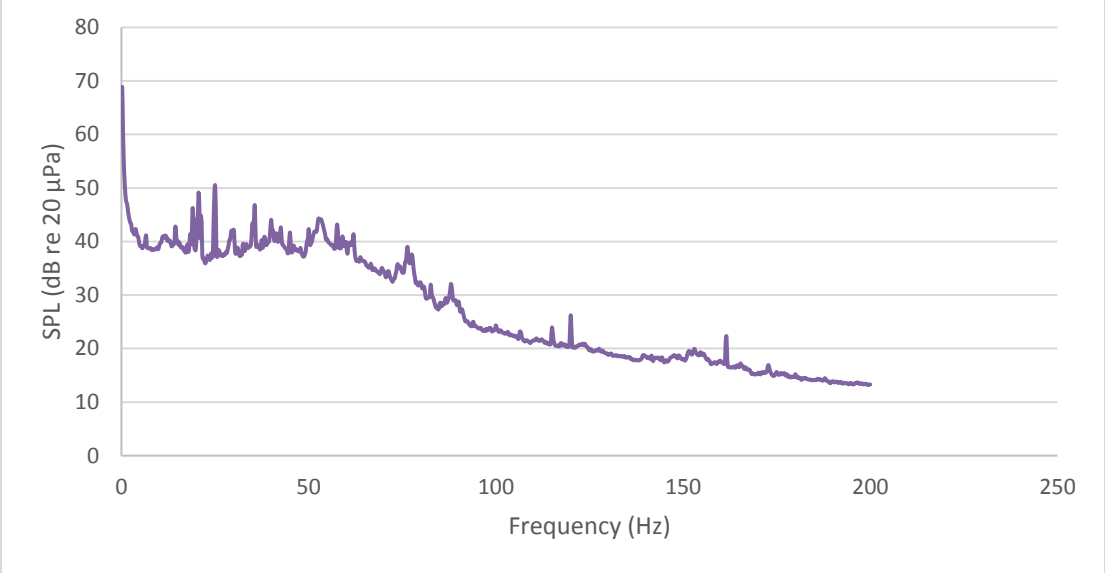

Figure 84: 8:00 AM

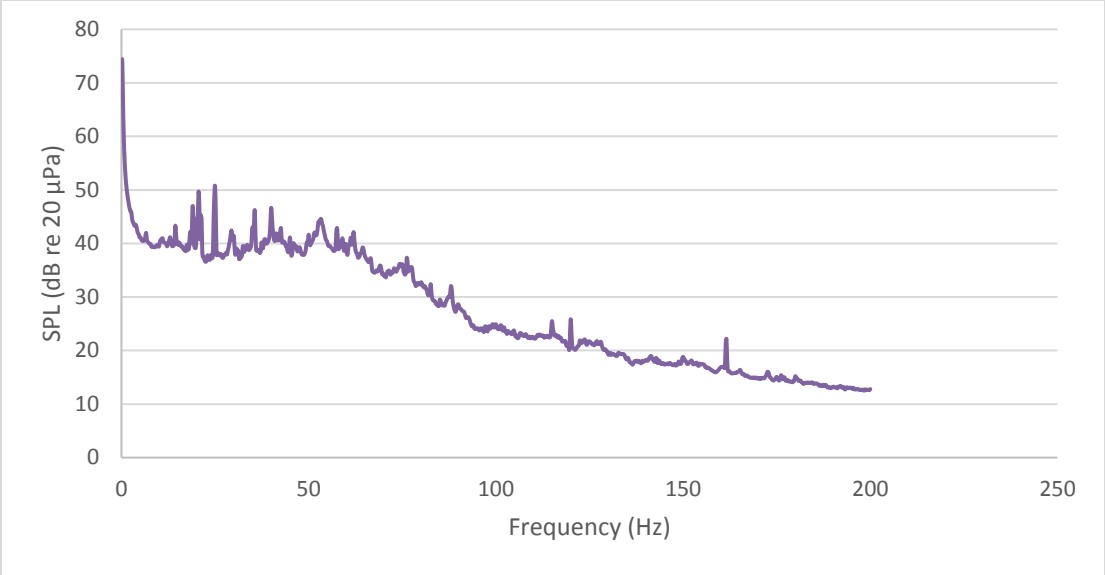

Figure 85: 9:00 AM

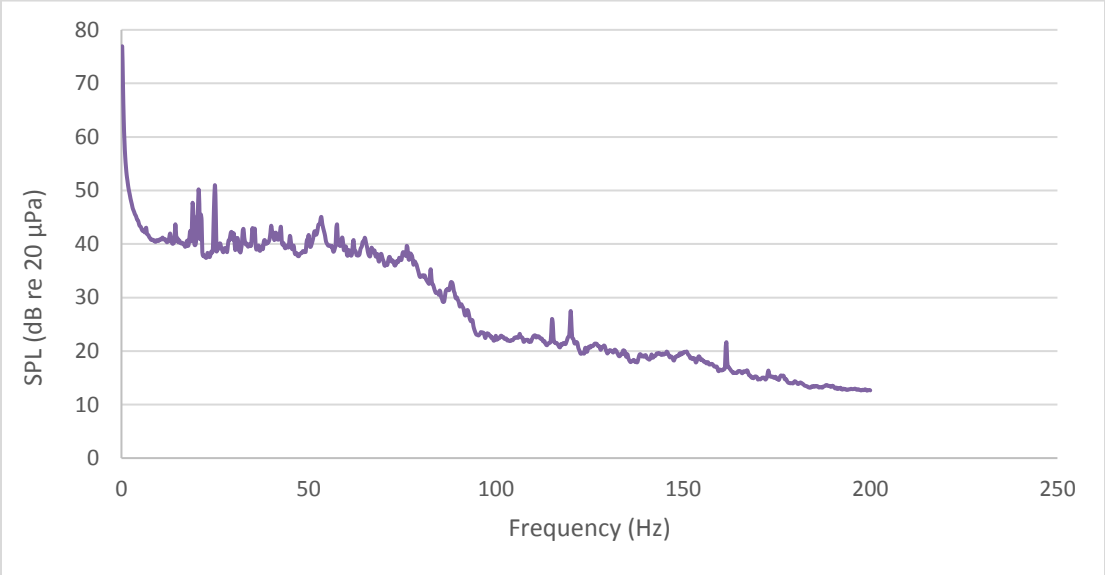

Figure 86: 10:00 AM

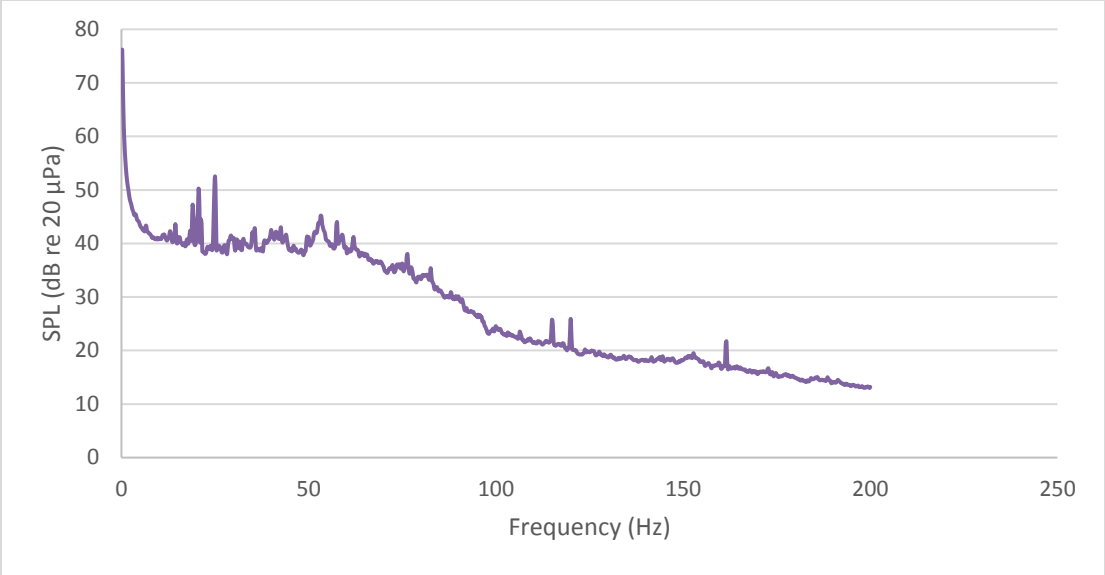

Figure 87: 11:00 AM

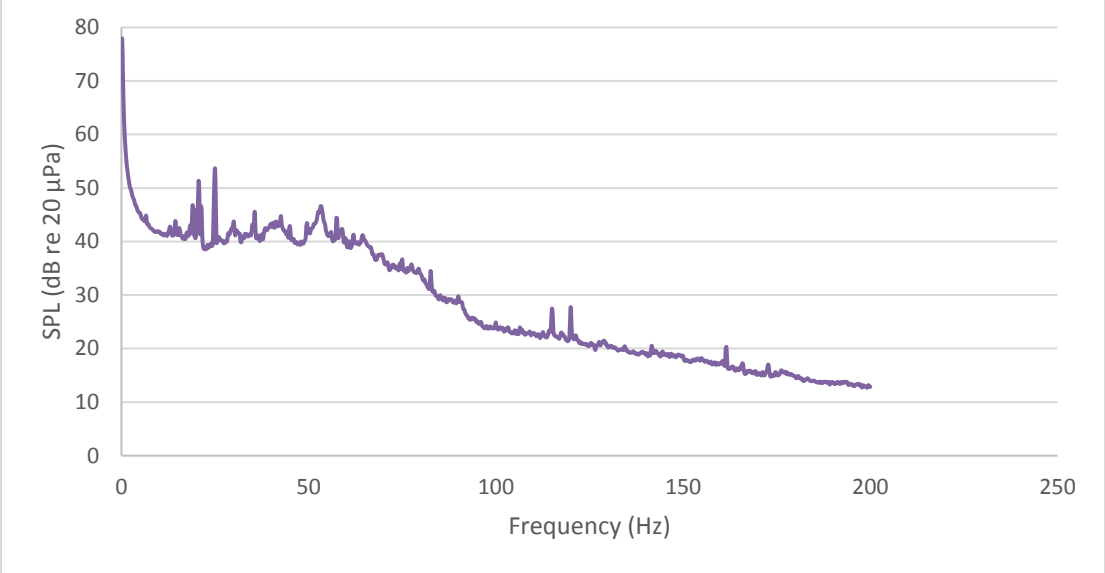

Figure 88: 1:00 PM

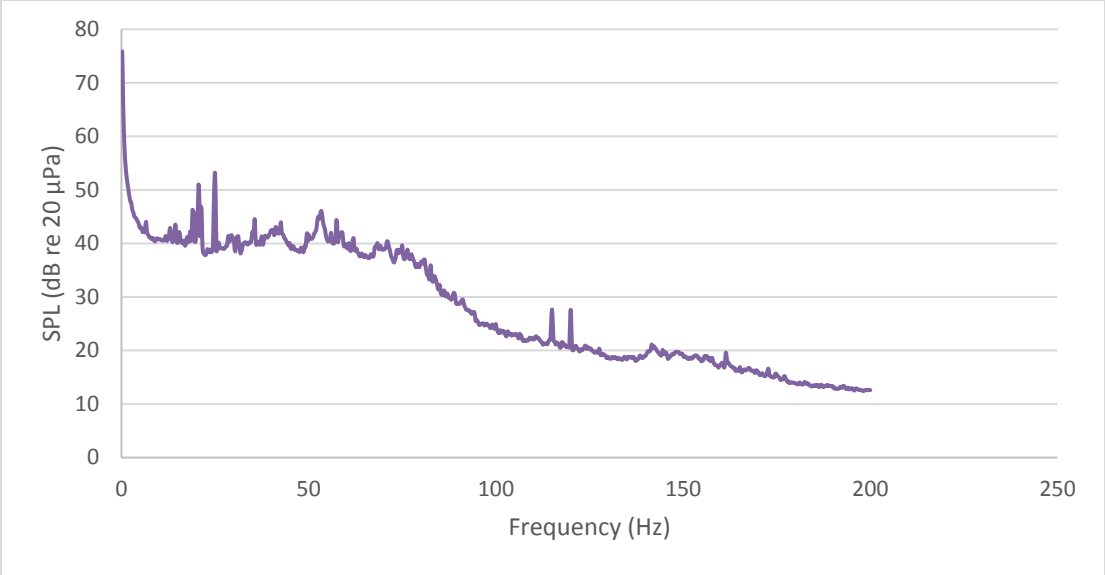

Figure 89: 2:00 PM

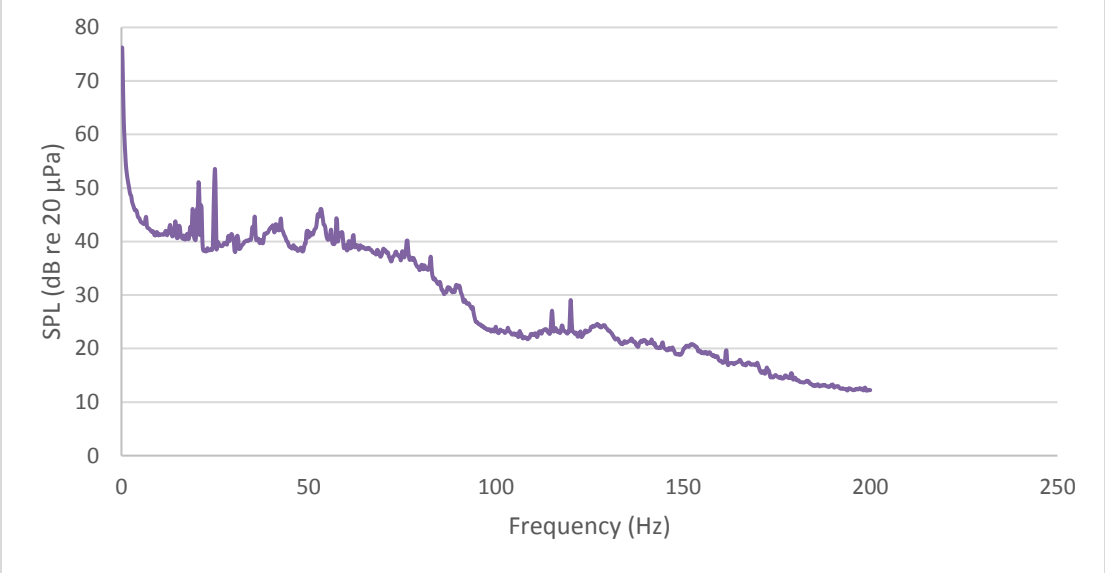

Figure 90: 3:00 PM

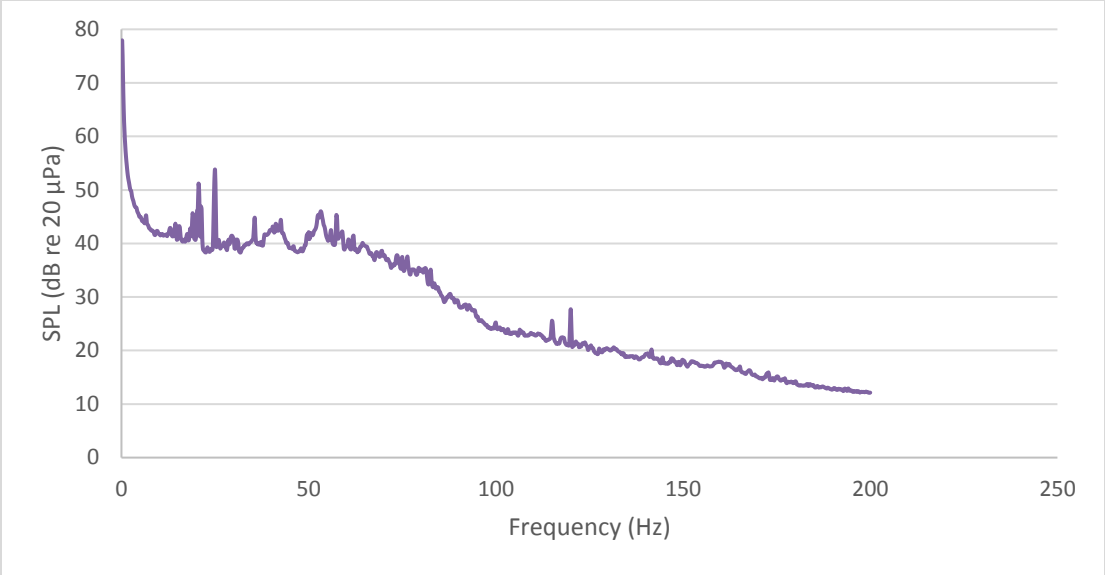

Figure 91: 4:00 PM

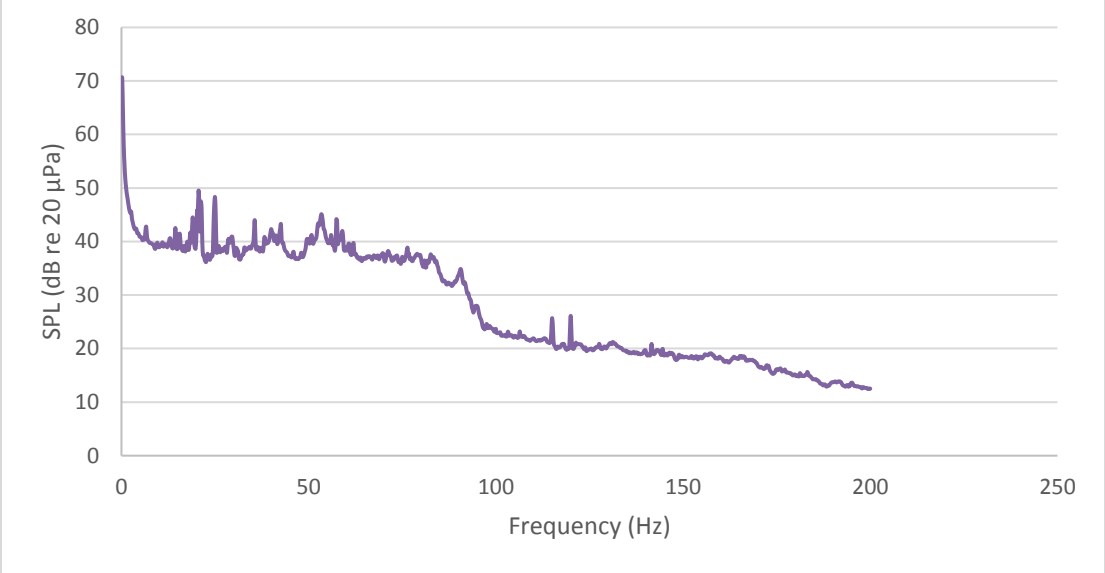

Figure 92: 6:00 PM

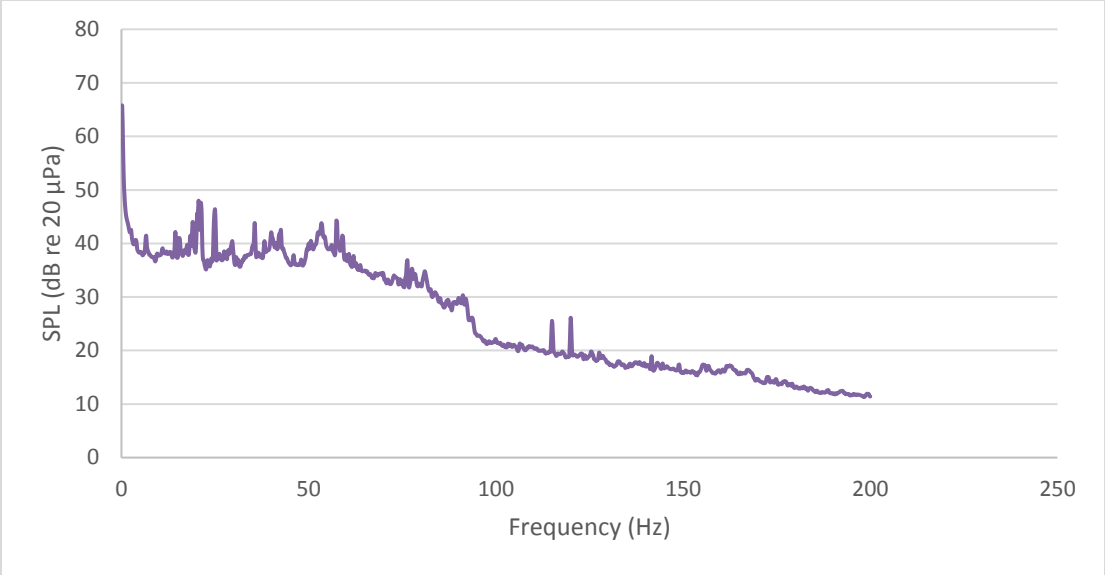

Figure 93: 7:00 PM

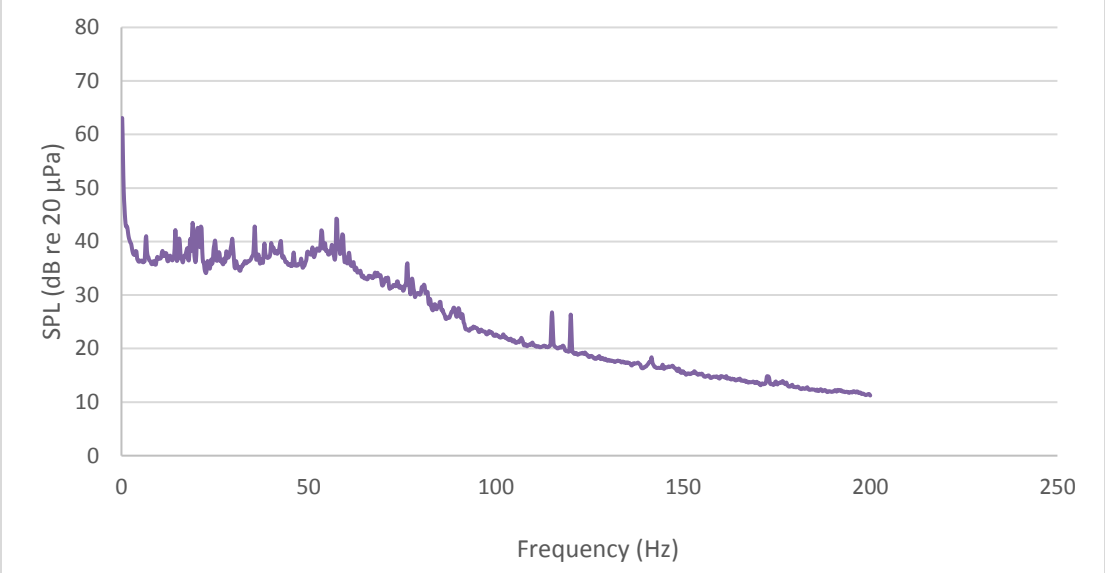

Figure 94: 8:00 PM

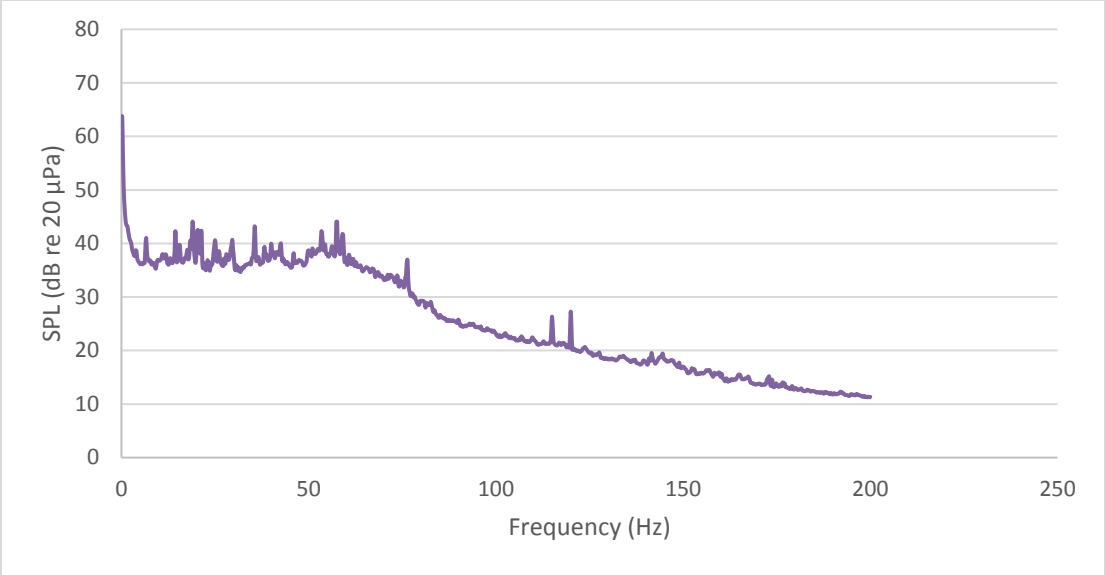

Figure 95: 9:00 PM

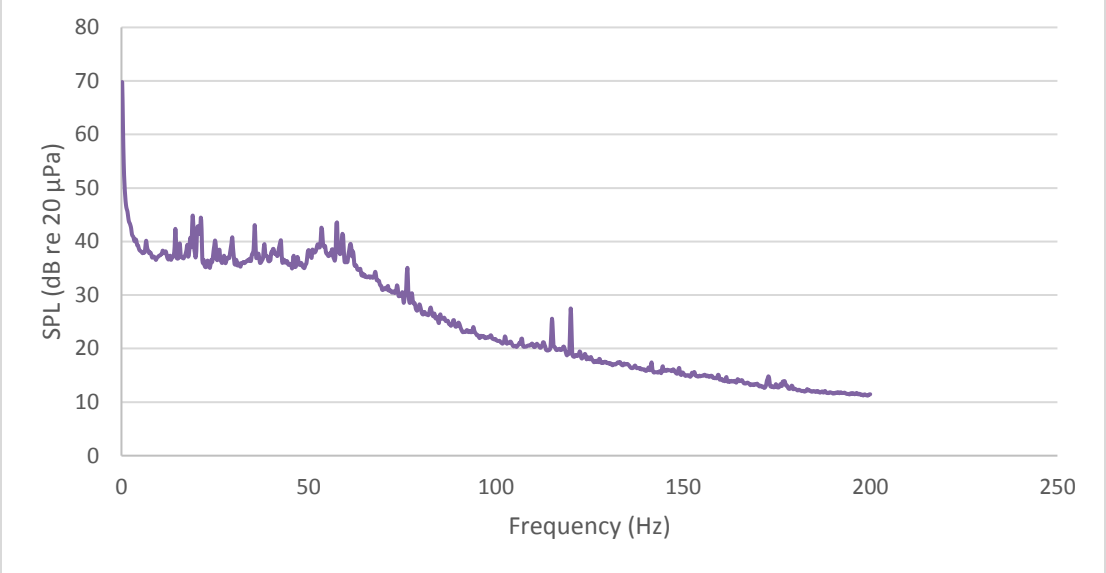

Figure 96: 10:00 PM

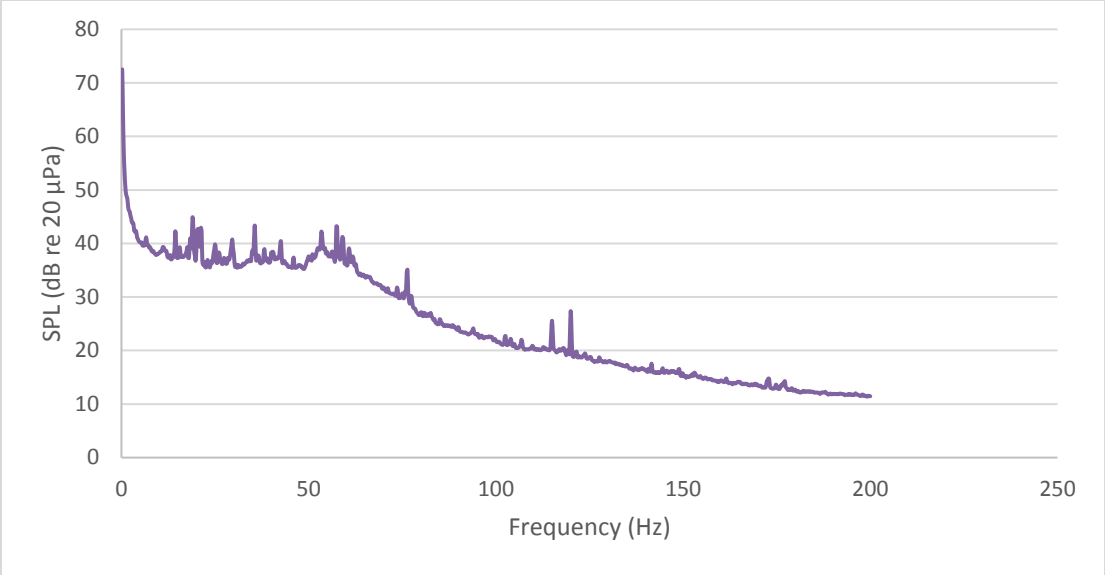

Figure 97: 11:00 PM

The following graphs are the other interesting earthquake spectra not shown in section 4.3.1.

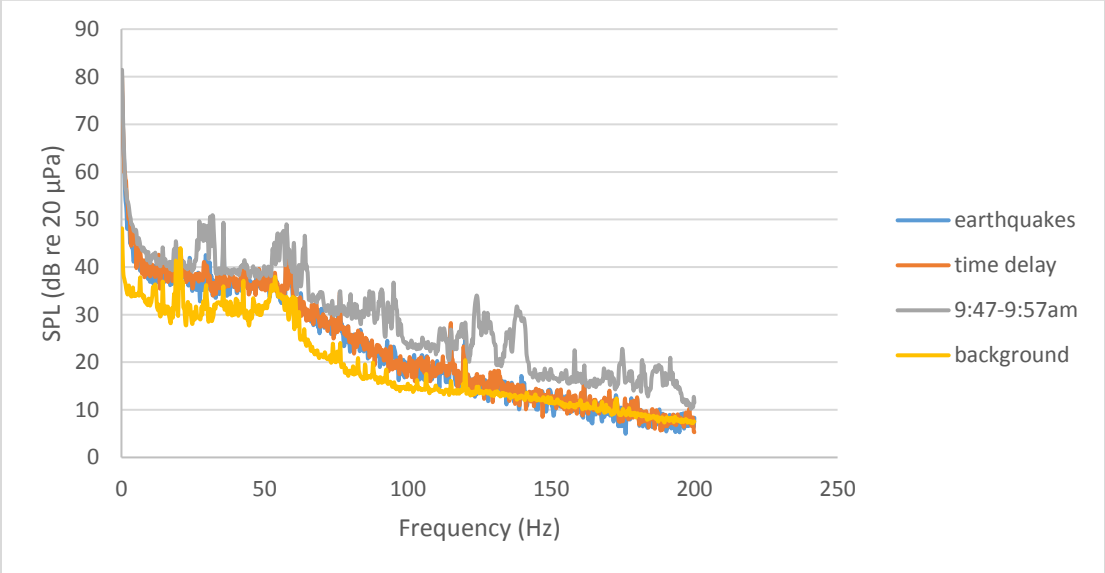

Figure 98: Earthquake recorded at 9:56 am on Sept 3, GPS location: 36.42, -96.87 (approx 23 miles from mic)

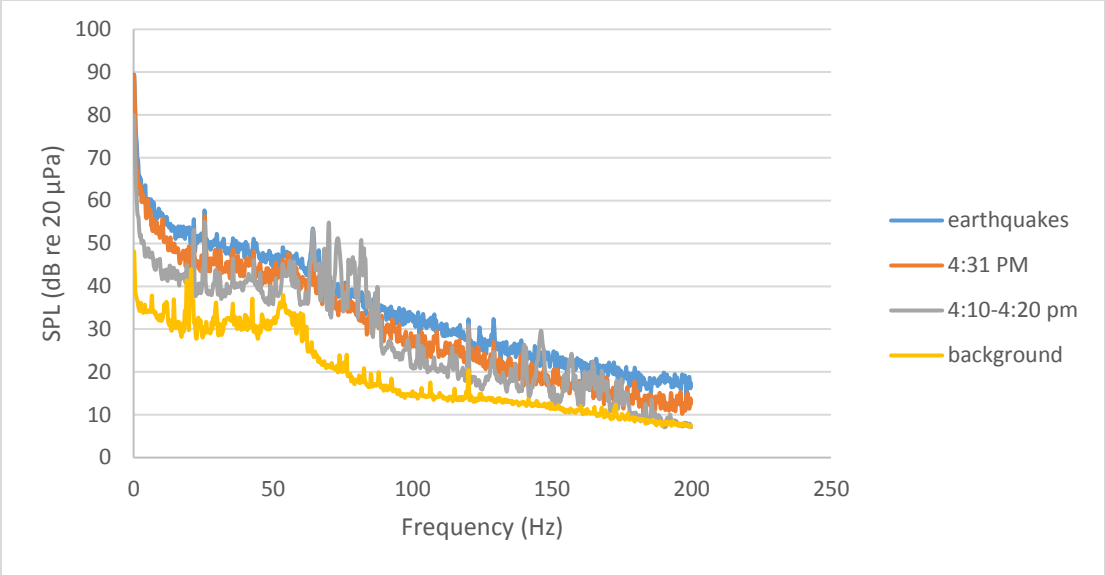

Figure 99: Earthquake recorded at 4:29pm on Sept 8, GPS location: 36.28, -97.52 (approx. 26.5 miles from mic)

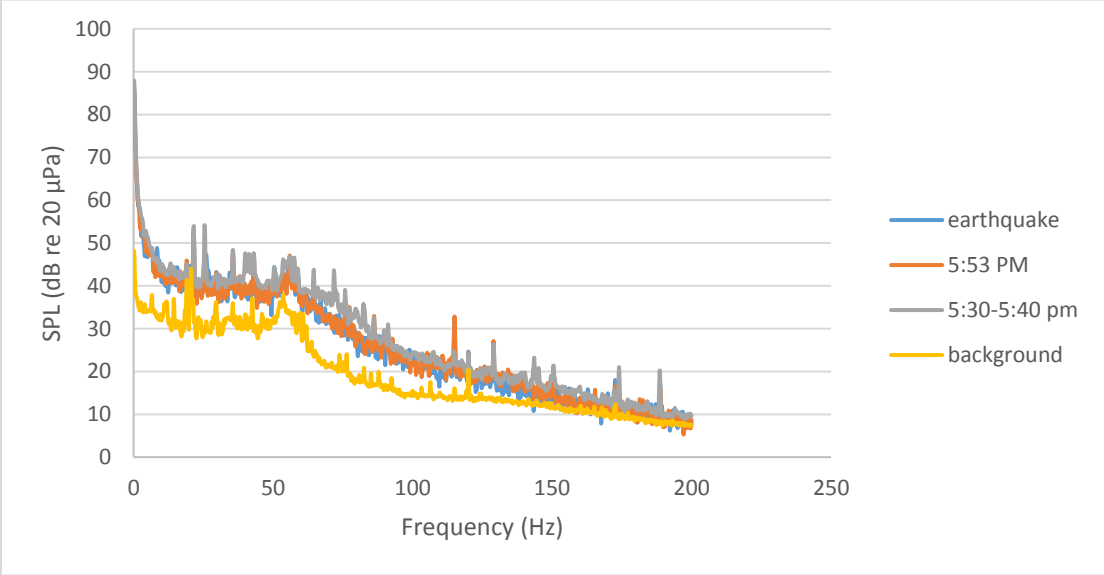

Figure 100: Earthquake recorded at 5:51pm on Sept 9, GPS location: 36.09, -96.74 (approx 20 miles from mic)

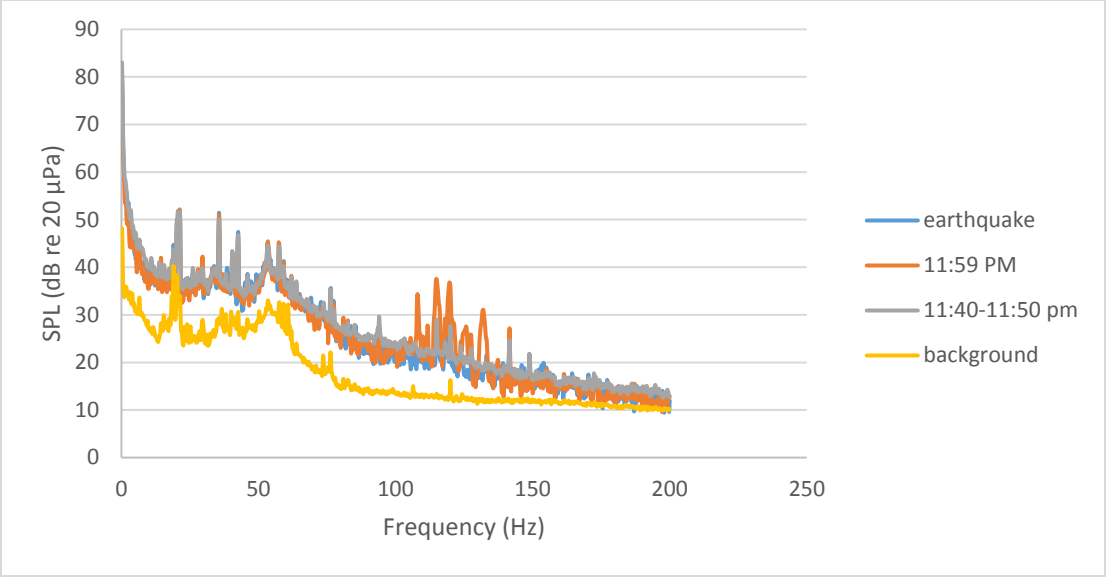

Figure 101: Earthquake recorded at 11:57pm on Sept 10, GPS location: 36.42, -96.91 (approx. 22 miles from mic)

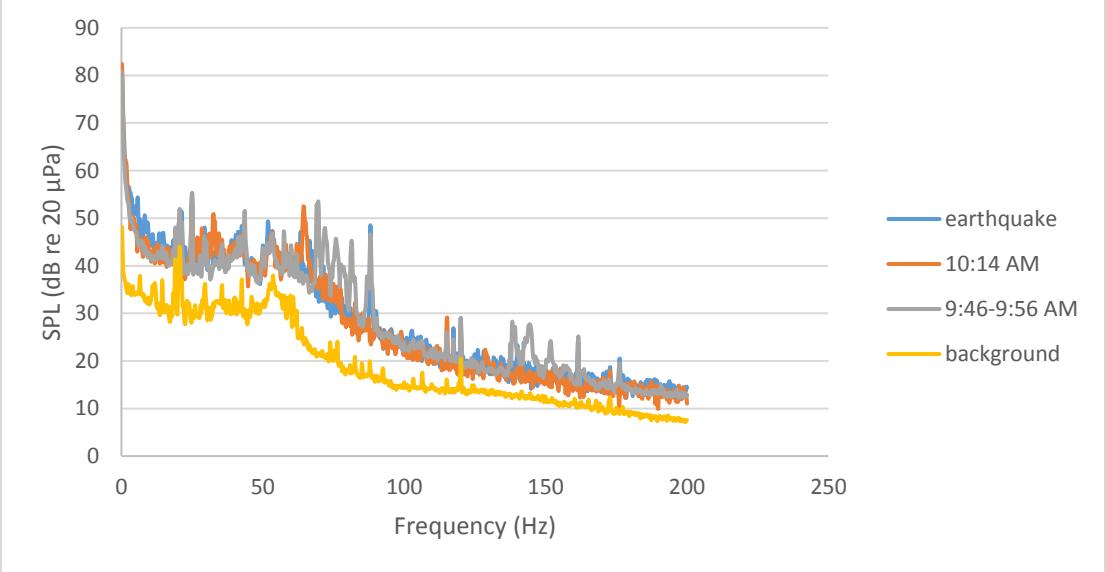

Figure 102: Earthquake recorded at 10:09am on Sept 13, GPS location: 36.78, -97.82 (approx. 61 miles from mic)

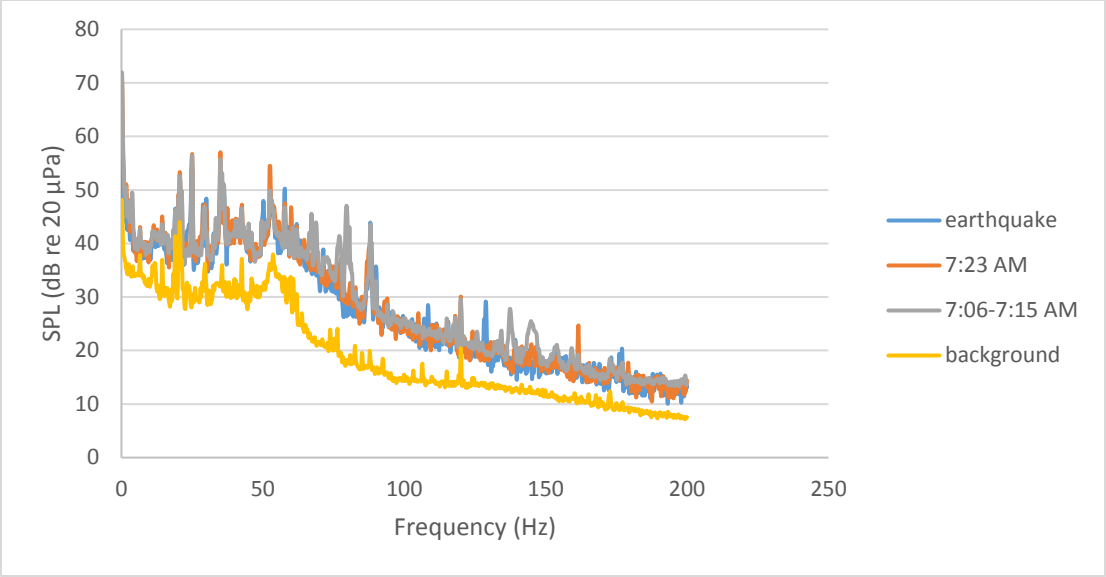

Figure 103: Earthquake recorded at 7:16 am on Sept 13, GPS location: 35.02, -97.88 (approx. 89 miles from mic)

VITA

Arnesha Renee' Threatt

Candidate for the Degree of

Master of Science

Thesis: INVESTIGATION OF NATURAL AND ANTHROPOMORPHIC SOURCES OF ATMOSPHERIC INFRASOUND

Major Field: Mechanical and Aerospace Engineering

Biographical:

Education:

Completed the requirements for the Master of Science in your Mechanical and Aerospace Engineering at Oklahoma State University, Stillwater, Oklahoma in December 2016.

Completed the requirements for the Bachelor of Science in Mechanical Engineering at Oklahoma State University, Stillwater, Oklahoma in 2014.